People's Democratic Republic of Algeria

Ministry of Higher Education and Scientific Research

University of Echahid Hamma Lakhdar-El-Oued

FACULTY OF TECHNOLOGY

DEPARTEMENT OF MECHANICAL ENGINEERING

Master thesis

Presented to fulfill the requirements to obtain

ACADEMIC MASTER DEGREE

Subject-Field: Sciences and Technology

Option: Mechanical engineering

Specialty: Energetics

Subject

Numerical study of mixed convection heat transfer in a ventilated cavity containing a heat fin

Thesis examination committee:

Dr. ATIA Abdelmalek: President.

Dr. KHECHEKHOUCHE Abderrahmane: Examiner.

Dr. BOUKHARI Ali: Supervisor.

Presented by:

KEDDOUDA Abdelhak

BOUDEBIA Mohammed Ridha

2019/2020

Dedications

This work is dedicated:

To my parents for their love, confidence, and motivation, may this work be a testimony of my deep gratitude.

To my brothers and sisters.

To my professors.

To all my family.

To all friends.

To anyone who ever gave me love, hope and support.

Abdelhak

Dedications

This work is dedicated:

To my mother for her love, faith, and support, may this work be an attestation to show a glimpse of my gratitude.

To my brothers and sisters.

To all my whole family.

To my professors.

To all friends.

Mohammed Ridha

Acknowledgments

First of all, we thank the Almighty Allah for endowing us the strength to successfully complete this thesis. We would like to express our gratitude to our respected supervisor Dr. BOUKHARI Ali, Associate professor, Department of mechanical engineering, University of El-Oued, for his generous amount of guidance, support and care provided through the process of conducting this research. We are indebted to him for his valuable help, patience in every step of this work; he will always be a source of inspiration for us.

We would like to thank the members of the thesis evaluation committee, Dr. Abdelmalek ATIA, Associate Professor, Department of mechanical engineering, University of El-Oued and Dr. Abderrahmane KHECHEKHOUCHE assistant professor, Department of mechanical engineering, University of El-Oued for their valuable comments and suggestions.

We would also like to express our sincere thanks and appreciation to Dr. GUERRAH Ayoub, Associate professor, Department of mechanical engineering, University of El-Oued, for extending his cordial support, guidance and comments during the operation of carrying out this dissertation.

We also want to profess our appreciation to anyone who lay a hand of help accomplishing this research, especially Mr. Nacer LEBBIHIAT, we also want to thank all professors of the department of the mechanical engineering at the University of El-Oued.

Last but not the least, we would like express our gratitude to our friends, families and our beloved ones for their continuous support, patience and confidence which made this work see the light on this day.

Table of contents

CHAPTER III : NUMERICAL TECHNIQUE

CHAPTER IV : RESULTS AND DISCUSSION

List of tables

List of figures

Nomenclature

A	Diagonal of coefficient matrix.	
AR	Aspect ratio.	
a	Vector field.	
B	Source term vector, Bottom.	
°C	Degree Celsius.	
C_p	Specific heat at constant Pressure.	$(J.kg^{-1}.K^{-1})$
d	Distance between cell and neighbor centroid.	(m)
D	Inlet, outlet dimension.	
F	Mass flux.	
g	Gravitational acceleration.	$(m.s^{-2})$
$\vec{g}$	Gravity field.	
H	Height.	(m)
h	Convective heat transfer coefficient.	$(W.m^{-2}.K^{-1})$
k	Thermal conductivity.	$(W.m^{-1}.K^{-1})$
K	Thermal conductivity ratio.	
L	Cavity length, Left.	(m)
m	Mass.	(kg)
$\dot{m}$	Mass flow.	$(kg.s^{-1})$
M	Coefficients matrix, Middle.	
$\vec{n}$	Normal vector.	
P	Dimensional pressure.	$(N.m^{-2})$
P^*	Dimensionless pressure.	
q	Heat transfer rate.	(W)
R	Right.	
S	Surface, Source term.	
t	Time.	(s)
T	Temperature.	(K)
ΔT	Temperature difference.	(K)
T^*	Dimensionless temperature.	
t^*	Dimensionless time.	
T	Top.	

u, v, w	Velocity components.	$(m.s^{1})$
$u^*,\ v^*,\ w^*$	Dimensionless velocity components.	
$\vec{V}$	Velocity vector.	
V	Volume of control volume.	
w	Weight function.	
x, y, z	Cartesian coordinates.	(m)
$x^*,\ y^*,\ z^*$	Dimensionless Cartesian coordinates.	

Greek Symbols

ρ	Density.	$(kg.m^{-3})$
μ	Dynamic viscosity.	$(kg.m^{-1}.s^{-1})$
β	Thermal expansion coefficient.	(K^{-1})
Φ	Transported quantity.	
Γ	Diffusion coefficient.	
ν	Kinematic viscosity.	$(m^2.s^{-1})$
α	Thermal diffusivity.	$(m^2.s^{-1})$
ϵ	Gradient error.	

Dimensionless numbers

Gr	Grashof number.
Nu	Nusselt number.
Pr	Prandtl number.
Ra	Rayleigh number.
Re	Reynolds number.
Ri	Richardson number.

Subscripts

ave	Average.
c	Constant.
cv	Control volume.
f	Fin, Face.
in	Inlet of control volume.
Loc	Local.
N	Neighbor.

out	Outlet of control volume.
P	Pivot.
s	Solid.
Φ	Transported quantity.
∞	Reference state.
w	Wall.
x, y, z	Direction, distance in Cartesian coordinates.

Abbreviations

FPSC	Flat plate solar collector.
BEM	Boundary element method.
CD	Central Differencing scheme.
CFD	Computational Fluid Dynamics.
FDM	Finite difference method.
FEM	Finite element method.
FVM	Finite volume method.
HVAC	Heating, ventilation, and air conditioning.
HTGR	High Temperature Gas-cooled nuclear Reactor.
PDE	Partial differential equation.
RCCS	Reactor Cavity Cooling System.
SEM	Spectral element method.
UD	Upwind Differencing scheme.

GENERAL INTRODUCTION

GENERAL INTRODUCTION

Energy exists in different forms according to thermodynamics, the science that deals with different forms of the energy, or more specifically, the amount of energy in which a system interacts with its surrounding, and the term energy here can refer to heat. However, in engineering, the interest is the rate of the transferred heat, which is a heat transfer science matter. The latter is the science that deals with the determination of that rate.

The heat transfer is encountered in many engineering applications such as cooling of electronic devices, thermal design of building, nuclear power, solar collectors, heat exchangers, refrigerators, radiators and many other systems. Those systems are mainly built on basis of heat transfer analysis, or in particular, convective heat transfer analysis for most of them, which is one of the mechanisms in which heat transfer occurs (in addition to conduction and radiation). Convection as an interdisciplinary requires an understanding of a two older disciplines, fluid mechanics and heat transfer.

Scientists and researchers have investigated many problems involving convective heat transfer phenomena in cavities, where both fluid flow and heat transfer have a significant importance, which makes the analytical solution of such problems very difficult to obtain, and mostly available for limited cases, as complexities can arise because of complex geometries and boundary conditions. To solve those problems and overcome those complexities and the high cost and time consumption of the experimental approach, the numerical solution is introduced which uses algorithms and computer development to yield a reliable solution for such problems.

In the present investigation, a more complex problem will be encountered since the mixed convection (combined free and forced) will be investigated in a new geometry with the objective of analyzing the heat transfer, thermal performance as well as the influencing geometry and fluid flow parameters and to provide a correlation for the heat transfer performance for such geometry. The solution will be obtained through solving the set of governing partial differential equations of continuity, momentum, and energy, using the commercial numerical, finite volume method based, CFD code of ANSYS Fluent.

Although we will employ the numerical approach, the difficulty of the problem requires assumptions and approximations, which we will build our solution around them, namely the Boussinesq approximation, the negligible viscous dissipation in the energy equation and the heat transfer by radiation, the incompressibility of the fluid and the constant thermos-physical properties, and the fluid flow will be exclusively laminar.

The dissertation illuminating the present work will consist of four main parts or chapters, in the first section, the basic fundamental concepts of the heat transfer in general, and mixed convection in particular, will be introduced with examples of industrial applications of the latter phenomena to point out its importance. Following that, a literature review of most recent works in the field of combined convection will be presented as well.

Afterwards, a second chapter will focus on the mathematical formulation of the studied problem, introducing the physical and mathematical model, relying on the cornerstone equations of the computational fluid dynamic and the employed assumptions. Those equations of continuity, momentum, and energy are then transformed into their dimensionless form to point out to the governing non-dimensional parameters.

Thereafter, a third section in which, the basics and advantages of the numerical analysis and the finite volume method will be presented, alongside the theory behind the latter numerical method formulation with details of discretization process of the governing equations. Algorithms of calculation and steps of setting up the solver from geometry modeling, meshing and selecting the different solution required parameters will be the final part in this chapter.

Eventually, a mesh independency test and validation of the employed CFD code will be conducted, and then a detailed presentation and discussion of the obtained results will be undertaken. Finally, the dissertation is rounded off with a conclusion conveying the outcomes and recommendations for present work.

CHAPTER I : GENERALITIES AND LITERATURE REVIEW

I.1 Introduction

Convective heat transfer, or just convection, is the study of heat conveyance process effected by the fluid flow. The very word convection has its roots in the Latin verbs convecto-are and convěho-věhěre [1],which mean to bring together or to carry into one place. Convective heat transfer has grown to the status of a contemporary science because of our need to understand and predict how a fluid flow acts as a ‘‘carrier’’ or ‘‘conveyor belt’’ for energy and matter [1].

To study the interdisciplinary is worthy, but it must take place after one acquires the major fields and branches, not counter wise. Obviously, convective heat transfer is a field in which two older fields meets: fluid mechanics and heat transfer. So, the study of any convective heat transfer issue must reset on a solid basic knowledge of the basic heat transfer and fluid mechanics principles.

The main objective of this chapter is to review these principles in order to establish a better understanding of the more specific issue addressed in present work.

I.2 Heat transfer mechanisms

The analysis of amount of heat transfer while a system goes through a transformation process from an equilibrium state to another is the thermodynamics’ concern. However, the determination of such energy transfers rate is the matter of heat transfer science, the transfer of energy as heat is always from the higher-temperature environment towards the lower-temperature one, the transfer stops when an equilibrium of temperature is reached.

Transfer of heat occurs within three mechanisms (modes): conduction, convection and radiation, the main requirement for each mode is the temperature difference existence [2].

I.2.1 Conduction

Conduction is the transport of heat from the more energetic particles of a substance to the neighboring less energetic ones as a result of interactions between the particles. Conduction can occur in solids, liquids, or gases. In liquids and gases, it is due to the clash and propagation of the molecules during their motion in random way. In solids, it is due to the combination of oscillation of the molecules in a lattice and the energy transport by free electrons. The rate of heat conduction in a medium depends on the medium's geometry, thickness, and its material, as well as the difference of temperature across that medium [2]. The theory behind the heat conduction was developed early in the nineteenth century by Joseph Fourier [3].

I.2.1.1 Thermal Conductivity

The thermal conductivity of a substance can be expressed as the rate of heat transfer within a unit thickness of the substance per unit area per unit temperature difference. The thermal conductivity of a substance is a measure of the capacity of the substance to conduct heat [2].

I.2.1.2 Thermal diffusivity

The thermal diffusivity is another material property that appears in the unsteady heat conduction analysis, which represents how fast heat diffuses through a substance, it is defined as the ratio of heat conduction to heat storage [2].

I.2.2 Convection

The convective heat transfer mode is comprised of two mechanisms. In addition to energy transfer due to random molecular motion (diffusion), energy is also transferred by the bulk, or macroscopic, motion of the fluid. This fluid motion is associated with the fact that at any instant, large numbers of molecules are moving collectively or as aggregates. Such motion, in the presence of a temperature gradient, contributes to heat transfer. Because the molecules in the aggregate retain their random motion, the total heat transfer is then due to a superposition of energy transport by the random motion of the molecules and by the bulk motion of the fluid. The term convection is customarily used when referring to this cumulative transport and the term advection refers to transport due to bulk fluid motion [4].

Convection is called forced convection if the fluid is forced to flow over the surface by external means such as a fan, pump, or the wind. In contrast, convection is called natural (or free) convection if the fluid motion is caused by buoyancy forces that are induced by density differences, due to the variation of temperature in the fluid [2].

Free and forced, mixed (or combined) convection, for short, mixed convection, is a coupled phenomenon of free and forced convection. As general case, the mixed convection is formed simultaneously by an outer forcing flow and inner volumetric force, while the latter is caused by the no-uniform density distribution of a fluid medium in a gravity field. Obviously, there has been much challenge in research of mixed convection over that of net free or forced convection [5]. The mixed convection is divided to two types, positive (adding) and negative (opposing) flows. For the former flow, free and forced convections are in the same direction, and the mixed convection parameter Gr (Grashof number) is positive. For the latter flow, free and forced convections are in the opposite directions, and the combined convection parameter Gr will be negative [5].

I.2.3 Radiation

Radiation is the energy emitted by matter in the form of electromagnetic waves (or photons) because of the changes in the electronic configurations of the atoms or molecules. Unlike conduction and convection, the transfer of heat by radiation does not require the presence of an intervening medium. In fact, heat transfer by radiation is fastest (at the speed of light) and it suffers no attenuation in a vacuum. This is how the energy of the sun reaches the earth [2].

I.3 Internal and external flows

Convective heat transfer is closely tied with fluid mechanics, which is the science that deals with the behavior of fluids at rest or in motion, and the interaction of fluids with solids or other fluids at the boundaries. There is a wide variety of fluid flow problems encountered in practice, and it is usually convenient to classify them on the basis of some common characteristics to make it feasible to study them in groups [2].

A fluid flow is classified into two categories; internal and external, depending on whether the fluid is forced to flow in a confined channel or over a surface. An internal flow is in a channel bounded on all sides by a solid surface except, possibly, for an inlet and exit. Flows through a pipe or in an air-conditioning duct are the examples of internal flow. Internal flows are dominated by the influence of viscosity throughout the flow field. The flow of an unbounded fluid over a surface is external flow [6].

I.4 Mixed convection heat transfer in cavities

Mixed convection in cavities is a matter of present-day importance, since cavities filled with fluid are central components in a long list of engineering and geophysical systems. The flow and heat transfer induced in a cavity differs fundamentally from the external mixed convection boundary layer. Mixed convection in a cavity, is the result of the complex interaction between finite size fluid systems in thermal communication with all the walls that confine it. The complexity of this internal interaction is responsible for the diversity of flows that can exist inside cavity [6].

The phenomenon of mixed convection in cavities is varied by the geometry and the orientation of the cavity. Judging by the potential engineering applications, the cavity phenomena can loosely be organized into two classes [6].

I.4.1 Vented cavity

In a vented cavity, where the interaction between the external forced stream provided by the inlet and the buoyancy driven flows induced by the heat source leads to the possibility of complex flows. Therefore it is important to understand the fluid flow and heat transfer characteristics of mixed convection in a vented cavity [6].

I.4.2 Lid-driven cavity

On the other hand, the fluid flow and heat transfer in a lid-driven cavity, where the flow is induced by a shear force resulting from the motion of a lid, combined with the buoyancy force due to non-homogeneous temperature of the cavity wall, provides another problem. Studied extensively by researchers to understand the interaction between buoyancy and shearing forces in such flow situation. The interaction between buoyancy driven and shear driven flows inside a closed cavity in a mixed convection regime is quite complex. Therefore, it is also important to understand the fluid flow and heat transfer characteristics of mixed convection in a lid-driven cavity [6].

I.5 Industrial application of mixed convection

Cavities and enclosures are frequent in different industries and equipment such as HVAC (Heating, ventilation, and air conditioning), heat exchangers, nuclear power, renewable energies [7]. Oil extraction, cooling of electronic equipment, design of heat exchangers, flow and heat transfer in solar ponds, crystal growth, dynamics of lakes and float glass productions [8]. In the following, some of these applications will be presented.

I.5.1 Solar collectors

Flat plate solar collector (FPSC) is one of the most popular equipment among solar energy systems, which can be utilized for heating of domestic or public buildings where the demands for hot water are quite indispensable. Although they have a number of benefits such as no need for sun tracking and low maintenance cost, their low thermal performance is considered as a hindrance in their extensive development [9].

The solar flat plate collector operating under different convective modes has low efficiency for energy conversion. The energy absorbed by the working fluid in the collector system and its heat transfer characteristics vary with solar insolation and mass flow rate. The performance of the system is improved by reducing the losses from the collector. Various passive methods have been devised to aid energy absorption by the working fluid [10].

Also, working fluids are modified using nanoparticles to improve the thermal properties of the fluid [10].

In numerical study that was conducted by Yurddaş Ali and Çerçi Yunus [11], revealed that the natural convection effects in the carrying pipe improves as the heat flux increases and thus, higher Nusselt numbers are obtained in mixed convection in comparison with forced convection.

I.5.2 Solar Ponds

Solar pond as a fairly new technology to collect and store solar energy. It seeks sustainable and environmentally benign methods to supply thermal energy for various applications. The first time the solar pond was discovered in the Middle East by Dave Grant in 1980 while he was working in an aquaculture project. The incident solar energy is mainly transmitted through the water layers, absorbed by the lined darkened bottom and probably the sides of the pond [12].

The accumulated heat will increase the water temperature in the lowest layer of the pond, which could reach 80-90 °C. Water in such temperature can be used for many purposes e.g. salty water desalination, aquaculture, and electricity generation [12].

I.5.3 Cooling of electronic components

Cooling requirements in microelectronics are among the toughest barriers of developing faster, smaller, and still more reliable systems. In the past three decades, electronics has developed to surround all faces of modern life. At the same time, with increasing number of applications reliability has become a real crucial problem. The failure of a brand-new stereo may be tolerable; however, a problem in the sophisticated computers supporting vital systems of business, health and defense could result in not only disruption of that service, but also disastrous events, perhaps, in terms of human lives. Realizing the importance of the problem, much emphasis has been given to the improvement of the reliability level as well as to the improvement of the electrical performances of the electronic devices [13].

The purpose of thermal design is to provide equipment to remove the heat from heat sources to one or more heat sinks in the environment. The main goal of thermal control is to maintain the temperatures of individual elements within their functional and maximum allowable limits. Functional temperature limit is the range in which the electronic element's performance is in accordance with the expectation of the electronic designer. If the operation temperature goes over the limit, degraded electrical performance and logic errors are very likely to occur. In order to meet the cooling requirements of microelectronics, the task of thermal design engineer is to find the most efficient thermal paths from the heat source to the ultimate heat sink. For this purpose, emphasis must be given to find ways of reducing both internal and external resistances [13].

I.5.4 The HVAC systems

Heat transfer by convection is when some substance that is readily movable such as air, water, steam, or refrigerant moves heat from one location to another [14].

An HVAC system uses convection in the form of air, water, steam and refrigerants in ducts and piping to convey heat energy to various parts of the system. When air is heated, it rises; this is heat transfer by "natural" convection. "Forced" convection is when a fan or pump is used to convey heat in fluids such as air and water. For example, many large buildings have a central heating plant where water is heated and pumped throughout the building to the final heated space. Fans then move heated air into the conditioned space [14].

I.5.5 Nuclear power

To achieve the massive production of hydrogen, a thermo-chemical cycle coupled to a High Temperature Gas-cooled nuclear Reactor (HTGR) is considered as one of the systems exhibiting high application potential. The Reactor Cavity Cooling System is a key safety system that ensures the integrity of the HTGR during accident conditions; therefore, it is necessary to verify its performance for the safety of the HTGR as well as for the reliability of the coupled hydrogen production system. The RCCS performance depends on the heat transfer rate of riser ducts; however, the mixed convection that is likely to occur in the riser ducts can complicate the verification process [15].

I.6 Literature review

Due to its practical importance, mixed convection in ventilated cavities has a great interest in many technological and industrial processes, such as thermal design of buildings, air conditioning, the cooling of electronic circuit boards, and the design of solar collectors.

Lately, enhancement of heat transfer using heat fins in cavities due to introduction of obstacles, partitions and fins attached to the wall(s) has gain great interest. A literature review on the topic reveals that many authors have investigated mixed convection in ventilated cavities with obstacles, partitions and fins, in the following section a literature survey on the heat transfer in cavities is introduced.

I.6.1 Natural convection

Calcagni et al. [16], carried out an experimental and numerical study of free convective heat transfer in a square enclosure heated from below. The study analyzed the heat transfer development inside the rectangular cavity with the increasing of the heat source length; the heat source was located at the bottom, and the cavity was cooled from the sidewalls (Figure I.1).

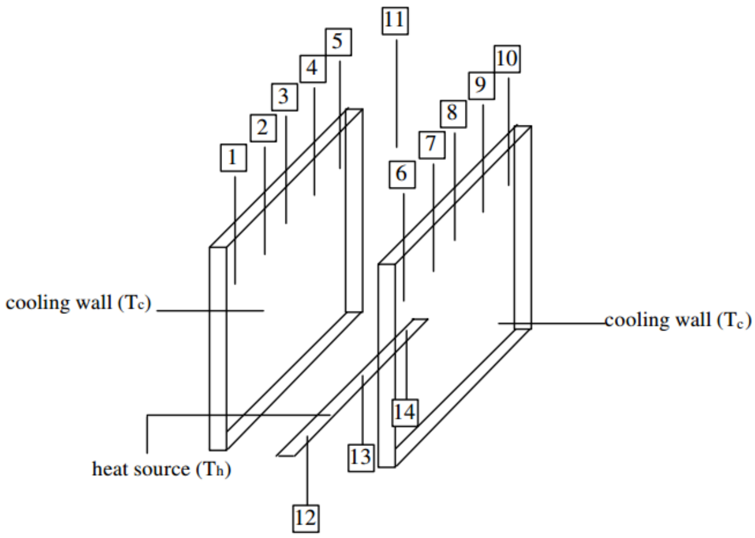

Figure I.1 *: Sketch of the position of the thermocouples [16].*

The experimental data was obtained by measuring the temperature distribution in the air layer by real-time and double-exposure holographic interferometry while the commercial finite volumes code Fluent 6.0 was used for the numerical study. The study was conducted for a range of Ra number of 10^3 to 10^6, and heat source varied from 1/5 to 4/5 of H, The study concentrates the attention on the effects of the dimension of the heat source on the convective heat transfer. The finding of this study pointed out a heat transfer prevalently conductive for Ra $\leq 10^4$ while the convective phenomenon develops completely for Ra $\cong 10^5$. As expected, an increase of the heat source dimension produces a raise in heat transfer particularly for high Ra.

I.6.2 Forced convection

Sourtiji et al. [17] carried out a numerical study of turbulent forced convection flow inside a square ventilated cavity. The position of the inlet port was fixed, while the outlet port was varied along the four walls of the cavity. The diagram of the local and total Nusselt numbers and the coefficient of the pressure drop were plotted with respect to the position of the outlet port in order to realize the best configuration of the system. The governing equations were iteratively solved by the finite-volume method using Patankar’s SIMPLE algorithm. The results indicated that the best position of the outlet port is specified by considering both the maximum overall Nusselt number and minimum system pressure drop in the cavity simultaneously. It was found that the case with the outlet port positioned on the right side of the bottom wall for the cases with wide ports, and the one with the outlet port located on the left wall for the cases with thin ports are the best positions to obtain the best performance of the system.

I.6.3 Mixed convection

Rahman et al. [18] carried out a computational study to investigate the effect of Reynolds number and Prandtl number on mixed convective flow and heat transfer characteristics in a ventilated cavity, with a solid circular heat generating obstacle at the center. The study was accomplished using Galerkin weighted residual finite element method to solve the governing equations of mass, momentum and energy, with the assumption of a two-dimensional, steady state, laminar and incompressible, mixed convection flow in the cavity, with a constant fluid properties and negligible radiation effects. In addition to the Boussinesq approximation. During their study, a wide range of Reynolds numbers ($50 \leq Re \leq 200$) and Prandtl numbers ($0.71 \leq Pr \leq 7.1$) was covered. Their findings indicated that the flow and thermal fields, the heat transfer rate, the Drag force and the average fluid temperature in the cavity depend significantly on the Reynolds and Prandtl number. For the last one, it has a remarkable influence on streamlines and isotherms; the increased Pr number values increased the average Nusselt number at the heated surface and the drag force, and decreased the average temperature of the fluid in the cavity. As for Re number, it has a significant effect on the flow and temperature fields. An increased value of Re, increased Buoyancy-induced vortex in the streamlines and the average Nusselt number, and made the thermal layer thin and concentrated near the heated surface, The Drag force decreased and increased in the forced and free convection region respectively. As for the average fluid temperature, it changed from highest to lowest as Ri number increased. In addition to that, Gupta et al. [19], examined the mixed convective transport in a ventilated square cavity in presence of a heat conducting circular cylinder placed at the center of the cavity. The fluid flow imposed through an opening at the bottom of the left cavity wall and taken away by a similar one at the top of the right wall (Figure I.2).

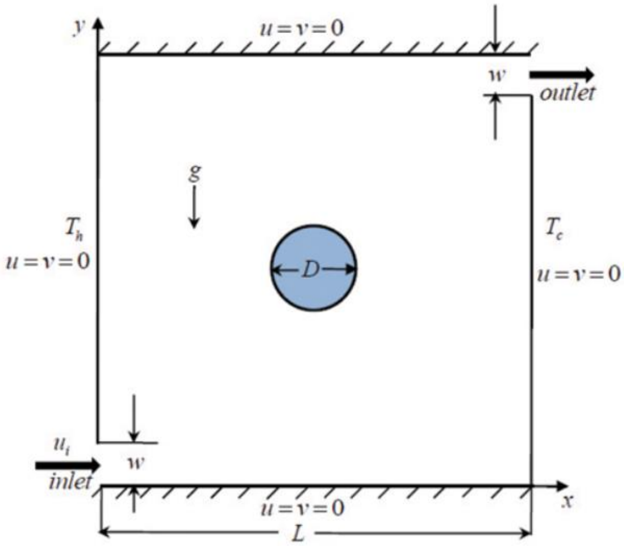

***Figure I.2** : Physical problem Schematic, Case I heated sidewalls [19].*

Two cases were considered depending on the thermal conditions of the cavity walls. In the first case, the left and right vertical walls were kept isothermal with different temperatures and the top and bottom horizontal walls were considered as thermally insulated. For the second case, the top and bottom walls were maintained at different constant temperatures and the left and right walls were considered adiabatic. Heat transfer due to forced flow, thermal buoyancy, and conduction within the cylinder was considered. Effect of the cylinder size ($0.1 \leq D \leq 0.5$) and the solid–fluid thermal conductivity ratio ($0.1 \leq K \leq 10$) were explored for various values of Richardson number ($0 \leq Ri \leq 5$) at fixed Reynolds ($Re = 100$) and Prandtl ($Pr = 0.71$) numbers. Assuming an incompressible flow with constant fluid properties along with Boussinesq approximation, the governing differential equations consisting of mass, momentum, and energy were solved using a finite volume based CFD package Fluent. It was found that the aforementioned parameters have significant influences on the fluid flow and heat transfer characteristics in the cavity. Moreover, Benderradji et al. [20] presented a numerical study of mixed convection heat exchange in a cubic cavity of a laminar three-dimensional (3D) incompressible flow. Their study predicted the behavior of the flow structure between Multi clear structure dominated by natural convection when the Reynolds number is small, and a Multi clear structure dominated by forced convection when the Reynolds number is high. They effected the study based on two aspects, the first was that the Grashof number is fixed and the

Reynolds number is varied (Re = 10 to 2000), and the second case was to present the effect of Grashof number (Gr = 10^3 to 10^6). The flow was considered three-dimensional, stationary and laminar, and the physical properties were assumed constant except for the density in the expression of the buoyancy force term, also the Boussinesq approximation was used. Viscous dissipation in the energy equation was neglected, the working fluid was air (Pr = 0.71). The coupled governing equations were solved using the finite volume method by the SIMPLE algorithm, and the convective terms are processed by the second order centered Upwind scheme. The obtained results of their study show that the size and shape of the cells of a Multi clear structure stationary flow regime depend strongly on the Grashof number and the Reynolds number

Ahammad et al. [21], studied the performance of different inlet and outlet locations on the flow and heat transfer for the MHD (Magnetohydrodynamic) mixed convection in a ventilated cavity in presence of a heat generating square block. A Galerkin weighted residual based finite element method was applied to obtain the numerical solutions of the governing equations. Four different inlet and outlet locations with Re = 100, Pr = 0.71(air), Ha = 10 was investigated for different Richardson numbers, (Ri = 0.1, 1, 10). with an adiabatic walls except for the bottom wall which was kept at constant temperature T_h and a applied magnetic field along the normal of the right vertical wall, and with the following assumptions : a two-dimensional, steady, laminar, and incompressible with constant fluid properties, no viscous dissipation, the radiation effects was neglected and the Boussinesq approximation was also considered. They concluded that both flow and thermal fields was strongly influenced by the position of inlet and outlet openings of the cavity and the BB configuration (An inlet port at the bottom of the left vertical wall, exit port situated at bottom of the opposite sidewall) generates more effective cooling than other configurations. In addition, Doghmi et al. [22], conducted a numerical study on mixed convection heat transfer in a three-dimensional ventilated cavity, for a combinations of thermal and geometrical parameters. Such as Reynolds number Re=100, Richardson number ($0.01 \leq Ri \leq 10$), relative height of the openings (B = h/L = 1/8) and relative width ($0.5 \leq A= w/L \leq 1$). In order to investigate numerically the effects of conjugated Richardson numbers and geometrical parameters on the thermal transport and fluid flow phenomena in the considered enclosure. The working fluid was air, (Pr = 0.71), and it was assumed laminar and incompressible with negligible viscous dissipation, All the thermo-physical properties of the fluid were assumed constant except the density, giving rise to the buoyancy forces (Boussinesq approximation). The mathematical model of their study was solved by the home-developed FORTRAN code, and the incompressible Navier-Stokes and energy equations are discretized by the finite volume method. The finding of this study was that the flow intensity and the heat transfer rate were improved significantly by an optimal choice of: the Reynolds and Richardson numbers, as well as the inlet configuration.

A numerical study has been performed by Rahman et al. [23] on mixed convection flow and heat transfer characteristics inside a square ventilated cavity with a heat-generating solid circular body at the center. The inlet was at the bottom of the left wall, while the outlet one is at the top of the right wall, and all the walls was assumed adiabatic (Figure I.3).

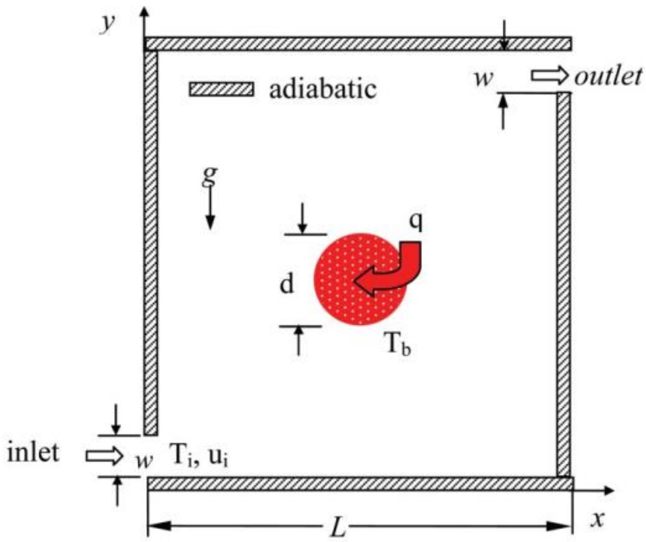

Figure I.3 *: Schematic diagram of the problem considered and coordinate system [23].*

A Galerkin weighted residual finite element method was used to solve the governing equations of mass, momentum, and energy. Their study incorporated the mentioned issue with the effects of dimensionless cylinder diameter D of the body, thermal conductivity ratio K between solid and fluid, and heat-generating parameter Q on the thermal and flow fields. The medium was considered as air with a Prandtl number of 0.71. With the assumption of a two-dimensional, steady state, laminar, incompressible, mixed convection flow, constant fluid properties, and a negligible radiation, in addition to the Boussinesq approximation. From their study, they managed to conclude that the previously mentioned parameters has remarkable effect on the streamlines and thermal field as well as the heat transfer rate and the dimensionless average drag force.

Furthermore, Karimi et al. [24] made a numerical study to investigate the steady-state mixed convection around two heated horizontal cylinders in a square 2-D enclosure. The cylinders was located at the middle of the enclosure height and the walls of the cavity was assumed adiabatic. The study was conducted to analyze the effects of cylinders diameter, Reynolds number and Richardson number on the heat transfer characteristics numerically. The working fluid was water (Pr =7.0) and the flow was laminar in all cases. The radiation effects was assumed negligible. It was further assumed that the water thermophysical properties were constants except for the density in the body force term of the y momentum equation, which follows the Boussinesq approximation. The flow was assumed to be steady state and viscous dissipation and compressibility effects was considered negligible. The finite volume method based CFD software package FLUENT was employed to solve the governing equations of continuity, momentum and energy. The obtained results indicated that the shape of streamlines was influenced by the size of the cylinders. The effect of natural convection on the left cylinder was more than that of right one at higher Richardson numbers. The average Nusselt number over the cylinder surfaces, and non-dimensional temperature inside the enclosure were also increased gradually by enlarging size of cylinders. In addition, they concluded that increasing Reynolds number from 50 to 200 at constant cylinder diameter (D=0.2), conduces to stronger circulating vortices in the flow domain and the natural convection heat transfer was very weak at Re=50.

Moreover, Mamun et al. [25], studied mixed convection heat transfer characteristics in a ventilated square cavity with a heated hollow cylinder at the center. The wall of the cavity was assumed adiabatic. Flows imposed through the inlet at the bottom of the left wall and exited at the top of the right wall of the cavity (Figure I.4).

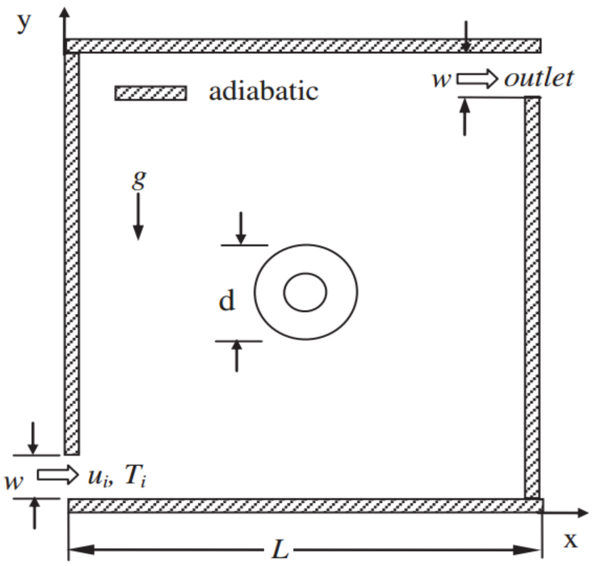

***Figure I.4** : Schematic diagram of the problem considered and coordinate system [25].*

The Emphasis was on the influences of the cylinder diameter and the thermal conductivity of the cylinder in the cavity. The study was conducted for a wide range of pertinent parameters such as Reynolds number, Richardson number, cylinder diameter and the solid-fluid thermal conductivity. Under consideration of a constant thermos-physical properties of the fluid, except the density in body force term of the v-momentum equation according to the Boussinesq approximation, with a steady, laminar and two-dimensional incompressible with negligible the radiation effects and viscous dissipation and pressure work. The laws of mass, momentum and energy were solved using the Galerkin finite element formulation is used to solve the governing equations along with boundary conditions. The obtained results indicated that the flow and thermal fields depended on diameter of the hollow cylinder, the maximum average Nusselt number and average fluid temperature was found for the largest value of the cylinder diameter. In addition, the thermal conductivity ratio was insignificant for Ri = 0.0, but significant at Ri=1.0 and 5.0. It was also observed that the maximum average Nusselt number was found for the lowest value of K. However, the maximum average fluid temperature was observed for the largest value of K. Chamkha et al. [26] have investigated mixed convection from a heated square solid cylinder located at the center of a vented cavity filled with air (Pr = 0.71). The horizontal walls and the right vertical wall were kept adiabatic, while the left vertical wall is maintained at a constant temperature T_c. The flow was assumed laminar, steady and of constant physical properties except for the density in the buoyancy term, which follows the Boussinesq approximation. The study aimed to investigates the effects of the outlet positions, Richardson numbers, Reynolds numbers, locations, and aspect ratios of inner square cylinder on the flow and the thermal fields. The parameters studied and their ranges was as follows: the Richardson number and Reynolds number was varied in the ranges from 0–10 and 50–200, respectively, location of the inner cylinder ($0.25 \leq L_X \leq 0.75$, $0.5 \leq L_Y \leq 0.75$), and aspect ratios of 0.1, 0.2, 0.3, and 0.4. A finite difference method based on successive over-relaxation iterative method was used to solve numerically the governing equations of continuity, momentum and energy of the developed mathematical model. A computational program was written in Fortran 90 language to compute the values of the required variables. The study showed that the average Nusselt number along the heated surface of the inner square values increases with increasing values of the Reynolds and Richardson numbers. The effect of the locations of the inner square cylinder and aspect ratio found to play a significant role in the streamline and isotherm patterns.

A numerical investigation of mixed convection flow through a copper–water Nano-fluid in a square cavity with inlet and outlet ports was carried out by Shahi et al. [27]. The natural convection effect was attained by heating from the constant flux heat source, which was symmetrical located at the bottom wall and cooling from the injected flow. The study was carried out for the Reynolds number in the range $50 \leq Re \leq 1000$, with Richardson numbers $0 \leq Ri \leq 10$ and for solid volume fraction $0 \leq \phi \leq 0.05$. The thermal conductivity and effective viscosity of Nano-fluid were calculated using Patel and Brinkman models, respectively. In addition, the effects of solid volume fraction of Nano-fluids on the hydrodynamic and thermal characteristics was investigated. A two-dimensional square cavity filled with a suspension of copper nanoparticles in water was considered. The shape and size of solid particles was assumed uniform and the diameter of them to be equal to 100 nm. In order to induce the buoyancy effect, the bottom horizontal wall had an embedded constant heat flux source, q'' on part of it. The non-heated parts and the remaining walls were insulated. The flow was entering the cavity from the bottom opening on left vertical wall and leaving from upper opening of the opposite vertical one. It was assumed that both the fluid phase and nanoparticles are in thermal equilibrium and there was no slip between them. Except for the density, the properties of nanoparticles and fluid was taken constant. It was further assumed that the Boussinesq approximation is valid for buoyancy force. Under these assumptions, the governing equations for the steady, two-dimensional laminar and incompressible mixed convection flow, were solved numerically based on the finite volume method using a collocated grid system. Central difference scheme was used to discretize the diffusion terms whereas a blending of upwind and central difference was adopt for the convection terms. The finding of this study indicates that the increase in solid concentration leads to increase in the average Nusselt number at the heat source surface and decrease in the average bulk temperature.

I.7 Motivation behind present work

In light of the literature review of previous studies, it is obvious that numerous numerical studies were carried out on mixed convection for different geometries, but no work has been done on a T-shaped heat fin placed at the center of a ventilated cavity, in addition, only few works were accomplished for 3D cavities. Moreover, mixed convection is a part of many industrial applications as mentioned in this chapter, and it can improve the performance and increase the lifetime of industrial equipments. Therefore, the present work was proposed with the objective of investigating mixed convective heat transfer in an enclosure with an isothermally heated T-shaped heat fin as a heat source at the center of a cavity with two ventilation ports on the sidewalls.

I.8 Conclusion

The purpose of this chapter was to present the fundamental principles of the heat transfer in general, and the mixed convection in particular, to provide a clear idea and a solid base for the problem discussed in this study.

This section of the thesis was also meant to present and discuss the difficulty of heat transfer and fluid flow problems in cavities and the importance of the phenomena for industrial activities and equipments such as the solar collectors, the HVAC systems and the nuclear power. A literature review was also a part of this chapter, in which we presented the most relevant previous works carried out to the studied problem of the present work. This review indicated that the study of this phenomenon is difficult, however, very important and can be controlled by different parameters and geometries.

For the next sections of this work, the mathematical and numerical representation of the studied problem will be introduced to carry out a detailed analysis of the heat transfer and fluid flow in a vented cavity with an isothermally heated T-shaped heat fin.

CHAPTER II : MATHEMATICAL MODELING

II.1 Introduction

The fluid mechanics and heat transfer problems are governed by a set of complex partial differential equation (PDE) that are solvable for only some limited cases, most of the times, using empirical correlations obtained from experiments and dimensional analysis. Because in order to solve a convection problem, we must solve the equations of fluid motion along with the energy equation. Therefore, we have to use a discretization method to solve those equations numerically using a computer to obtain an approximated solution. As much as the precision and quality of experimental results depends on the quality of the used tools, the precision and quality of the numerical results depends on the quality of the used discretization method.

The purpose of this chapter is to introduce the basic conservation equations corresponding to mixed convection. For this intent, the general conservation equations of continuity, momentum and energy are expressed to deeply understand fluid convection.

II.2 Physical model

The geometry sketch of the investigated problem is represented in Figure II.1. The system is composed of a rectangular cavity with side's length of L and a height of H (meters or physical unites). The cavity is supplied with two ventilating opening, an inlet at the bottom left side and an outlet at the top right side. The cavity contains a heat generating T-shaped solid fin with foot length of H_f, and a thermal conductivity k_s. The walls are considered adiabatic except for the cold side of the top wall.

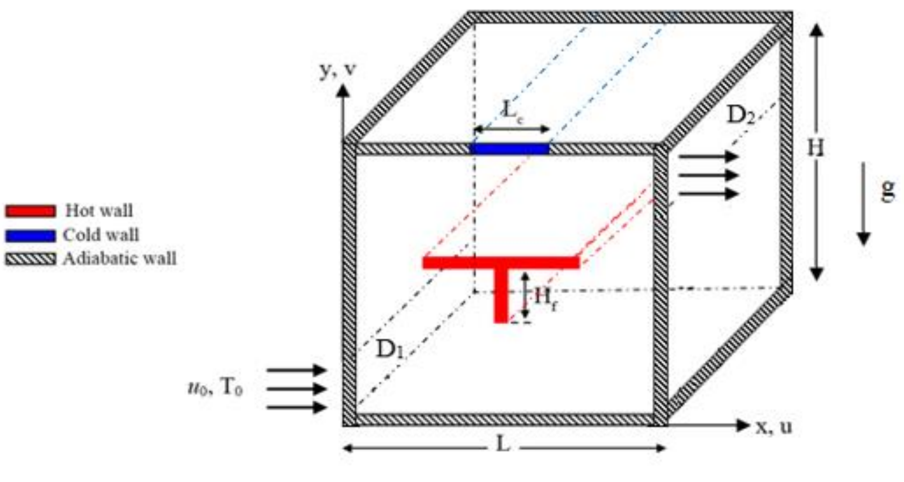

***Figure II.1** : 3D Schematic view of the physical model.*

II.3 The fundamental principles

The fundamental of computational fluid dynamics is the governing equations of continuity, momentum and energy, these equations speaks the physics, and they are the mathematical representation of three fundamental physical principles upon which fluid dynamics is founded [28].

II.3.1 Conserved mass

The first principle to review is undoubtedly the oldest: It is the conservation of mass in a closed system or the ‘‘continuity’’ of mass through a flow (open) system [1].

$$\frac{\partial m_{cv}}{\partial t} = \sum_{in} \dot{m} - \sum_{out} \dot{m}$$

Where m_{cv} is the mass that is trapped instantaneously inside the control volume, while the $\dot{m}$’s are the mass flow rates associated with flow into and out of the control volume [1].

From this principle, we can derive a general differential equation for conservation of mass, known as the continuity equation:

$$\frac{\partial \rho}{\partial t} + \vec{\nabla}.\left(\rho \vec{V}\right) = 0 \qquad \text{II.1}$$

Where ρ is the fluid density.

II.3.2 Newton’s second law

Newton’s second law is an expression for momentum balance and can be stated as the net force acting on the control volume is equal to the mass times the acceleration of the fluid element within the control volume, which is also equal to the net rate of momentum outflow from the control volume. We express Newton’s second law of motion for the control volume as [2]:

$$(\text{Mass})x \begin{pmatrix} Acceleration \\ in\ a\ specific\ direction \end{pmatrix} = \begin{pmatrix} net\ force\ (body\ and\ surface) \\ acting\ in\ that\ direction \end{pmatrix}.$$

II.3.3 Conserved energy

The heat transfer part of the convection problem requires a solution for the temperature distribution through the flow. The additional equation for accomplishing this ultimate objective is the first law of thermodynamics or the energy equation [1].

$$\begin{pmatrix} Rate\ of\ energy \\ accumilation \\ in\ the\ CV \end{pmatrix} = \begin{pmatrix} Net\ transfer \\ of\ energy\ by \\ fluid\ flow \end{pmatrix} + \begin{pmatrix} Net\ heat \\ transfer\ by \\ conduction \end{pmatrix} + \begin{pmatrix} Net\ of\ internal \\ heat\ generation \end{pmatrix} - \begin{pmatrix} Net\ work \\ transfer\ from\ the\ CV \end{pmatrix}.$$

II.4 The governing equations

From these fundamental principles, we can derive the differential equations of fluid motion, namely, conservation of mass (the continuity equation). Newton's second law (the Navier–Stokes equations). These equations apply to every point in the flow field and thus enable us to solve for all details of the flow everywhere in the flow domain. Unfortunately, most differential equations encountered in fluid mechanics are very difficult to solve and often require the aid of a computer [29].

For the fluid flow and heat transfer, these equations must be coupled with additional equations, such as an equation of state and an equation for energy [29].

II.4.1 Simplifying hypotheses

Due to fact that the governing equations of fluid flow and heat transfer can be very complicated, we adopt the following hypotheses to model of the problem of the current study:

- The heat transfers by radiation and mass are negligible.
- The fluid is Newtonian incompressible fluid.
- The fluid flow and heat transfer are three-dimensional.
- The flow is laminar.
- Viscous dissipation is neglected in the energy equation.
- At the interface, we have a thermal and dynamic balance.
- The thermo-physical properties of the fluid are assumed to be constant, except for the density on the buoyancy term which is temperature dependent and the Boussinesq approximation is used

Using the mentioned assumption and applying the fundamental laws of conservation of mass, Newton's second law (momentum balance) and energy conservation, we can express the governing equations of the fluid flow and heat transfer problems with as set of coupled, nonlinear, partial differential equations.

II.4.2 Continuity equation

$$\frac{\partial u}{\partial x}+\frac{\partial v}{\partial y}+\frac{\partial w}{\partial z}=0 \qquad \text{II.2}$$

Where u, v and w are the velocity components in x, y and z direction respectively.

Equation II.2 is the incompressible form of the continuity equation in Cartesian coordinates; it is applicable for both steady and unsteady flow. (Density is not a function of time or space) [29].

II.4.3 Momentum Equations (Navier-Stokes Equations)

$$\rho\frac{D\vec{V}}{Dt}= -\vec{\nabla}P+\mu\nabla^2\vec{V}+\rho\vec{g} \qquad \text{II.3}$$

Equation II.3 is known as the Navier-Stocks equations, it has four unknowns (three velocity components and pressure), yet it represents only three equations (three components since it is a vector equation). Obviously, we need another equation to make the problem solvable; the fourth equation is the incompressible continuity equation. Equation II.3 is an unsteady, nonlinear, second order, partial differential equation, it is valid in any orthogonal coordinate system [29].

The Navier–Stokes equations is expanded in Cartesian coordinates (x, y, z) and (u, v, w) respectively as follows [29]:

$$\rho\left(\frac{\partial u}{\partial t}+u\frac{\partial u}{\partial x}+v\frac{\partial u}{\partial y}+w\frac{\partial u}{\partial z}\right)=-\frac{\partial P}{\partial x}+\mu\left(\frac{\partial^2 u}{\partial x^2}+\frac{\partial^2 u}{\partial y^2}+\frac{\partial^2 u}{\partial z^2}\right)+\rho g_x \qquad \text{II.4}$$

$$\rho\left(\frac{\partial u}{\partial t}+u\frac{\partial u}{\partial x}+v\frac{\partial u}{\partial y}+w\frac{\partial u}{\partial z}\right)=-\frac{\partial P}{\partial y}+\mu\left(\frac{\partial^2 u}{\partial x^2}+\frac{\partial^2 u}{\partial y^2}+\frac{\partial^2 u}{\partial z^2}\right)+\rho g_y \qquad \text{II.5}$$

$$\rho\left(\frac{\partial u}{\partial t}+u\frac{\partial u}{\partial x}+v\frac{\partial u}{\partial y}+w\frac{\partial u}{\partial z}\right)=-\frac{\partial P}{\partial z}+\mu\left(\frac{\partial^2 u}{\partial x^2}+\frac{\partial^2 u}{\partial y^2}+\frac{\partial^2 u}{\partial z^2}\right)+\rho g_z \qquad \text{II.6}$$

Where P is the pressure, ρ is the fluid density, g is the gravitational constant and μ is fluid viscosity.

II.4.3.1 Boussinesq approximation

Fluid motion in free convection is driven by density change and gravity. Thus, the assumption of constant density can not be made in the analysis of free convection problems. Instead, an alternate simplification called the Boussinesq approximation is made. The basic approach in this approximation is to treat the density as constant in the continuity equation and the inertia term of the momentum equation, but allow it to change with temperature in the gravity term [30].

Assuming that ρ is constant in the inertia (first) term but not in the gravity term ρg. Thus, equation II.3 is rewritten as

$$\rho_\infty \frac{D\vec{V}}{Dt} = -\vec{\nabla}P + \mu\nabla^2\vec{V} + \rho\vec{g} \qquad \text{II.7}$$

Where ρ_∞ is fluid density at some reference state, such as far away from an object where the temperature is uniform and the fluid is either stationary or moving with uniform velocity. Thus at the reference state we have

$$\frac{D\overrightarrow{V_\infty}}{Dt} = \nabla^2\overrightarrow{V_\infty} = 0 \qquad \text{II.8}$$

Applying equation II.7 at the reference state ∞ and using equation II.8 gives

$$\rho_\infty\vec{g} - \nabla P_\infty = 0 \qquad \text{II.9}$$

Subtracting equation II.9 from equation II.7.

$$\rho_\infty \frac{D\vec{V}}{Dt} = -\vec{\nabla}(P - P_\infty) + \mu\nabla^2\vec{V} + (\rho - \rho_\infty)\vec{g} \qquad \text{II.10}$$

Now we eliminate the $(\rho - \rho_\infty)$ term in equation II.10 and express it in terms of temperature difference. This is accomplished through the introduction of the coefficient of thermal expansion β, defined as

$$\beta = \frac{1}{\rho}\left[\frac{\partial\rho}{\partial T}\right]_P \qquad \text{II.11}$$

Pressure variation in free convection is usually small and in addition, the effect of pressure on β is also small. In other words, in free convection β can be assumed independent of P. We further note that over a small change in temperature the change in density is approximately linear [30]. Thus, we can write.

$$\beta = \frac{1}{\rho}\frac{(\rho - \rho_\infty)}{(T - T_\infty)} \qquad \text{II.12}$$

This result gives:

$$(\rho - \rho_\infty) = -\beta\rho_\infty(T - T_\infty) \qquad \text{II.13}$$

Equation II.13 relates density change to temperature change [30]. The importance of this approximation lies in the elimination of density as a variable in the analysis of free convection problems. However, the momentum and energy equations remain coupled [30].

II.4.3.2 Momentum equation in y direction

The Boussinesq approximation leads to simplify the momentum equation in y direction, by substituting $(\rho - \rho_\infty)$ from the equation II.13 in equation II.5.

$$\rho\left(\frac{\partial u}{\partial t} + u\frac{\partial u}{\partial x} + v\frac{\partial u}{\partial y} + w\frac{\partial u}{\partial z}\right) = -\frac{\partial P}{\partial z} + \mu\left(\frac{\partial^2 u}{\partial x^2} + \frac{\partial^2 u}{\partial y^2} + \frac{\partial^2 u}{\partial z^2}\right) + g\beta(T - T_\infty) \qquad \text{II.14}$$

Where β is the volumetric coefficient of thermal expansion, T and T_∞ are the fluid temperature and the reference temperature respectively.

II.4.4 Energy equation

Then the energy equation for the three dimensional flow of a fluid with constant properties and negligible shear stresses is obtained by the following equation [2]:

$$\rho C_p\left(\frac{\partial T}{\partial t} + u\frac{\partial T}{\partial x} + v\frac{\partial T}{\partial y} + w\frac{\partial T}{\partial z}\right) = \mathrm{k}\left(\frac{\partial^2 T}{\partial x^2} + \frac{\partial^2 T}{\partial y^2} + \frac{\partial^2 T}{\partial z^2}\right) \qquad \text{II.15}$$

In addition to these equations, the heat conduction for the solid fin is valid and it is given in the following equation:

$$\frac{k_s}{\rho C_p}\left(\frac{\partial^2 T}{\partial x^2} + \frac{\partial^2 T}{\partial y^2} + \frac{\partial^2 T}{\partial z^2}\right) = 0 \qquad \text{II.16}$$

Where C_p is the fluid specific heat, k and k_s are the thermal conductivity of fluid and solid respectively, and $\frac{k_s}{\rho C_p}$ is the thermal diffusivity.

II.5 Dimensional analysis

Sometimes it is preferable to put the governing equations in dimensionless form to generalize the analysis of the physical problem considered. In order to do that we have to select a characteristic quantities that describes the flow, such as a characteristic length, velocity, pressure and temperature…etc. Using these characteristic quantities, we can obtain the following non-dimensional parameters

$$t^* = \frac{t}{L/u_\infty} \ , x^* = \frac{x}{L} \ , y^* = \frac{y}{L} \ , z^* = \frac{z}{L} \ , u^* = \frac{u}{u_\infty} \ , v^* = \frac{v}{u_\infty} \ , w^* = \frac{w}{u_\infty},$$

$$P^* = \frac{P - P_\infty}{\rho u_\infty^2} \ , T^* = \frac{T - T_\infty}{\Delta T}, K = \frac{k}{k_s}$$

Where T^* is dimensionless temperature, K is thermal conductivity ratio. These non-dimensional parameters can be used to obtain the dimensionless form of the governing equations and to identify the governing parameters.

II.5.1 Continuity equation

$$\frac{\partial u^*}{\partial x^*} + \frac{\partial v^*}{\partial y^*} + \frac{\partial w^*}{\partial z^*} = 0 \qquad \text{II.17}$$

II.5.2 Momentum equation in x-direction

$$\frac{\partial u^*}{\partial t^*} + u^* \frac{\partial u^*}{\partial x^*} + v^* \frac{\partial u^*}{\partial y^*} + w^* \frac{\partial u^*}{\partial z^*} = -\frac{\partial P^*}{\partial x^*} + \frac{1}{Re}\left(\frac{\partial^2 u^*}{\partial x^{*2}} + \frac{\partial^2 u^*}{\partial y^{*2}} + \frac{\partial^2 u^*}{\partial z^{*2}}\right) \qquad \text{II.18}$$

II.5.3 Momentum equation in y-direction

$$\frac{\partial v^*}{\partial t^*} + u^* \frac{\partial v^*}{\partial x^*} + v^* \frac{\partial v^*}{\partial y^*} + w^* \frac{\partial v^*}{\partial z^*} = -\frac{\partial P^*}{\partial y^*} + \frac{1}{Re}\left(\frac{\partial^2 v^*}{\partial x^{*2}} + \frac{\partial^2 v^*}{\partial y^{*2}} + \frac{\partial^2 v^*}{\partial z^{*2}}\right) Ri.T^* \qquad \text{II.19}$$

II.5.4 Momentum equation in z-direction

$$\frac{\partial w^*}{\partial t^*} + u^* \frac{\partial w^*}{\partial x^*} + v^* \frac{\partial w^*}{\partial y^*} + w^* \frac{\partial w^*}{\partial z^*} = -\frac{\partial P^*}{\partial z^*} + \frac{1}{Re}\left(\frac{\partial^2 w^*}{\partial x^{*2}} + \frac{\partial^2 w^*}{\partial y^{*2}} + \frac{\partial^2 w^*}{\partial z^{*2}}\right) \qquad \text{II.20}$$

II.5.5 The energy equation

$$\frac{\partial T^*}{\partial t^*} + u^* \frac{\partial T^*}{\partial x^*} + v^* \frac{\partial T^*}{\partial y^*} + w^* \frac{\partial T^*}{\partial z^*} = \frac{1}{Re\,.\,Pr}\left(\frac{\partial^2 T^*}{\partial x^{*2}} + \frac{\partial^2 T^*}{\partial y^{*2}} + \frac{\partial^2 T^*}{\partial z^{*2}}\right) \qquad \text{II.21}$$

II.5.6 The heat equation in the solid fin

$$\frac{\partial^2 T^*}{\partial x^{*2}} + \frac{\partial^2 T^*}{\partial y^{*2}} + \frac{\partial^2 T^*}{\partial z^{*2}} = 0 \qquad \text{II.22}$$

II.6 Dimensionless numbers

It is obvious that the dimensionless equations are very similar to their dimensional form and there are four governing parameters in them, which characterize the flow of the fluid and the heat transfer inside the cavity.

II.6.1 Grashof number

The Grashof number (G_r) is a dimensionless number in a fluid dynamics and heat transfer that approximates ratio of the buoyancy to viscous force acting on a fluid. It frequently arises in the study of situations involving natural convection. The transition to turbulent flow occurs in the range $10^8 < G_r < 10^9$ for natural convection from vertical flat plates. At higher Grashof number, the boundary layer is turbulent; at lower Grashof numbers, the boundary layer is laminar [31].

$$Gr = \frac{g\beta\,.\,\Delta T.\,L^3}{\nu^2} \qquad \text{II.23}$$

II.6.2 Prandtl number

The Prandtl number is a fluid property that represents the ratio of kinematic viscosity ν, also known as momentum diffusivity of the fluid, to the thermal diffusivity α of the fluid. With definitions of fluid kinematics viscosity ν and thermal diffusivity α, the new form of Prandtl number Pr can be defined as [32] :

$$Pr = \frac{\nu}{\alpha} = \frac{(\mu/\rho)}{\left(k/\rho c_p\right)} = \frac{\mu\,.\,C_p}{K} \qquad \text{II.24}$$

II.6.3 Nusselt number

Nusselt number Nu is a dimensionless temperature gradient of the fluid at a surface [32], and it is also described as a rate of two heat transfer coefficients or the ratio the contribution of convection, to the contribution of heat conduction. Therefore, the Nusselt number can be written generically as [33]:

$$Nu = \frac{hL}{k} \tag{II.25}$$

II.6.4 Reynolds number

Fluid flow is generally categorized into two flow regimes: laminar and turbulent. Laminar flow is characterized by smooth and constant fluid motion. Whereas turbulent flow is characterized by vortices and inertial flow fluctuations. Physically, the two regimes differ in terms of the relative importance of viscous and inertial forces. The relative importance of this two types of forces for a given flow condition, or to what extent the fluid is laminar, is measured by the Reynolds number (Re) [34]:

$$Re = \frac{\rho\, u_{\infty} L}{\mu} \tag{II.26}$$

II.6.5 Richardson number

It expresses the ratio of the buoyancy term to the flow shear term. If the Richardson number is much less than unity, buoyancy unimportant in the flow. If it is much greater than unity, buoyancy is dominant (in the sense that there is insufficient kinetic energy to homogenize the fluids). If the Richardson number is of order unity, then the flow is likely to be buoyancy driven: the energy of the flow derives from the potential energy in the system originally. In thermal convection problems, the Richardson number represents the importance of natural convection relative to the forced convection. Typically, the natural convection is negligible when Ri < 0.1, forced convection is negligible when Ri > 10, and neither is negligible when 0.1< Ri <10. It may be noted that usually the forced convection is large relative to natural convection except in case of extremely low forced flow velocities [31].

$$Ri = \frac{Gr}{Re^2} \tag{II.27}$$

II.7 Dimensionless boundary conditions

The developed mathematical model is used to examine mixed convection heat transfer in a vented cavity with a T-shaped heat fin placed at the center; the domain is subject to the following dimensionless boundary conditions.

- At the inlet

$$u^* = 1,\ v^* = w^* = 0 \qquad \text{II.28}$$

- At the outlet

$$\frac{\partial U}{\partial x} = 0, \frac{\partial U}{\partial y} = 0, \frac{\partial U}{\partial z} = 0, \frac{\partial T^*}{\partial x} = 0, \frac{\partial T^*}{\partial z} = 0 \qquad \text{II.29}$$

- At the hot fin

$$u^* = v^* = w^* = 0,\ T^* = 1 \qquad \text{II.30}$$

- At the cold wall

$$u^* = v^* = w^* = 0,\ T^* = 0 \qquad \text{II.31}$$

- At the horizontal and vertical walls

$$u^* = v^* = w^* = 0, \frac{\partial T^*}{\partial x} = \frac{\partial T^*}{\partial y} = \frac{\partial T^*}{\partial z} = 0 \qquad \text{II.32}$$

II.8 Evaluation of Nusselt number

As a result of temperature difference between a fluid and a solid wall, heat will flow into the wall or out from it, depending on which one is hotter than the other. The heat flux at the wall q_w depends on the velocity and temperature fields in the fluid; their evaluation is quite complex and can lead to considerable problems in calculation. However, we can write [35]:

$$q_w = h(T_w - T_\infty) \qquad \text{II.33}$$

Were h is known as the convective heat transfer coefficient At the very adjacent to wall fluid, the fluid velocity is zero, the energy is transferred through heat conduction, and Fourier's law, which states that heat flux is given by equation II.34, is valid [35]:

$$q_w = -k\left(\frac{\partial T}{\partial y}\right)_w \qquad \text{II.34}$$

Thus, we can say that the heat transfer coefficient can be expressed as follows:

$$h = -k \frac{\left(\frac{\partial T}{\partial y}\right)_w}{T_w - T_\infty} \qquad \text{II.35}$$

Using the non-dimensional parameters $y^* = \frac{y}{L}$ and $T^* = \frac{T - T_\infty}{\Delta T}$ we can write the convective heat transfer coefficient in a non-dimensional form, then equation II.35 gives:

$$h = \frac{-k}{L} \frac{\left(\frac{\partial T^*}{\partial y^*}\right)_w}{T^*_w - T^*_\infty} \qquad \text{II.36}$$

Alternatively, we can write:

$$\frac{hL}{k} = -\frac{\left(\frac{\partial T^*}{\partial y^*}\right)_w}{T^*_w - T^*_\infty} \qquad \text{II.37}$$

The right and left hand sides of the equation II.37 are different expressions for the dimensionless parameter known as Nusselt number [35]. This equation indicates that Nusselt number is the dimensionless temperature gradient normal to the wall, this is the local Nusselt number (Nu_{Loc}), the average Nusselt number can be calculated as the integral of the local Nu over a given surface, one could write:

$$Nu_{ave} = \frac{1}{S} \iint_s \frac{\partial T^*}{\partial x^* \partial y^*} dS \qquad \text{II.38}$$

II.9 Conclusion

This section of present work stands for the main conservation laws that governs the mixed convective heat transfer in the cavity and the fundamental basic principles behind them, and presents the physical and mathematical model of the present study.

Using the previously mentioned assumptions and through one of the derivation methods, the governing equations are presented, first in their dimensional form as a set partial differential equations. Then afterwards those equations are transformed into dimensionless form to present the non-dimensional governing parameters of the problem, which makes it possible to assume that Re and Ri numbers are among the principle influencing parameters. Finally the boundary condition corresponding to present problem are presented as the final principle component to make the study valid, this section was closed with the method of evaluation of average Nusselt number since it is an important parameter to represent the thermal performance.

Based on this chapter, the next chapter will introduce the numerical method to derive an approximate solution of the problem using the finite volume method.

CHAPTER III : NUMERICAL TECHNIQUE

III.1 Introduction

Physical phenomena are represented mathematically using partial differential equations, these equations include analytical or numerical solution, and as much as any other phenomena, fluid mechanics and heat transfer problems involves a lot of this kind of equations, but the solution for them is limited to only a number of flows.

In order to obtain an approximate numerical solution, we need to approximate the governing partial differential equations to a system of algebraic equations that we can solve using a computer. This simplifying process is applied to a small part of the domain in which we can obtain a numerical solution, and then we can provide the whole result through the integration of the values of the discretized location. The discretization process is a very important factor for the solution, it is also important for the numerical procedure so it should match our desired results.

III.2 Advantages of Numerical Analysis

Researchers and scientists have performed many experimental investigations on heat transfer and fluid flow problems. But, the experimental approach is not desirable for many cases due to the fact that it is very costly and time consuming process, to reduce and avoid those problems, the numerical approach is becoming more usually performed to solve such problems today, which on the other hand provides time reduction and accurate results. The most important advantages of this technique are mentioned below:

- Direct and exact solution (if exists).
- Time reduction much less costly.
- Very useful and powerful for cases with complex structures or geometries.
- It discretizes the model to small domains.
- Converts the geometrical problems from complex to simpler.

III.3 Solution of differential equations

In many cases sufficient precision of the solution is obtained with the use of well defined finite number of components (discontinuous problems), for the other problems, infinite number of sub-divisions or elements is possible (continuous problems). However, a finite number of elements is used to solve continuous problems; this is because the capacity of computational machines is limited (finite). Therefore, to make the problem domain subdivided to a number of points, elements or volumes, a number of computational methods are suggested. Based on the way of discretization there are different types of solving methods such as finite difference method **(**FDM**)**, finite element method **(**FEM**)** and finite volume method **(**FVM**)**.

Many other methods are available such as BEM and SEM.to solve a CFD problem. Moreover, there is many software packages such as ANSYS, COMSOL Multiphysics today. For the present work, we will be using ANSYS Fluent for the simulations, which is a code based on the FVM [36].

III.4 Finite volume method

The finite volume method **(**FVM**)** is a numerical technique used to find the approximate solution for CFD problems through the transformation (discretization) of the governing partial differential equations to a set of algebraic equation over a finite volume, element or cell the first step in the solution process is to discretize the geometrical domain to a finite volumes. Then the partial differential equations are also discretized to algebraic equations by integrating them over each discrete element. The system of algebraic equations is then solved to compute the values of the dependent variable for each of the elements [37].

In the finite volume method, some of the terms in the conservation equation are turned into face fluxes and evaluated at the finite volume faces. Because the flux entering a given volume is identical to that leaving the adjacent volume, the FVM is strictly conservative. This inherent conservation property of the FVM makes it the preferred method in CFD [37].

For the next section, we are going to be covering how we can discretize the governing equation and to write them in the form of system of algebraic equation in the following form:

$$M\ \Phi = \mathrm{B} \qquad \text{III.1}$$

Were M is coefficients matrix.

The control volume shown in Figure III.1 illustrates a centroid point P , E and W (East and West) the neighbors points in **x** direction while N and S (North and South) are the neighbors in **y** direction. The faces of the control volume are at *e* and *w* in x direction, *n* and *s* in y direction.

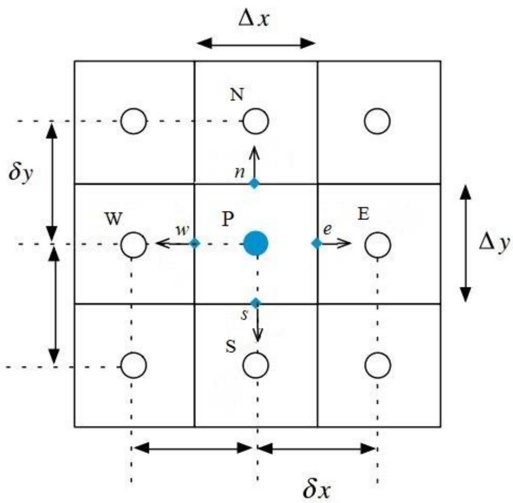

***Figure III.1** : Finite volume method notation [37].*

III.5 Discretization of the governing equations

III.5.1 Basic concept

Similar to other numerical methods, the finite volume method transforms the set of governing partial differential equations to a system of linear algebraic equations. However, the discretization process of the finite volume method is quite different and distinctive, it involves to major steps, firstly the partial differential equations are integrated over the control volume and this involves transforming the volume integrals to surface integrals using Gauss theorem (Divergence theorem), which results a set of semi-discretized equations. Then as a second step, we need to approximate the variables variation within the finite volume and relate the surface values to their cell values and which results a set of algebraic equations, this can be achieved by choosing interpolation profiles.

III.5.2 The transport equation

The conservation equations mentioned in CHAPTER II can be written in the form of a single equation over a given control volume (Figure III.2).

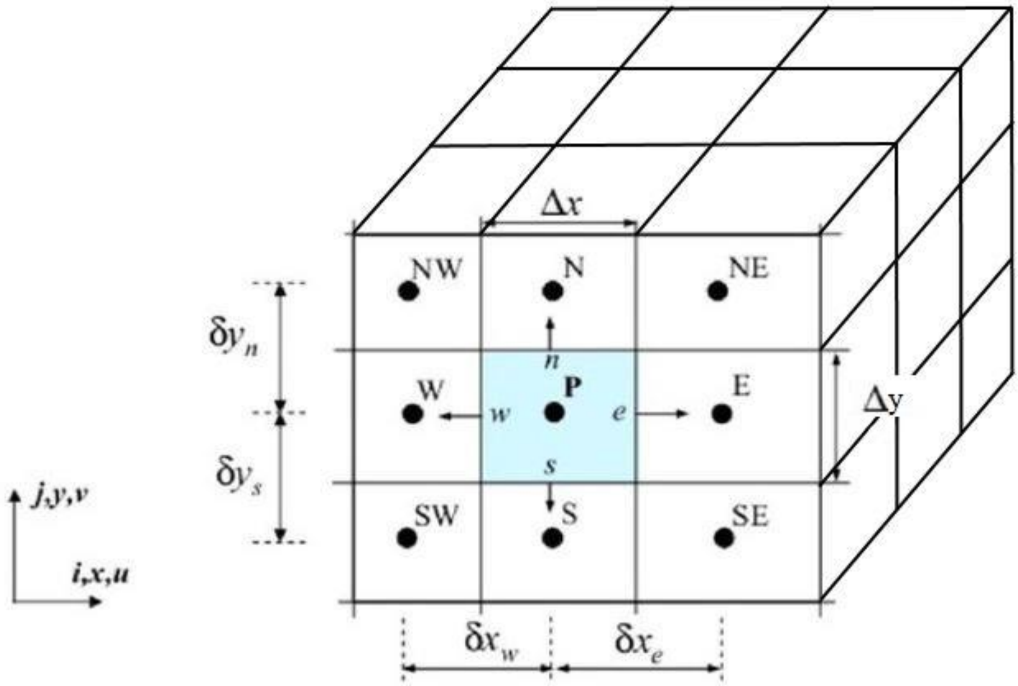

Figure III.2 *: Typical control volume in 3D.*

This equation provides us the ability to discretize the governing equations for one time only; this equation is called the transport equation [37].

$$\frac{\partial(\rho\Phi)}{\partial t} + \nabla.(\rho v\Phi) = \nabla.(\Gamma_\Phi \nabla\Phi) + S_\Phi \qquad \text{III.2}$$

Were Φ is the transported quantity such as velocity, mass or temperature … etc. Γ_Φ is the transported quantity's diffusion coefficient. This equation is a second order equation since the diffusion term involves a second order derivative of Φ in space [38]. Table III.1 summarizes the definition of diffusion coefficient Γ_Φ, the source term S_Φ, and the transported quantity Φ for the governing equations mentioned in CHAPTER II.

***Table III.1** : Cases for transport equation for fluid domain.*

Quantity	Φ	Γ_Φ	S_Φ
Equation II.17	1	0	0
Equation II.18	u^*	$\frac{1}{Re}$	$-\frac{\partial P^*}{\partial x^*}$
Equation II.19	v^*	$\frac{1}{Re}$	$-\frac{\partial P^*}{\partial y^*}+Ri.\theta$
Equation II.20	w^*	$\frac{1}{Re}$	$-\frac{\partial P^*}{\partial z^*}$
Equation II.21	0	$\frac{1}{Re.Pr}$	0

III.5.3 Discretization of the transport equation

We can right the equation III.1 in the integral form over a given control volume V as the one shown in Figure III.2 as follows [38]:

$$\int_V \frac{\partial \rho \Phi}{\partial t}\, dV + \int_V \nabla.(\rho u \Phi) dV = \int_V \nabla.(\Gamma_\Phi \nabla \Phi) dV + \int_V S_\Phi(\Phi) dV \qquad \text{III.3}$$

III.5.3.1 Gauss theorem

A very important theorem in the FVM. It states that the volume integral of a divergence of a vector field equals to the surface integral of the outward flux normal to face of the control volume, this theorem can be written as follows [39] :

$$\int_V \nabla.a\, dV = \int_S \vec{n}\, dS\,.\,a \qquad \text{III.4}$$

Were S is the surface the control volume's face and dS is the infinitesimal surface element with the normal n outward of **S**. Using this theorem, we can derive the following equation out of equation III.2.

$$\frac{\partial}{\partial t}\int_V (\rho\Phi)\, dV + \int_S (\rho\vec{u}\Phi)\, \vec{n}.dS = \int_S (\Gamma_\Phi \nabla\Phi)\, \vec{n}.dS + \int_V S_\Phi(\Phi) dV \qquad \text{III.5}$$

The equation above is a statement of conservation that the change of the quantity Φ in the control volume equals the diffusive and convective fluxes across the faces of control volume plus the rate of creation of that quantity in the control volume.

III.5.3.2 Approximation of surface and volume integrals

To calculate the surface integrals in equation III.4 we need to find out the value of Φ on the faces of the control volume, but since the variables are calculated at the center of the control volume, the value of Φ is unknown at the faces of the control volume so we need to take an approximation. We assume that Φ varies linearly over all faces f of the control volume, so that we can represent it by its mean value at the face center, now we can use the midpoint rule to approximate the surface integral as a product of transported quantities at the face centroid f and the area of the face [40].

Using those assumptions and approximations, the fluxes in equation III.4 can be expressed as follows [40] :

$$\oint_S (\rho u \Phi)\, n.dS = \sum_f \int_S (\rho u \Phi.\vec{n})_f \,\mathrm{dS} \approx \sum_f S_f \,.\, (\overline{\rho u \Phi})_f = \sum_f S_f \,.\, (\rho u \Phi)_f \qquad \text{III.6}$$

$$\oint_S (\Gamma_\Phi \nabla \Phi)\, n.dS = \sum_f \int_S (\Gamma_\Phi \nabla \Phi.\vec{n})_f \,\mathrm{dS} \approx \sum_f S_f \,.\, (\overline{\Gamma_\Phi \nabla \Phi})_f = \sum_f S_f \,.\, (\Gamma_\Phi \nabla \Phi)_f \qquad \text{III.7}$$

For the approximation of the volume integrals in equation III.4 we make a similar assumption, that is Φ varies linearly over the control volume, which we are integrating over, thus we write [38] :

$$\int_S \Phi(\mathrm{x})\mathrm{dV} = \int_V \left[\Phi_\mathrm{p} + \left(\mathrm{x} - \mathrm{x_p}\right).(\nabla\Phi)_\mathrm{p}\right]\mathrm{dV}$$

$$= \Phi_p \int_V dV + \left[\int_V \left(x - x_p\right).(\nabla\Phi)_p dV\right].(\nabla\Phi)_p$$

$$= \Phi_p V \qquad \text{III.8}$$

If Φ varies linearly or constant this approximation becomes exact, otherwise it is considered as a second order approximation. Introducing equations III.5 into equation III.4, we get:

$$\frac{\partial}{\partial t}\rho\Phi V + \sum_f S_f\,.\,(\rho u\Phi)_f = \sum_f S_f\,.\,(\Gamma_\Phi \nabla\Phi)_f + S_\Phi V_p \qquad \text{III.9}$$

Since all variables are computed and stored at the control volumes centroid, the face values in equation III.8, the convective flux [S. $(\rho u\Phi)$] and diffusive flux [S. $(\Gamma_\Phi \nabla\Phi)_f$] in or out of the faces need to be determined using some form of interpolation from the centroid and the neighboring control volumes

III.5.3.3 Convective term spatial discretization

We can write the convective term obtained in equation III.8 in another form as follows [38].

$$\sum_f S_f\,.\,(\rho u.\vec{n}\Phi)_f = \sum_f S_f\,.\,(\rho u.\vec{n})_f\Phi_f = \sum_f \dot{F}\,.\,\Phi_f \qquad \text{III.10}$$

Were $\dot{\boldsymbol{F}}$, is the mass flux through the face.

$$\dot{F} = S_f.(\rho u.\vec{n})_f \qquad \text{III.11}$$

This flux is obviously depends on the face value of u and ρ which can be calculated similarly to Φ_f, with keeping in mind that the velocity field from which the fluxes are derived must satisfy continuity equation

$$\int_V \nabla.u dV = \oint_S u.\vec{n}dS = \sum_f\left(\int_f u.\vec{n}dS\right) = \sum_f S_f.(\rho u)_f = \sum_f \dot{F} = 0 \qquad \text{III.12}$$

The interpolation schemes of the convection are used to compute the value of the transported quantity Φ on the faces f, therefore, using the neighbors control volumes to compute the value of the transported quantity, and here we present tow of most used schemes, which we are going to use combined.

i. Central Differencing (CD) scheme

Known also as the linear interpolation, this scheme indicates that the variation of the dependent variables is linear. The face value is computed from a weighted linear interpolation between the control volume V_P and its neighbor V_N [40].

The simple case is when the face is at midway of the two neighboring control volumes (uniform mesh), this approximation is then reduced to the following average:

$$\Phi_f = \frac{(\Phi_P + \Phi_N)}{2} \qquad \text{III.13}$$

For the other cases, we use the following interpolation formula [40]:

$$\Phi_P = f_x \Phi_P + (1 - f_x)\Phi_N \qquad \text{III.14}$$

Were f_x is the ration of the distances fN and PN, given by the following formula and shown in Figure III.3

$$f_x = \frac{fN}{PN} = \frac{|x_f - x_N|}{|d|}$$

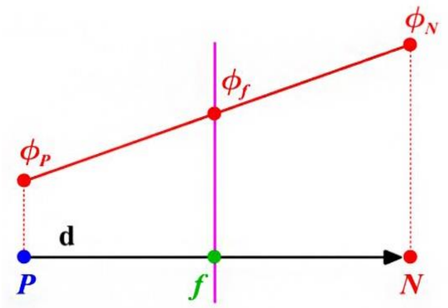

Figure III.3 *: Face interpolation, CD scheme.*

ii. Upwind Differencing scheme

An alternative scheme called the Upwind differencing scheme (UD), in which the face value is determined according to the flow's direction as shown in Figure III.4 [40].

$$\Phi_f = \begin{cases} \Phi_f = \Phi_P & for \qquad \dot{F} \geq 0 \\ \Phi_f = \Phi_N & for \qquad \dot{F} < 0 \end{cases}$$

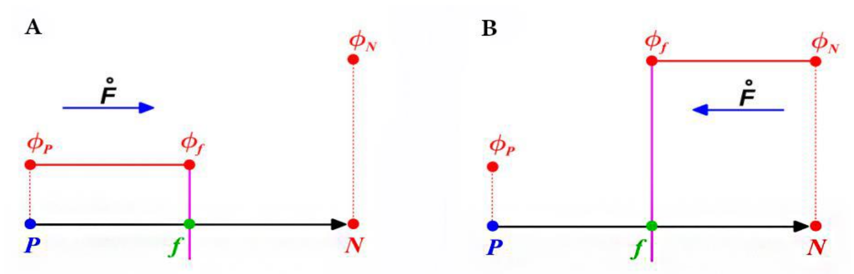

Figure III.4 *: Face interpolation, UD scheme, A)* $\dot{F} \geq 0$. *B)* $\dot{F} < 0$.

This scheme has the advantage of the boundedness, but, it is a first order accurate while the central differencing scheme (CD) scheme is a second order, however, it causes non-physical oscillation in the solution for convection problems. Therefore, in order to overcome those issues, linear combination of Upwind scheme (UD) and central differencing scheme (CD) to fit to the accuracy of the discretization and preserve the boundedness and stability of the solution [40].

For the present study, we are going to use a second order upwind scheme for the momentum and energy equation.

III.5.3.4 Diffusion term spatial discretization

The discretization of the diffusion term is obtained using a similar approach as before in the equation III.6

$$\int_V \nabla.(\rho\Gamma_\Phi \nabla\Phi)dV = \sum_f S_f.(\rho\Gamma_\Phi \nabla\Phi)_f = \sum_f (\rho\Gamma_\Phi)_f\, S_f.(\nabla\Phi)_f \qquad \text{III.15}$$

In equation III.13 [40], Γ_Φ is the diffusion coefficient, for the case of a uniform Γ_Φ its value is the same for all control volumes. However, for situations where Γ_Φ is non-uniform, it can be computed using linear interpolation between the control volume V_P and V_N as shown in Figure III.5

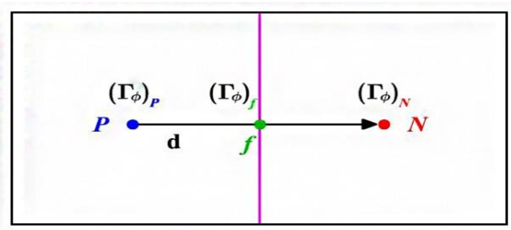

Figure III.5 : Diffusion coefficient Γ_Φ variation in neighboring control volumes.

The interpolation for Γ_{Φ} is shown in the following formula [40] :

$$(\Gamma_{\Phi})_f = f_x(\Gamma_{\Phi})_P + (1 - f_x)(\Gamma_{\Phi})_P \qquad \text{With} \qquad f_x = \frac{fN}{PN} = \frac{|x_f - x_N|}{|d|} \qquad \text{III.16}$$

For the case where the face f is midway between the control volumes V_P and V_N (uniform control volumes), f_x is equal to 0.5 and $(\Gamma_{\Phi})_f$ is equal to the arithmetic mean. However in this method and if $(\Gamma_{\Phi})_N$ is equal to 0, there would be no diffusion out of the face f but in fact equation III.15 do approximate a value for $(\Gamma_{\Phi})_f$.

For a better approximation for the variation, and as a solution to this issue, we use the harmonic mean, which is expressed in the following equation:

$$(\Gamma_{\Phi})_f = \frac{(\Gamma_{\Phi})_N(\Gamma_{\Phi})_P}{f_x(\Gamma_{\Phi})_P + (1 - f_x)(\Gamma_{\Phi})_P} \qquad \text{With} \qquad f_x = \frac{fN}{PN} = \frac{|x_f - x_N|}{|d|} \qquad \text{III.17}$$

- **The gradient term**

From the process of discretization of the diffusive terms, a face gradient come out namely $(\nabla\Phi)_f$ (equation III.15), this gradient can be computed using a central difference approximation or the Green-Gauss cell based gradient evaluation, but for the present study we are going to use the Least-Square fit. Which is a method that assumes a linear variation of Φ and evaluate the gradient error at each neighboring control volume using the following expression:

$$\epsilon_N = \Phi_N - (\Phi_P + d.(\nabla\Phi)_p) \qquad \text{III.18}$$

Were the objective is to minimize the least-square error at the centroid of control volume V_P given by

$$\epsilon_P^2 = \sum_N w_N^2 \epsilon_P^2 \qquad \text{III.19}$$

Were the function w is given by $w_N = 1/|d|$, then we use the following expression to evaluate the gradient at the centroid of control volume V_P.

$$(\nabla\Phi)_P = \sum_N w^T.w.G^{-1}.d^T(\Phi_N - \Phi_P)$$

$$G = \sum_N w^T.w.d^T d$$

Were G can be easily inversed since it is a symmetric matrix N x N were N is the number of spatial dimension. After evaluation, the neighbor control volume gradient, they can be interpolated to the face.

III.5.3.5 Source term spatial discretization

All The terms of the transport equation other than convection diffusion or temporal are generally classified as source terms, in general and as a function of Φ, needs to be linearized first, such that [38]:

$$S_{\Phi}(\Phi) = S_c + S_P \Phi \qquad \text{III.20}$$

Were S_c is the constant part of the source term, S_P depends on Φ

Following equation III.8 the volume integral of the source term is computed as [38]:

$$\int_V S_{\Phi}(\Phi)\, dV = S_c V + S_P V \Phi_p \qquad \text{III.21}$$

III.5.3.6 Temporal discretization

Considering the time derivative of equation, and integrating in time we get

$$\int_t^{t+\Delta t} \left[\int_V \frac{\partial \rho \Phi}{\partial t}\, dV + \int_V \nabla . (\rho u \Phi) dV \right] dt = \int_t^{t+\Delta t} \left[\int_V \nabla . (\Gamma_{\Phi} \nabla \Phi) dV + S_{\Phi}(\Phi)\, dV \right] dt \qquad \text{III.22}$$

Using equations III.6. and equation III.21 we can write equation III.22 as

$$\int_t^{t+\Delta t} \left[\left(\frac{\partial \rho \Phi}{\partial t} \right)_P V + \sum_f S_f . (\rho u \Phi)_f \right] dt = \int_t^{t+\Delta t} \left[\sum_f S_f . (\Gamma_{\Phi} \nabla \Phi)_f + S_c V + S_P V \Phi_p \right] dt \qquad \text{III.23}$$

This expression is called the semi-discretized form of the transport equation; keeping in mind the assumed variation of Φ with t, the temporal derivative and time integral can be calculated as follows [38]:

$$\left(\frac{\partial \rho \Phi}{\partial t} \right)_P = \frac{\rho_P^n \Phi_P^n - \rho_P^0 \Phi_P^0}{\Delta t} \qquad \text{III.24}$$

$$\left(\frac{\partial \rho \Phi}{\partial t} \right)_P = \frac{\rho_P^n \Phi_P^n - \rho_P^0 \Phi_P^0}{\Delta t} \qquad \text{III.25}$$

Were $$\Phi^n = \Phi(t+\Delta t) \qquad \text{III.26}$$

$$\Phi^0 = \Phi(t) \qquad \text{III.27}$$

Assuming that the density and diffusivity keeps constant with time, equations III.23, III.24 and III.25 gives [38] :

$$\frac{\rho_P^n \Phi_P^n - \rho_P^0 \Phi_P^0}{\Delta t} V + \frac{1}{2}\sum_f F\Phi_f^{\mathrm{n}} - \frac{1}{2}\sum_f (\rho\Gamma_\Phi)_f \,\mathrm{S}.(\nabla\Phi)_f^n + \frac{1}{2}\sum_f F\Phi_f^0$$
$$-\frac{1}{2}\sum_f (\rho\Gamma_\Phi)_f \,\mathrm{S}.(\nabla\Phi)_f^0 = S_u V + \frac{1}{2}\, S_P V \Phi_f^{\mathrm{n}} + \frac{1}{2}\, S_P V \Phi_f^{\mathrm{n}-1} \qquad \text{III.28}$$

This form of discretization is called the Crank-Nicholson method, which is a second order accurate [38].

Using the appropriate scheme for convection term and the diffusion term, we can now apply a general form of the equation to each control volume in the domain to create our linear algebraic system, which will be solved later on using a CFD code (ANSYS Fluent) using an appropriate algorithm, this equation is of the following form:

$$a_P \Phi_P^n + \sum_f a_N \Phi_N^n = B \qquad \text{III.29}$$

This will create a system of algebraic equations of the form:

$$M\,\Phi = B \qquad \text{III.30}$$

Were M is a square matrix, with the coefficient a_P on the diagonal and a_N off the diagonal, Φ is the transported quantity vector for all control volumes and B is the source term vector.

This discretization method is applicable for any shape of control volumes and any type of mesh and for three dimension transient problems, for the steady state cases, we just drop the transient term in equation III.2 and following the same process of discretization, we get our linear algebraic system of equations.

Now, we have our system of linear equation we need to solve it in order to get our solution, however, this process is not that easy, and there is a lot of algorithms to solve the Navier-Stocks equations numerically such as the SIMPLE algorithm (Semi-Implicit Method for Pressure-Linked Equations). Created by Patankar, in the early 1970s [38], which is going to be used for in present work.

III.5.4 SIMPLE algorithm

Since we have only the Navier-Stocks and the continuity equations in x, y and z directions and four unknowns, namely the three components of velocity filed u, v, w and the pressure filed P. Nevertheless, we cannot solve this system of equation because we do not have an equation for the pressure. And here comes the key tricks of the SIMPLE algorithm, which are to derive an equation for pressure from the momentum and continuity equations, and derive a corrector for the velocity filed, so that is satisfy the continuity equation [40]. The processes and steps of this algorithm are summarized in the following steps:

- The first stage is to express the momentum equations in the general matrix form:

$$M\,\Phi = -\nabla P \qquad \text{III.31}$$

Were the matrix M is the coefficient matrix that are calculated by discretizing the terms in the equation. These coefficients are all known.

- The second step is to separate the matrix M into a diagonal and off-diagonal components:

$$A\,\Phi - H = -\nabla P \qquad \text{III.32}$$

Were A is diagonal of M and the matrix H is evaluated from the off-diagonal terms and the velocity from the previous iteration, hence it is known.

$$H = A\,\Phi - M\,\Phi \qquad \text{III.33}$$

Now that we have the decomposed form of the momentum equations (equation III.32) and the continuity equation, $\nabla\,\Phi = 0$, we can derive an equation for the pressure.

- The next step is to rearrange the momentum equation and substitute into the continuity equation.

$$\Phi = -A^{-1}H - A^{-1}\,\nabla P \qquad \text{III.34}$$

$$\nabla[-A^{-1}H - A^{-1}\,\nabla P] = 0 \qquad \text{III.35}$$

We get a Poisson equation for pressure.

$$\nabla.[-A^{-1}\nabla P] = \nabla.[A^{-1}H] \qquad \text{III.36}$$

Now we have all our equations (velocity components and pressure equation), but we still have to solve them in the following manner:

- Solve the momentum equation (equation III.31) for the velocity field. However, the velocity field does not satisfy the continuity equation

- Solve the Poisson equation (equation III.36) for the pressure filed and use it to correct the velocity filed so that it satisfies the continuity equation. (equation III.34)

- The velocity filed now does not satisfy the momentum equations.

- Repeat the cycle

Since we use it to correct the pressure, it is called a pressure corrector algorithm, it is iterative because it is in the form of a loop, and we can add the energy equation to the loop to get the following diagram.

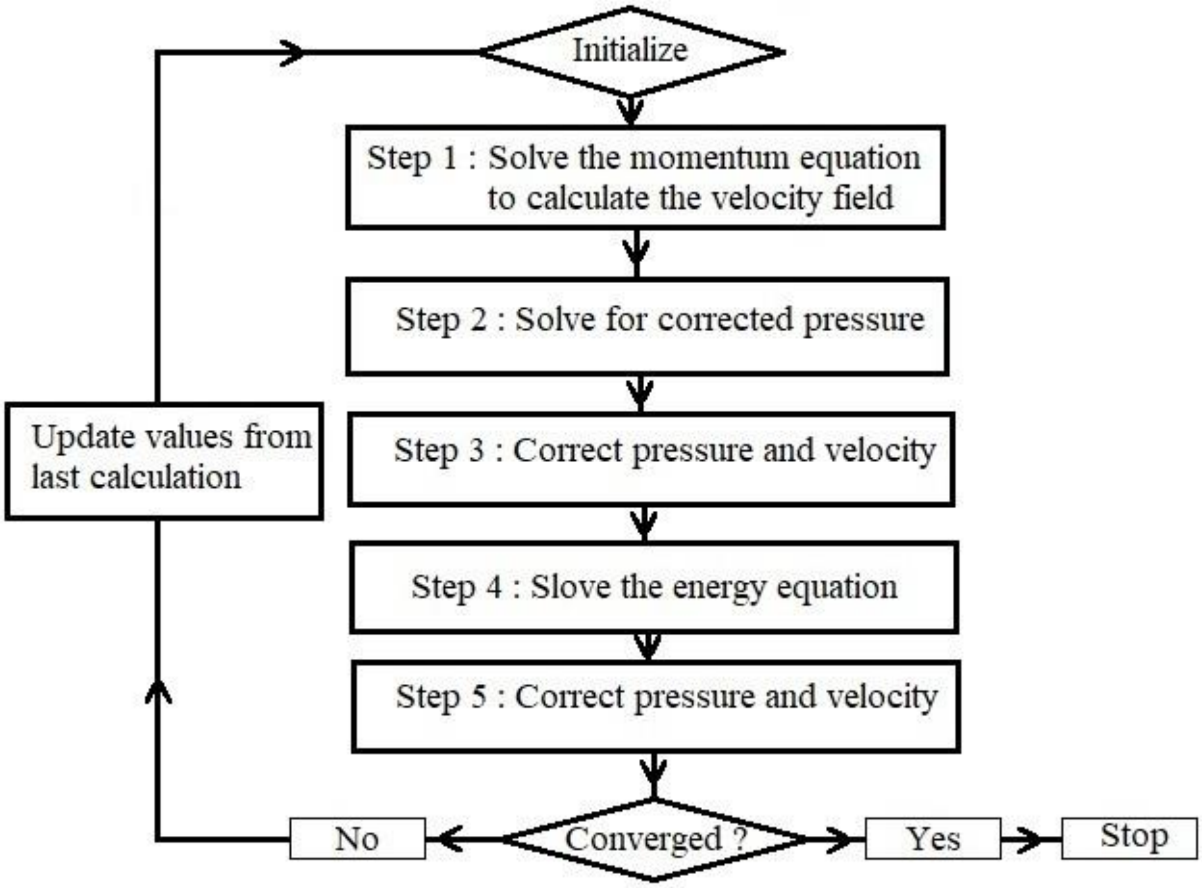

Figure III.6 *: The SIMPLE algorithm diagram [37].*

III.6 Numerical procedure

ANSYS Fluent is a state-of-the-art computer program for modeling fluid flow, heat transfer, and chemical reactions in complex geometries. ANSYS Fluent is written in the C computer language and makes full use of the flexibility and power offered by the language. Consequently, true dynamic memory allocation, efficient data structures, and flexible solver control are all possible [41].

ANSYS Fluent provides complete mesh flexibility, including the ability to solve flow problems using unstructured meshes that can be generated about complex geometries with relative ease. Supported mesh types include 2D triangular, quadrilateral, 3D tetrahedral, hexahedral, pyramid, wedge, polyhedral, and mixed (hybrid) meshes. ANSYS Fluent also enables to refine or coarsen mesh based on the flow solution [41].

As all CFD problems, our fluid flow and heat transfer solution process goes through three major steps, preprocessing, processing and the post processing, in the following section we are going to discuss the first two steps and leave the post-processing to CHAPTER IV.

III.6.1 Preprocessing

Before executing the analysis, and after we have defined the objectives that need to be achieved through the CFD analysis of our problem, figure out the necessities, and the requirements such as the objectives, modeling options, required physical models, boundary conditions, domain space ... etc. and by identifying the assumptions and model simplification that will be required during the analysis. We are set to start the analysis, starting with the following first main steps.

III.6.1.1 Geometry model

Since we have enough information available, the next step is to develop the geometrical model based on the assumptions and simplifications decided. For that, the built-in geometry builder ANSYS Design Modeler will be used, the application is intended for the purpose to be used as a geometry editor of computer-aided design models. The geometry model of present study consists of a solid T-shaped heat fin of 0.01 m in thickness, 1 m length in z direction, 0.5 m in x, and 0.3 of its width in y, surrounded by 1 m cube of air domain (L x H x W), sliced into two sub-domains; a 0.7x0.35 m at the fin surrounding, and the rest is a far of the fin surrounding. The fluid domain contains an inlet at the left bottom side and an outlet at the top opposite side of a dimension $D_1 = D_2$. The top wall contains a cold part of H/4. The resulted geometry is shown in Figure III.7.

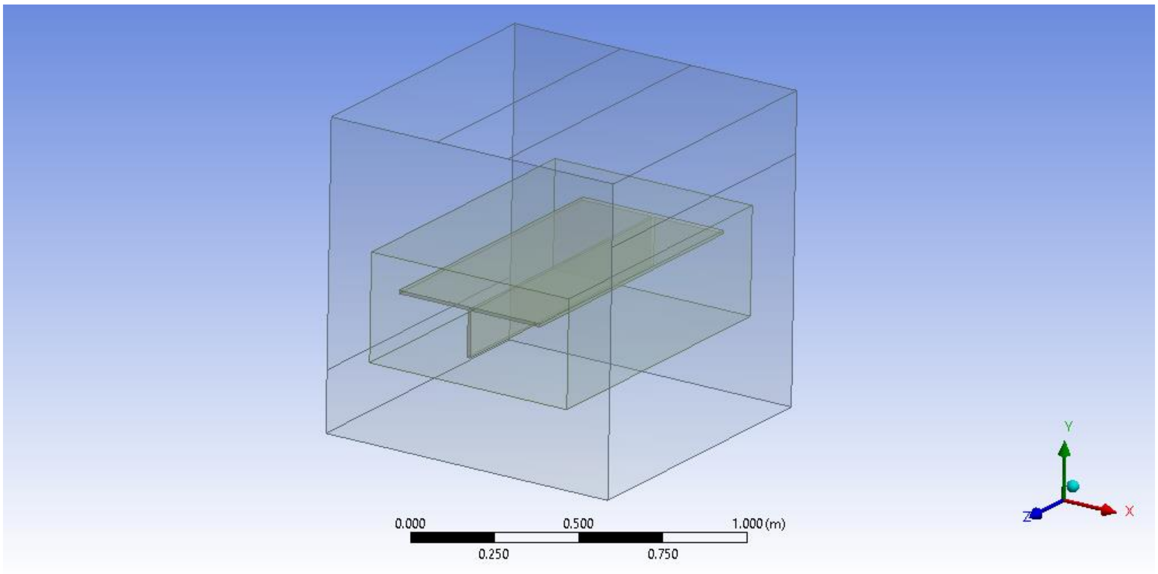

***Figure III.7**: The computational domain geometry.*

III.6.1.2 Meshing

It is well known that the entire simulation relies on how well the computational domain is transformed into small elements (control volumes). This process known as Meshing, is one of the most important aspects for any CFD simulation, and should be precise enough to consider the complexity in geometry, flow and achieve accurate results. Depending on that fact and knowing that regions with high gradients should be identified and the mesh must be refined accordingly. the meshing of present investigated problem domain was done with extra caution, a very fine mesh with over a million element was used to assure the precision of the solution, it was done using a body sizing of 10 mm and a Multi-zone method for the solid fin mesh, a bit bigger body sizing of 15 mm body size with Multi-zone method as well for the far-surrounding fluid, while a smaller and finer than the latter body sizing, with a 13 mm was assigned for the fin surrounding fluid. To assure more accuracy, an inflation at the fin boundaries of 5 layers was added for a better capture of the phenomena, the mesh and the meshing process detail, characteristics, with the assigned various geometrical faces and volume entities are shown in Figure III.8 and Figure III.9 respectively.

As for the heat transfer between the fluid and the solid, a contact region was established, to assure the connection and interaction solid-fluid, and since we have divided the fluid domain into two sub-regions, and to get fine mesh. The meshing process was arranged in such a way so that the fin surrounding fluid fits to the other regions, this was established by meshing it last. As result, worksheet for the mesh was needed to keep the order of created mesh.

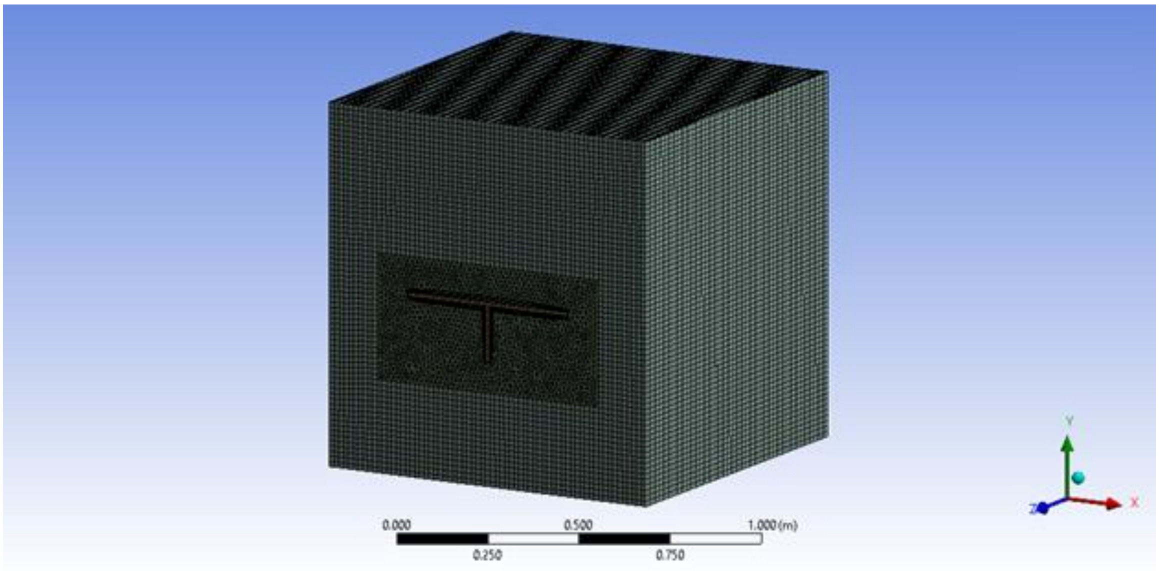

Figure III.8 *: The discretized domain.*

(a) (b)

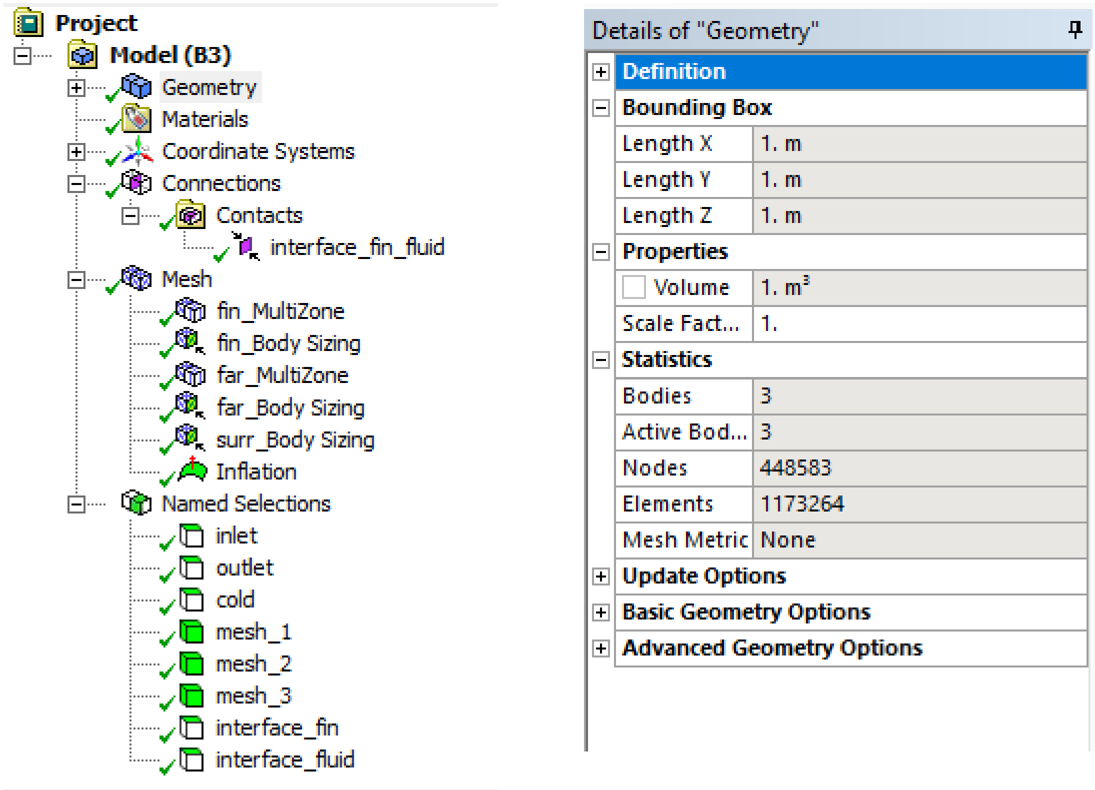

***Figure III.9** : Various geometrical faces and volume entities (a), and Mesh details (b).*

III.6.2 Processing

III.6.2.1 Selecting the solver type

The following step after meshing is to decide to the type of the needed solver. for our case and since we have an incompressible fluid flow and heat transfer problem, we used the pressure based solver with the steady solver for the time independent cases, and unsteady for time dependent cases.

The basic principle of this type of solver is to use a projection method, in the projection method, wherein the constraint of mass conservation (continuity) of the velocity field is achieved by solving a pressure (or pressure correction) equation. The pressure equation is derived from the continuity and the momentum equations in such a way that the velocity field, corrected by the pressure, satisfies the continuity. Since the governing equations are nonlinear and coupled to one another, the solution process involves iterations wherein the entire set of governing equations is solved repeatedly until the solution converges [42].

There is two types of the pressure-based solvers the coupled, and segregated algorithm, which is used by the SIMPLE algorithm in our case, is illustrated in figure. Figure III.10.

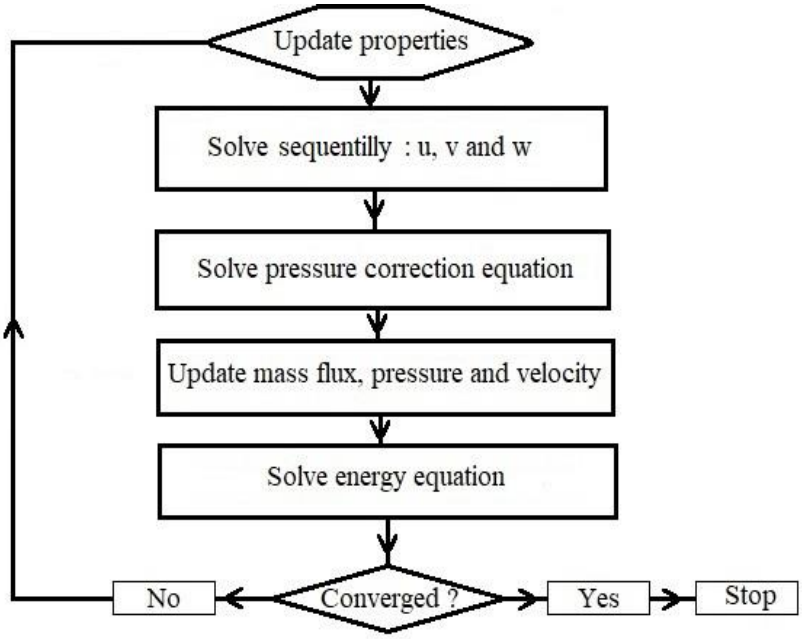

***Figure III.10** : The Pressure-Based Segregated Algorithm [42].*

III.6.2.2 Physical model

The next step is to select the physical model; ANSYS Fluent is a very powerful CFD code that provides comprehensive modeling ability for a wide range of flows, laminar, turbulent, compressible and incompressible ... etc. Steady-state or transient analyses can be performed, and for that it provides us with a wide range of mathematical models for transport phenomena such as heat transfer, for our case and according to the objectives and assumptions we have chosen the laminar model for the fluid flow, and we have activated the energy equation for the heat transfer phenomena as shown in Figure III.11.

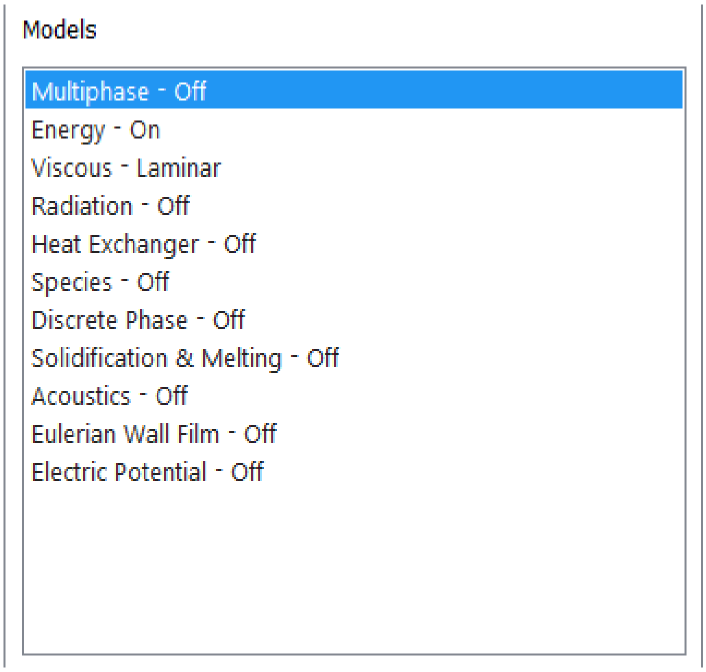

***Figure III.11** : Selecting the appropriate Models.*

III.6.2.3 Material properties, operating and boundary conditions

Following the selection of solver and physical model, is the step of defining the material properties, operating and boundary conditions. Regarding the material properties, a Boussinesq approximation for buoyancy flow was established, and the material properties of the working fluid air was taken to so that the air is at 20 °C. The following table and Figure III.12 summarizes the different properties of the working fluid.

Table III.2 *: Thermophysical properties of air at 20 °C [43].*

Thermophysical property	Magnitude
Density : ρ	1.204 kg/m3
Specific Heat : Cp	1007 J/kg/K
Thermal conductivity : k	0.025 W/m.K
Thermal diffusivity : α	2.074. 10^{-05} m2/s
Dynamic viscosity : μ	1.82. 10^{-05} kg/m2.s

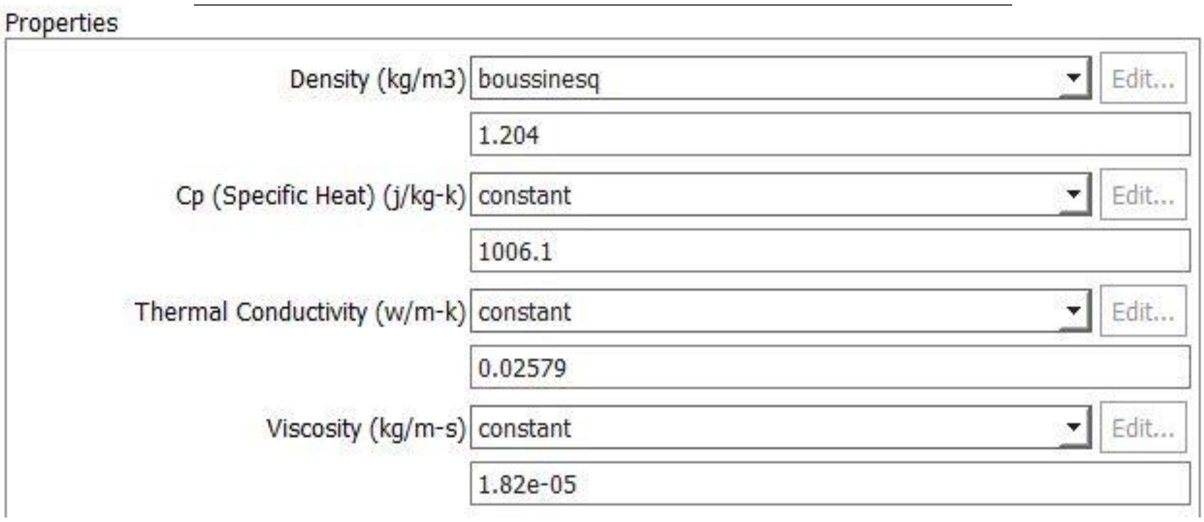

Figure III.12 *: Air properties implemented to Fluent.*

ANSYS fluent is has a wide range of boundary condition types, for our computational domain which was a cavity with an inlet and outlet we had 3 types of boundary condition according to the assumption and the boundary conditions discussed in CHAPTER II, a velocity inlet, a pressure outlet and walls (Figure III.13). Those boundary conditions were implemented to ANSYS fluent in proportion to each of the simulation cases.

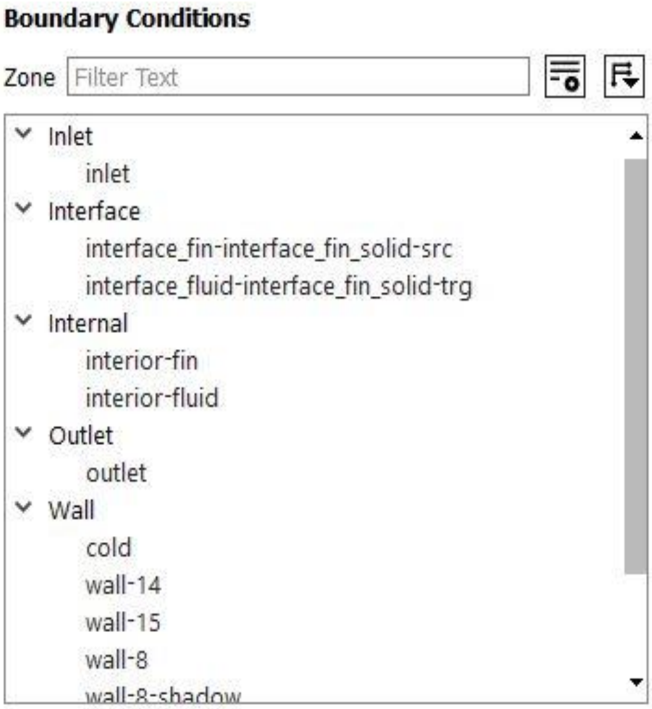

Figure III.13 *: Boundary conditions.*

For the operating condition, it was set to perform the assumption of the Boussinesq approximation under the ambient pressure, temperature and density of 1 atm, 293 K and 1.204 kg/m^3 respectively, also in presence of the gravitational filed in y direction of 9.81 m/s^2. Figure III.14 shows the operating conditions implemented to ANSYS Fluent.

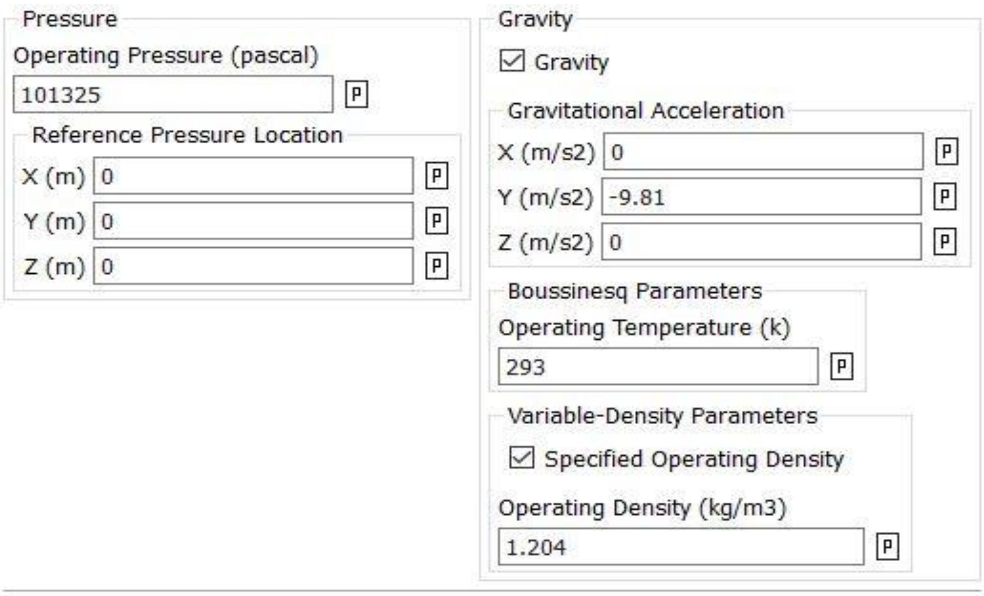

Figure III.14 *: Operating conditions in ANSYS Fluent.*

III.6.2.4 The solution methods

The most important task in solving a CFD problem is setting up the solution methods to specify the schemes of solving algorithms and the accuracy of the code. For our simulations we used the SIMPLE algorithm for the pressure-velocity coupling, Least Squares Cell based for the gradient term evaluation of the diffusion terms and a second order upwind for the momentum and energy equation,. All these algorithms and schemes were presented previously in this Chapter, and shown in Figure III.15.

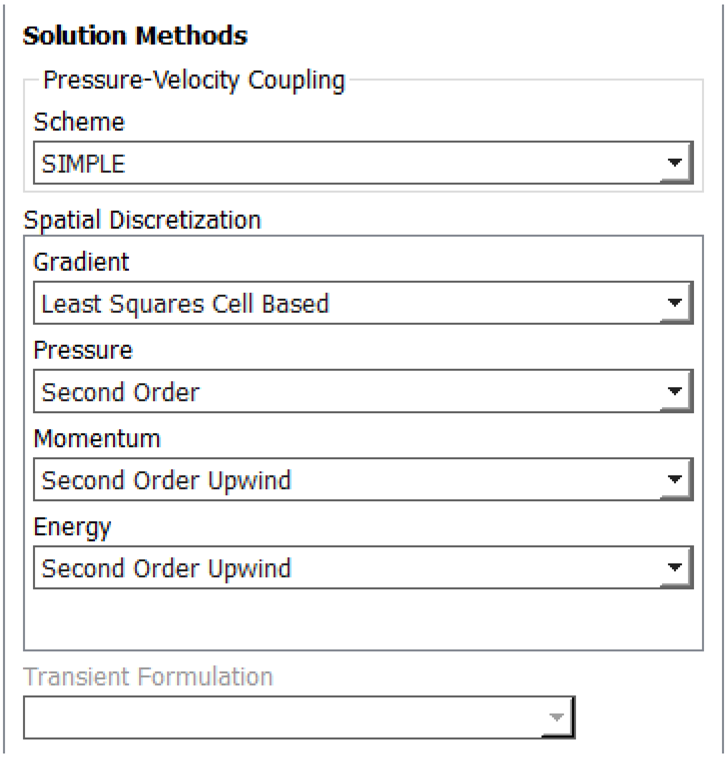

Figure III.15 *: Solution methods in ANSYS Fluent.*

III.6.2.5 Solution monitoring

Solution monitoring during computing process is also important, it helps in determining the accuracy of the physical models, meshing and problem setup. For that we have established two convergence monitors for convergence criteria on each of the 157 simulations, first one is the residuals, which was set to 10^{-06} for the energy equation and 10^{-04} for the continuity and momentum equations, the second is the stability of the average Nusselt number over the fin surface during iterating process, both of those convergence monitors are shown in Figure III.16. Once it is all done, the domain, mesh, solver and physics are set up; we initialize the flow field to start the solving process.

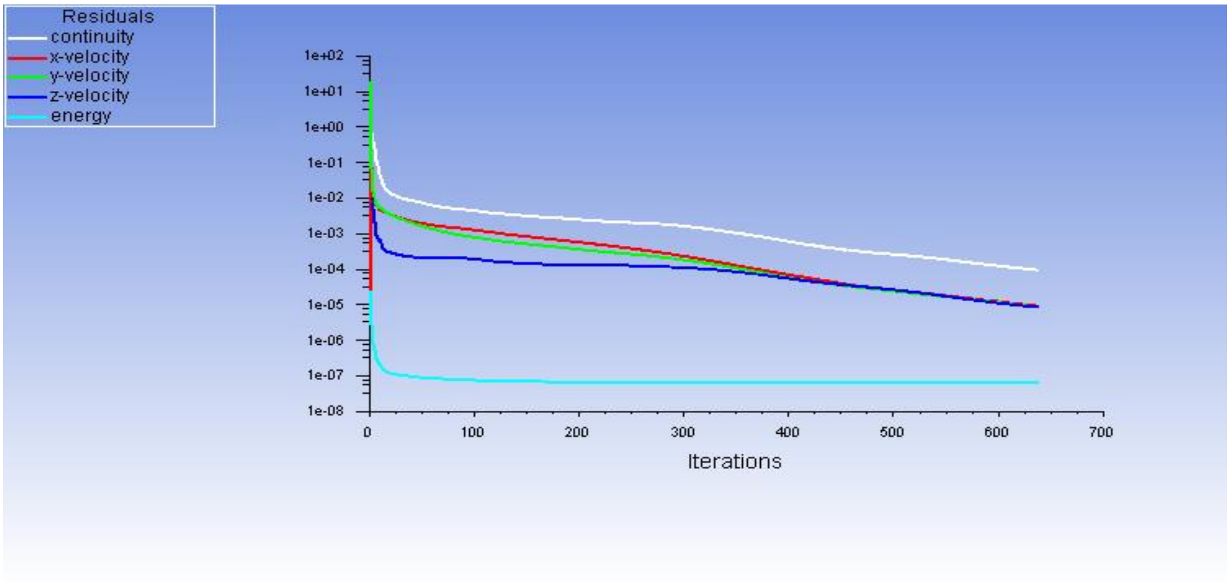

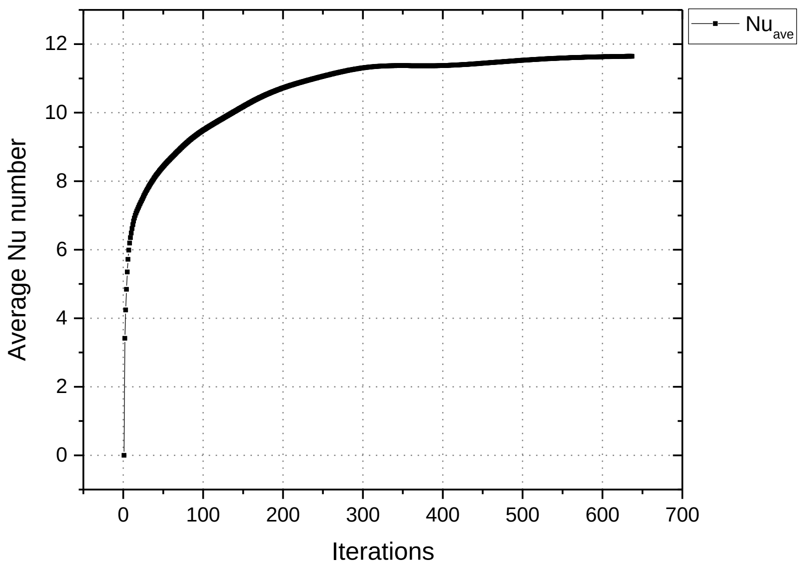

***Figure III.16** : Monitoring the convergence criteria.*

III.7 Computing average Nusselt number

The average Nusselt number in Figure III.16 and following sections was calculated using the surface heat transfer coefficient and the surface Nu Number as defined in ANSYS Fluent [44]:

$$h_{eff} = \frac{q}{T_w - T_{ref}} \quad \text{III.37}$$

$$Nu = \frac{h_{eff}\, L_{ref}}{k} \quad \text{III.38}$$

Using equation III.37 and III.38:

$$Nu = \frac{q\, L_{ref}}{k(T_w - T_{ref})} \quad \text{III.39}$$

III.8 Algorithm of numerical procedure

The CFD code of ANSYS Fluent is built around numerical algorithms that can tackle fluid flow problems, the general steps of solving a fluid flow and heat transfer problem using this CFD code are summarized in the following algorithm (Figure III.17).

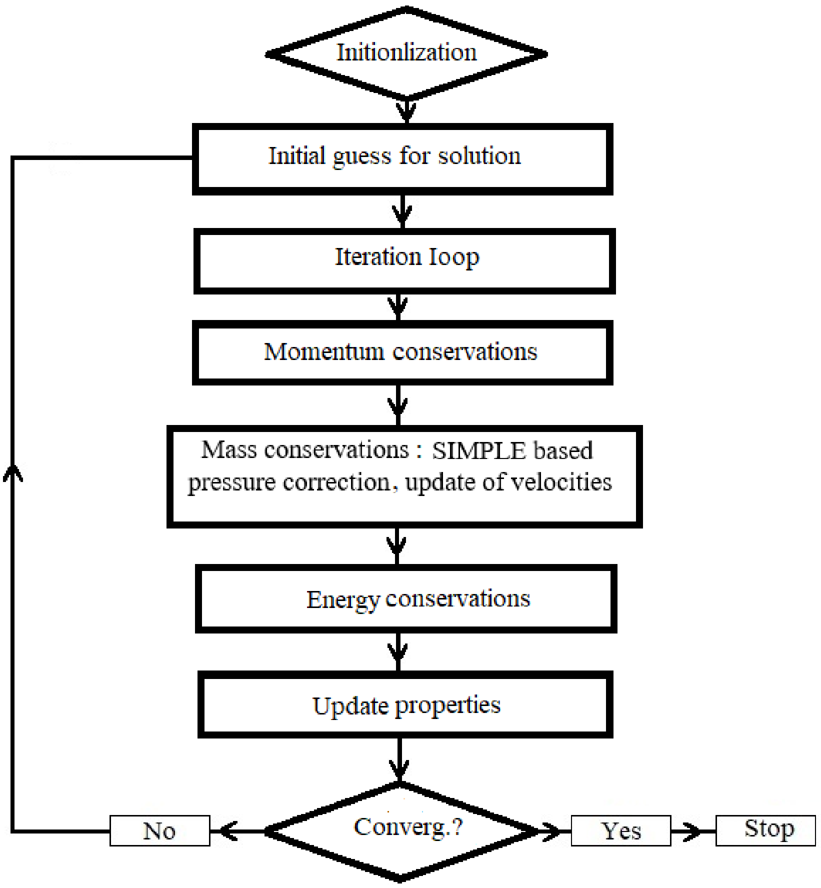

***Figure III.17** : General SIMPLE-based numerical procedure.*

III.9 Conclusion

The intent of this chapter was to clarify and elaborate on the numerical solution introduced in present work, where the point was to provide the reader a summarized and useful sense of the used numerical schemes involved to derive a CFD problem solution.

In spite of ultimate effort, the restricted framework of the thesis has compelled to introduce only brief notion about numerical formulation and theory behind it. After a short introduction on the methods used to derive a numerical solution, the finite volume methods with discretization of the governing equation is provided alongside the different numerical schemes and algorithms used for each term of the governing equations. Afterwards the numerical procedure of ANSYS Fluent CFD solver is then presented with detailed description of each step.

The next section of the thesis will consist of a mesh test and code validation to provide validity to the CFD code used for present study, and then a detailed analysis of the provided solution.

CHAPTER IV : RESULTS AND DISCUSSION

IV.1 Introduction

In this Chapter, different features of mixed convection heat transfer in a ventilated cavity in the presence of T-shaped heat fin are studied, a wide range of Reynolds numbers, Richardson numbers and Prandtl numbers (10-1500), (0.1- 10) and (0.71-7.10) are respectively covered in this analysis, Firstly, the effects of the mentioned dimensionless numbers on the governing equations are focused. Then the effect of K the thermal conductivity ratio between the fluid and the solid fin is also investigated in wide range of (0.1-10). Further, the effect of different geometrical parameters is also examined, namely, the inlet and outlet dimensions and locations, the fin foot length and location, in addition to effect of AR**,** i.e. the aspect ratio of the height to the length of the cavity. The qualitative analysis is mainly developed by the use of isotherms and streamlines contours at the cavity canter (z = 0.5). The quantitative analysis which is the analysis of the heat transfer rate, is accomplished using average Nusselt number at fin surface.

The objective of this chapter is to present a clear idea about the addressed problem by showing, commenting and interpreting the results accomplished on this work, to explain the physics behind the phenomena, and to provide a correlation relating the dimensionless parameters (Re and Ri) corresponding to this new geometry. Since we will be interested in the final temperature distribution and the overall thermal performance, we will be performing a steady state analysis.

IV.2 Mesh sensitivity test

For numerical solution of different fluid flow and heat transfer problems, a mesh sensitivity test is performed to reduce the cost of computation and emphasize on the accuracy of the numerical solution, generally, higher number of cells (volumes or elements) provides more accurate solution. However, increasing the number of element in the computational domain has a limit up on which a more accurate solution can be obtained by increasing elements number, that limit is reached when a particular derived parameter becomes constant with the increase of the elements number, then a more mesh refinement is not necessary and it is just more computational cost. Depending on this concept and since high number of elements involves high number of calculation operations, which produces more calculation time and cost. To avoid this, a particular parameter is selected to observe the change in its value for alteration of number of elements or nodes while all other parameters kept constant. Once the number of elements is sufficiently high for satisfactory of the solution, implementing a finer mesh does not change the value of the selected parameter significantly. That mesh is considered optimum and standard for the solution.

The results of the mesh test for present work are shown in Figure IV.1. The test was performed for Reynolds number, Re = 100, Richardson number, Ri = 1, Prandtl number, Pr = 0.71, thermal conductivity ration, K = 0.1, inlet and outlet location of BT configuration, H/5 in dimension, fin length H_f = 0.3, location at the cavity center, and cavity aspect ratio, AR = 1.

The figure shows that increasing the number of elements increases the value of average Nusselt number over the fin surface. However, from about a number of 1173264 cell elements, the value of average Nusselt number becomes constant at 5.158, and further increment in elements number does not change Nu_{ave} significantly. Hence, for all subsequent simulations, the mesh grid having number of 1173264 elements is selected as optimum mesh size.

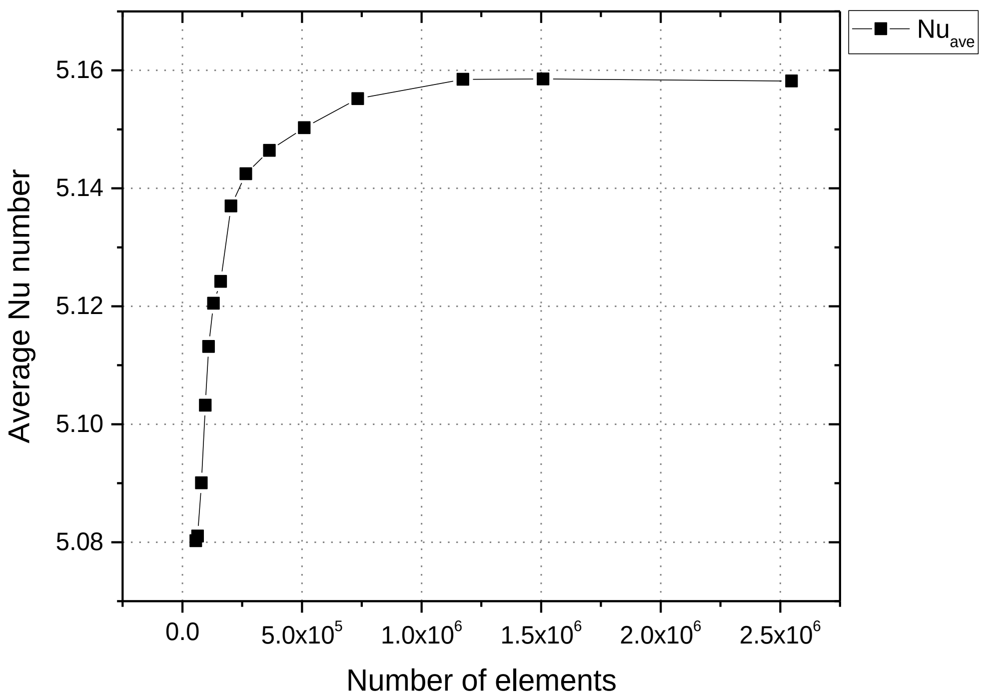

***Figure IV.1** : Variation of average Nusselt number with different mesh size for Re = 100, Ri = 1, Pr = 0.71, K = 0.1, inlet and outlet of BT configuration, H/5 dimensions, fin location at the cavity center, H_f = 0.3, and AR = 1.*

IV.3 Validation of the model

An important part of all CFD analysis is the validation of the model that is under study. The accuracy of used CFD code must be verified with respect to other previously validated numerical models, in present work validation is checked qualitatively and quantitatively using isothermal, temperature contours and average Nu_{ave} number respectively, with the experimental and numerical studies of Calcagni et al [16].

Comparison of average Nusselt number has been accomplished for $\varepsilon = 4/5$ and $H_f = 0$, between present study and the experimental and numerical outcomes of Calcagni et al [16]. Results are presented in Table IV.1.

***Table IV.1** : Comparison of average Nu number at the isothermal heat source, for $\varepsilon = 4/5$ and $H_f = 0$ between the present study (numerical) and the experiments of Calcagni et al [16].*

	Calcagni et al	Present study (numerical)	Error
Experimental ($Ra = 1.205 \times 10^5$)	7.15	6.81	4.75 %
Numerical ($Ra = 10^5$)	6.4895	6.4301	0.9 %

For isotherms and temperature contours validation, a comparison with the experimental and numerical results of Calcagni et al.[16], and present numerical study was realized, temperature contours of their study (a, b) on top, and (c) present study on bottom respectively for $Ra = 10^5$, $\varepsilon = 4/5$ and $H_f = 0$, (Figure IV.2). From the two comparison between the results, it can be said that the numerical method and CFD code for the present study is reliable.

(a)

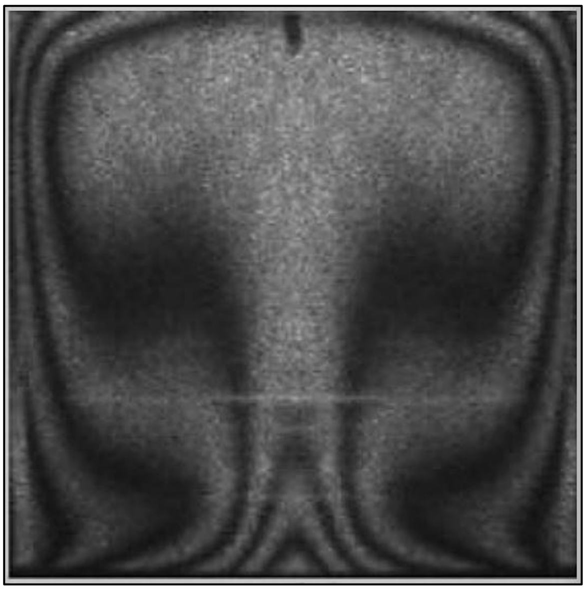

(b)

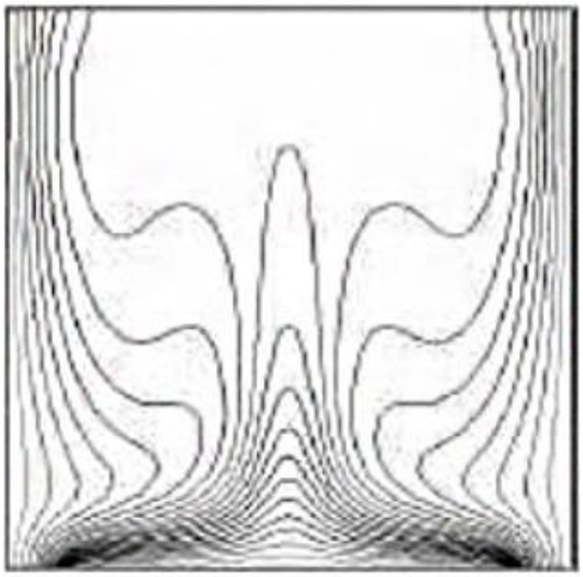

(c)

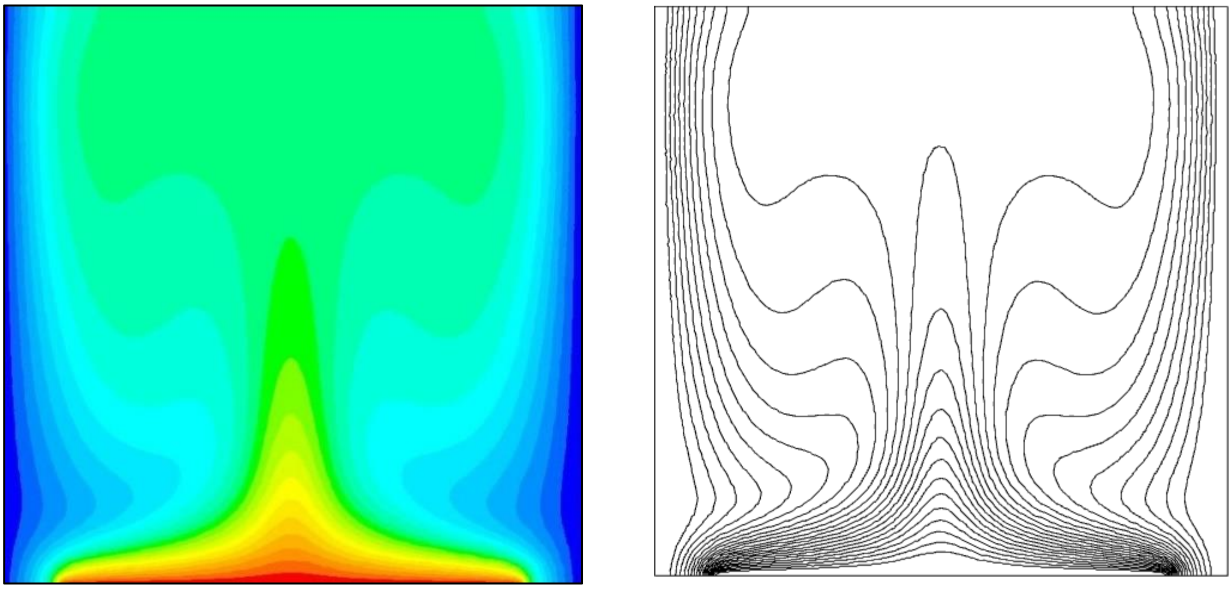

Figure IV.2 *: Temperature contours comparison for the experimental and numerical results of Calcagni et al [16] (a, b) respectively and (c) present numerical study* $Ra = 10^5$, $\varepsilon = 4/5$ *and* $H_f = 0$.

IV.4 Effects of dimensionless parameters

For this section, all geometry parameter mentioned above are kept constant in the following manner: inlet and outlet dimensions of (D_1 = D_2 = H/5), at location of BT configuration, fin length H_f = 0.3, at the cavity center, having an aspect ratio AR = 1.

IV.4.1 Effects of Reynolds number (ventilation velocity)

Ventilation in the cavity can be controlled by changing Reynolds number. As Richardson number was fixed so that the convection regime is mixed Ri = 1, Pr = 0.71, K = 0.1. We note that the increase of Re (velocity) causes a decrease in temperature (Figure IV.3), for the heat transfer, i.e. heat flux, the increase of Reynolds number results in an increase in the Nu_{ave}, thus we can conclude that the Reynolds number has a remarkable effect on fin cooling process. Effects of Re number on the temperature and flow fields are shown in Figure IV.4, the effect of Re number is clearly evident and significant since we note that at low Re number (Re = 10) the convection regime is dominated by the buoyancy flow driven convection. As Re increases, the convection is shifted from natural to forced convection dominant, and vortices start to appear in the cavity (Figure IV.5).

(a)

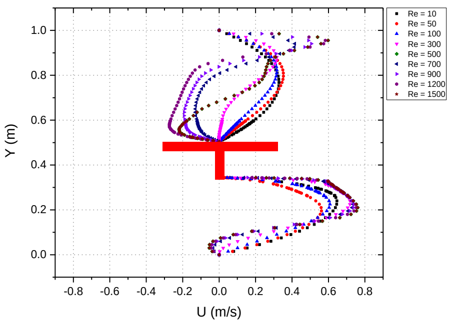

(b)

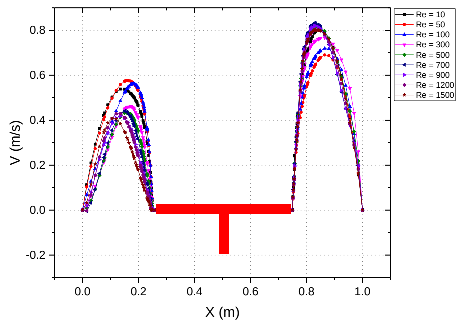

(c)

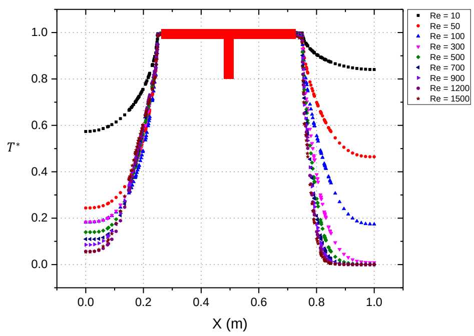

(c)

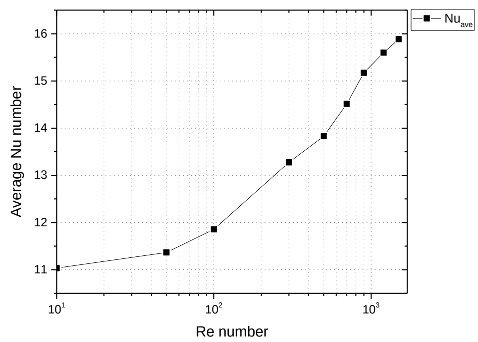

***Figure IV.3** : Velocity components U, V, and temperature profiles and Nu_{ave} at the cavity canter.*

(a)

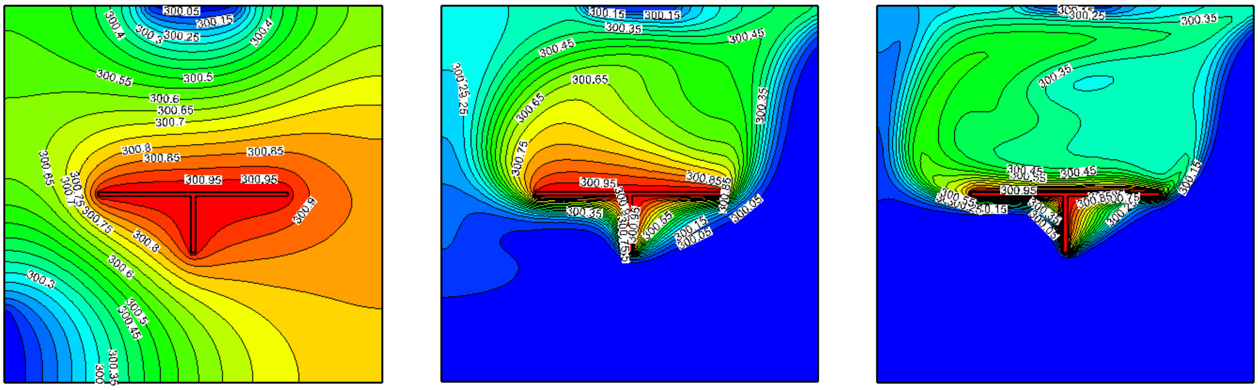

(b)

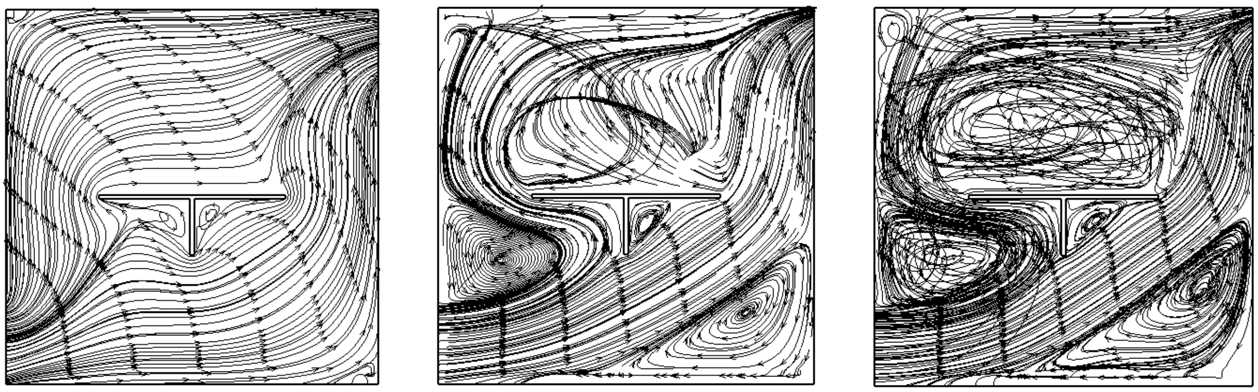

Re = 10 Re = 500 Re = 1500

Figure IV.4 *: Temperature contours (a) and streamlines (b) for different Re numbers (Ri = 1, Pr = 0.71 K = 0.1).*

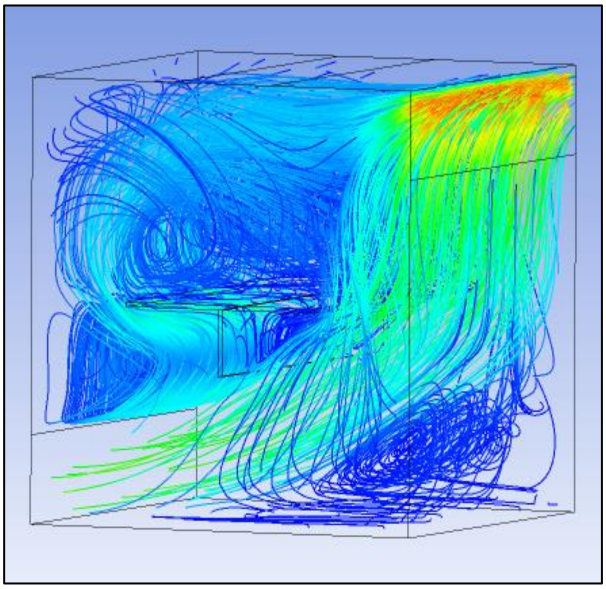

Figure IV.5 *: 3D streamlines for Re = 500, (Ri = 1, Pr = 0.71 K = 0.1).*

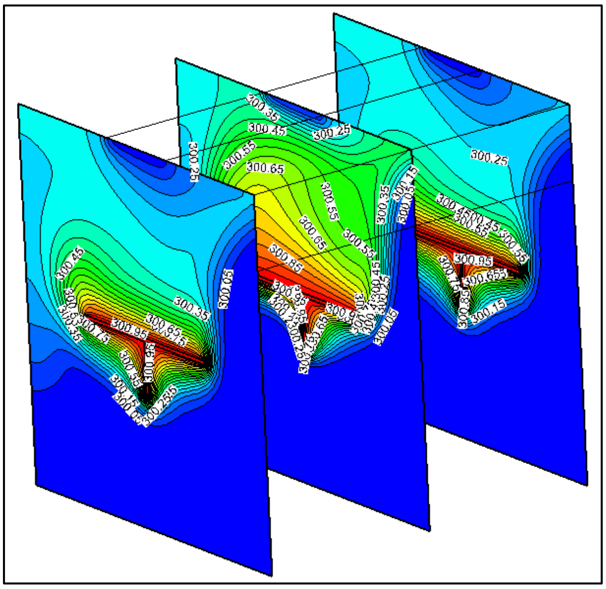

Figure IV.6 *: Slices of temperature contours at z = 0, 0.5, for Re = 500, (1, Ri = 1, Pr = 0.71 K = 0.1).*

IV.4.2 Effects of Richardson number (convection regime)

The effect of Richardson number on the average Nusselt number (due to the change of Grashof number) over the fin surface at constant Reynolds number is illustrated in Figure IV.7. It was found that Nu_{ave} increases with the increase of Ri number while preserving a constant Re number, and this shows the effect of the buoyancy induced convection, which becomes more dominant over the forced convection for higher Ri number. For low Ri values ($0.1 < Ri < 1$), the rate of change of Nu_{ave} is small, however that change gets steeper as Ri increases ($1 < Ri < 10$).

Figure IV.8 shows the effect of Richardson number on the flow and thermal fields for constant Re number. For Ri > 0.1, and since the external driving force remains constant as Re was fixed, the isotherms contours are more disseminated and vortex in the cavity appears at Ri = 10. Therefore as Ri number increase, Gr number also increases, and thus the induced buoyancy flow (distorted isotherms in Figure IV.8) indicates that the natural convection is dominant over the forced convection. The natural convection is so dominant at high Ri values ($Ri \geq 1$) which makes the hot fluid from the fin tends to the top of the cavity towards the outlet (Figure IV.9).

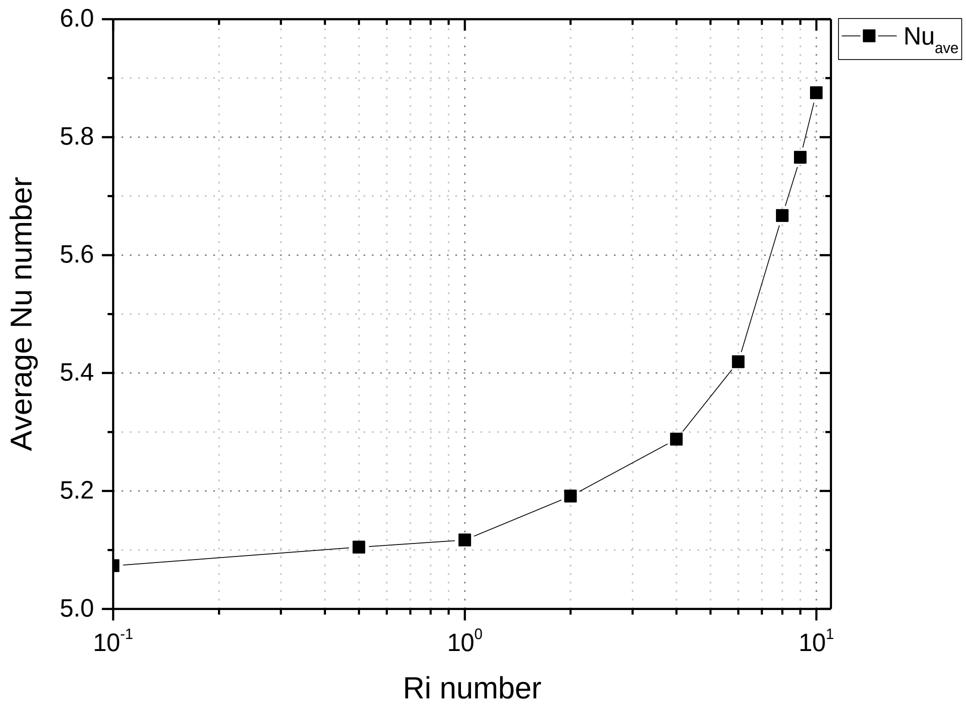

Figure IV.7 *: Average Nu number for different Ri values at Re = 100 (Pr = 0.71, K = 0.1).*

(a)

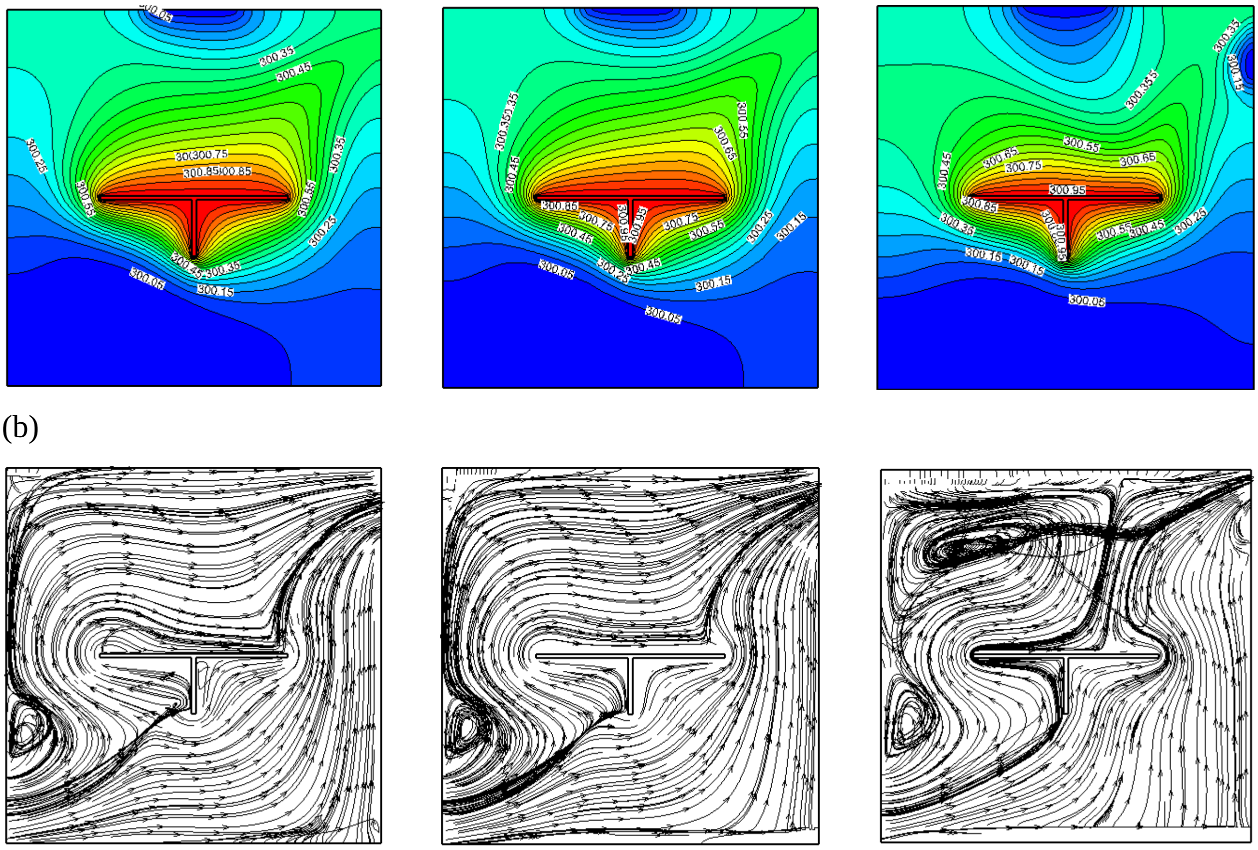

(b)

Ri = 0.1 Ri = 1 Ri = 10

Figure IV.8 *: Temperature contours (a) and streamlines (b) for different Ri numbers (Re = 100, Pr = 0.71 K = 0.1).*

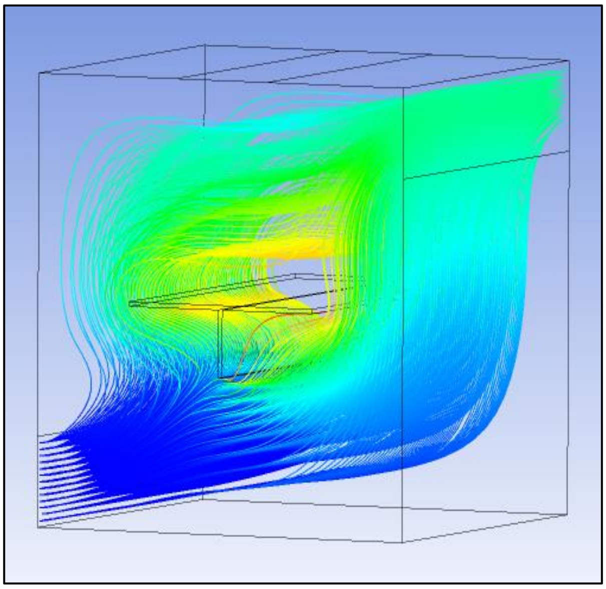

Figure IV.9 *: 3D streamlines for Ri = 1, (Re = 100, Pr = 0.71, K = 0.1).*

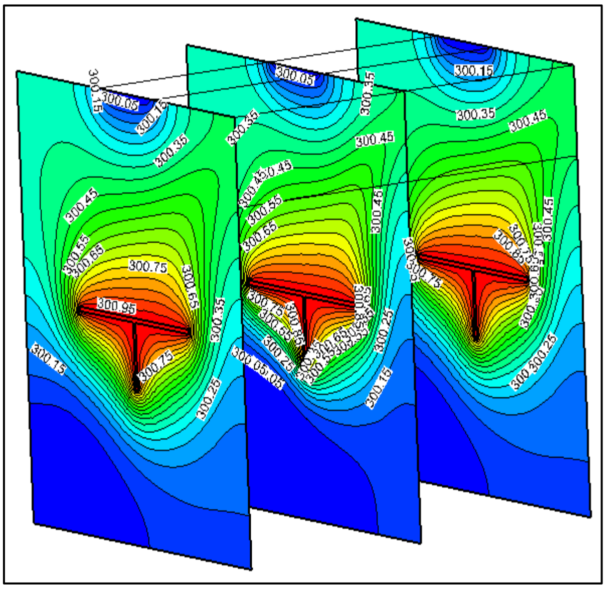

Figure IV.10 *: Slices of temperature contours at z = 0, 0.5, 1 for (Ri = 1, Re = 100, Pr = 0.71 K = 0.1).*

IV.4.3 Effects of Prandtl number

The variation of average Nusselt number for different Pr number values at constant Re and Ri numbers (Re = 500, Ri = 1, K = 0.1) at the hot fin surface is shown in Figure IV.11, it is clearly noted that the increase in Pr number causes an increase in the average Nu number and reaches the highest values for Pr = 7.1. This is because the fluid with high Pr number can carry more heat away from the fin and dissipate it through the outlet of the cavity.

The flow and temperature fields for different Pr number values at (Re = 500, Ri = 1, K = 0.1) are shown in Figure IV.12. The temperature fields indicates that the increase in Pr number reduces the thermal boundary layers, and the isothermal lines are denser near the hot fin (Pr = 7.10), it is also noted that the isothermal lines almost disappear in the low part of the cavity for high Pr number (Pr ≥ 3.91) as shown in Figure IV.14, oppositely to the low Pr values. This is due to constricting the thermal boundary layers in small region for the viscous fluid and the forced convection. For the flow field, for low Pr number (Pr = 0.71) it is remarked a small vortices starting to appear in the cavity, those vortices becomes larger with the increase of Pr number (Figure IV.13), this is due to the effect of the inertia forces.

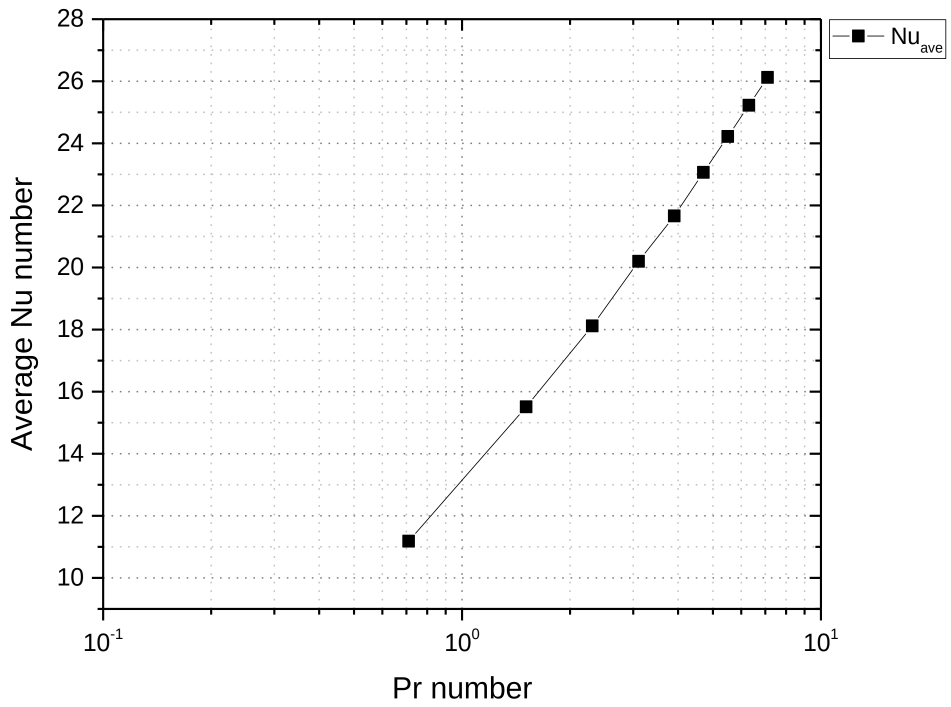

***Figure IV.11** : Variation of Nu_{ave} number for different Pr numbers (Re = 500, Ri = 1, K = 0.1).*

(a)

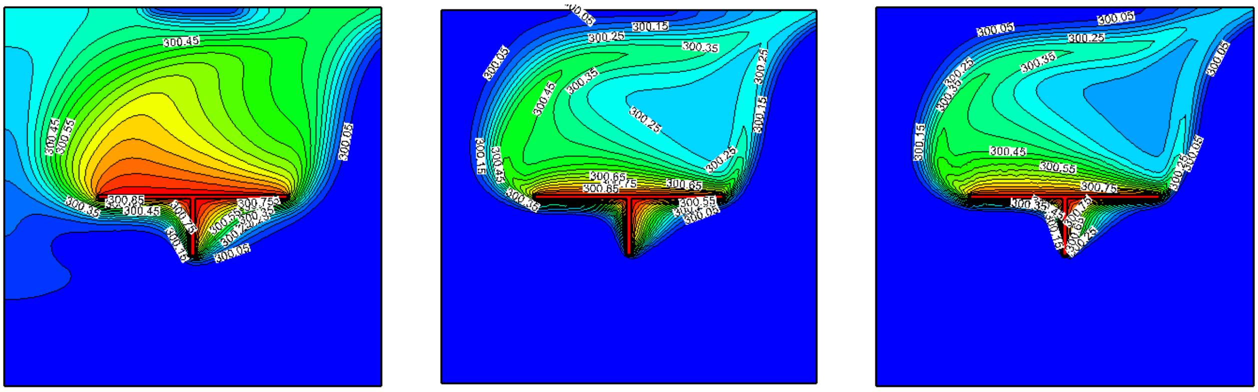

(b)

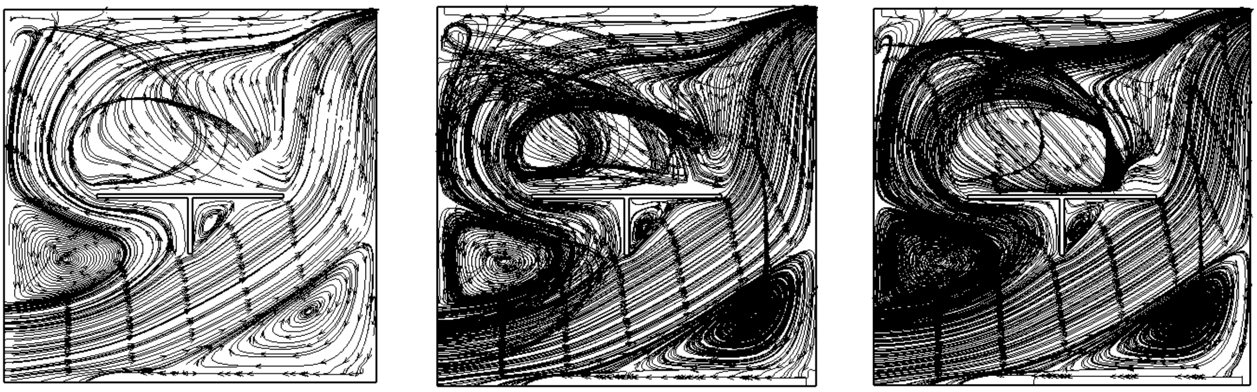

Pr = 0.71 Pr = 3.91 Pr = 7.10

***Figure IV.12** : Temperature contours (a) and streamlines (b) for different Pr numbers (Re = 500, Ri = 1 K = 0.1).*

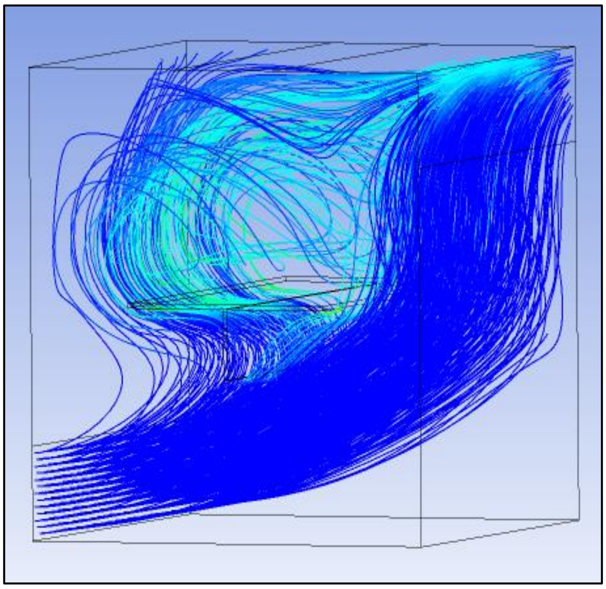

***Figure IV.13** : 3D streamlines for (Pr = 3.91, Re = 500, Ri = 1 K = 0.1).*

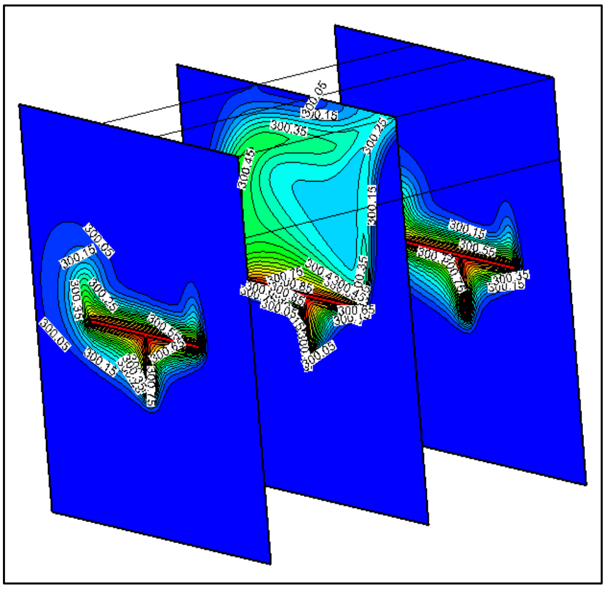

***Figure IV.14** : Temperature contours at z = 0, 0.5,1 for (Pr = 3.91, Re = 500, Ri = 1, K = 0.1).*

IV.4.4 Effects of the thermal conductivity ratio

The effect of the fluid-solid thermal conductivity ratio on the average Nusselt number for Re = 1, Ri = 1, Pr = 0.71 is shown in Figure IV.15, it is remarkable the thermal conductivity ratio has a significant effect on the heat transfer rate since the increase in K value causes a decrease in the average Nu number. This is because the solid fin becomes more conductive while the fluid becomes less conductive. Thus, the fluid becomes carrying less heat from the hot fin towards the outlet.

The illustration of the effect of the thermal conductivity ratio on the flow and thermal fields for constant Re, Ri and Pr numbers is represented in Figure IV.16. It is evident that for the higher values of K, the temperature gradient is concentrated around the hot fin, this is because low conducting fluid draws less heat from the hot fin (Figure IV.18). With the decrease in thermal conductivity ratio the fluid carries more heat from the fin and the isothermal lines becomes more widely spreading around the fin. On the other hand, K has insignificant effect on the flow fields for different K values (K = 0.1 - 10).

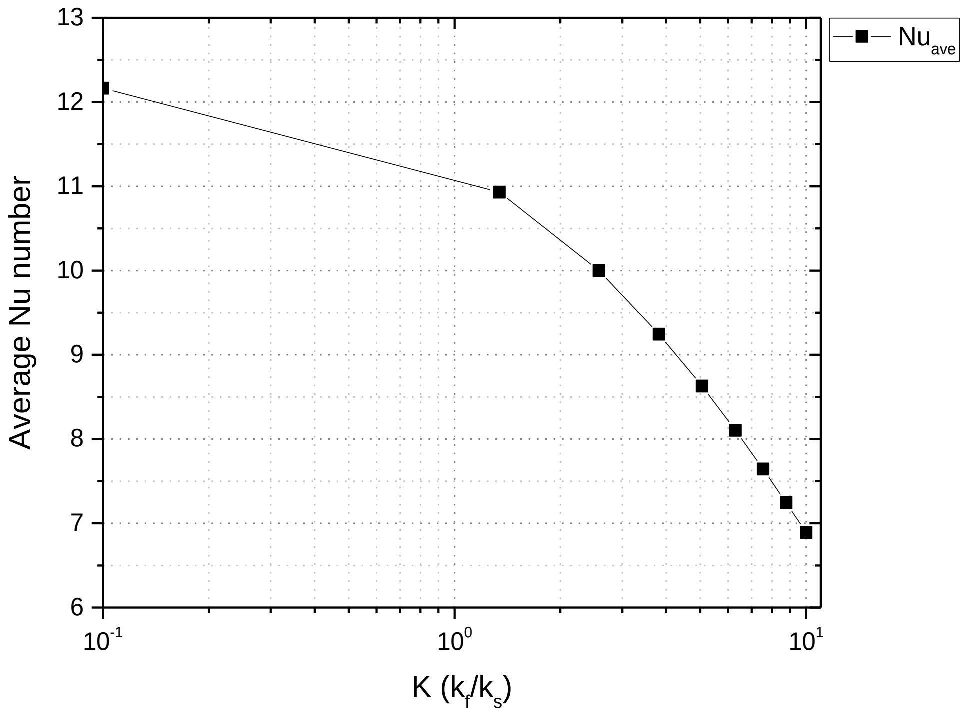

***Figure IV.15** : Variation of average Nu number for different K values (Re = 500, Ri = 1, Pr = 0.71).*

(a)

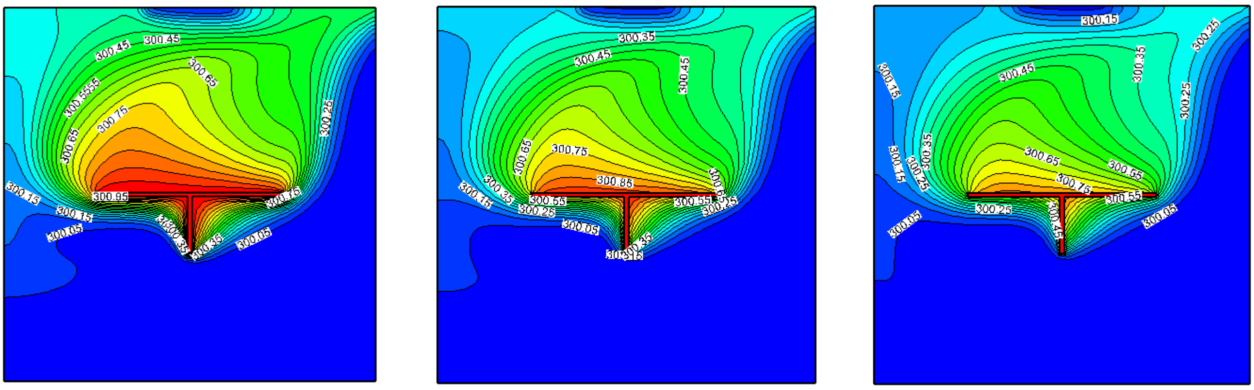

(b)

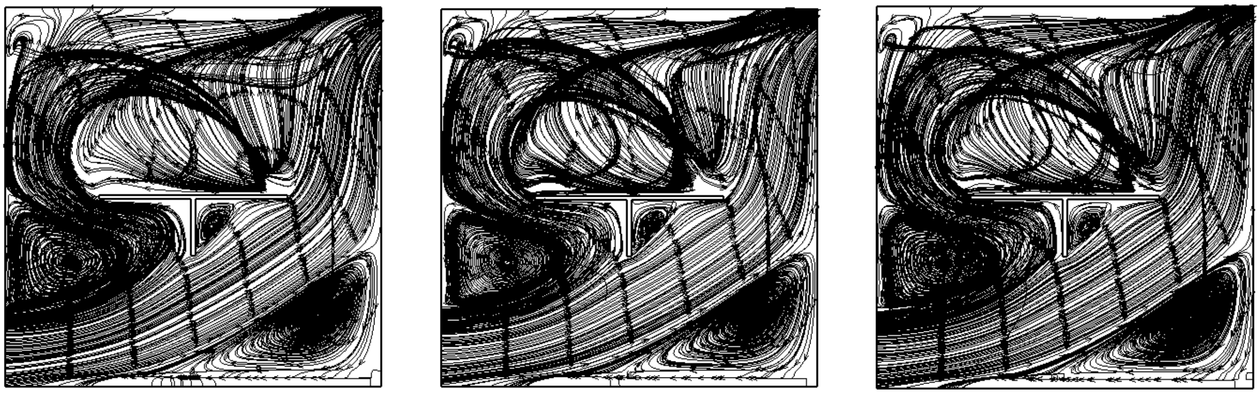

K = 0.1 K = 5.05 K = 10

Figure IV.16 *: Temperature contours (a) and streamlines (b) for different Pr numbers (Re = 500, Ri = 1 K = 1).*

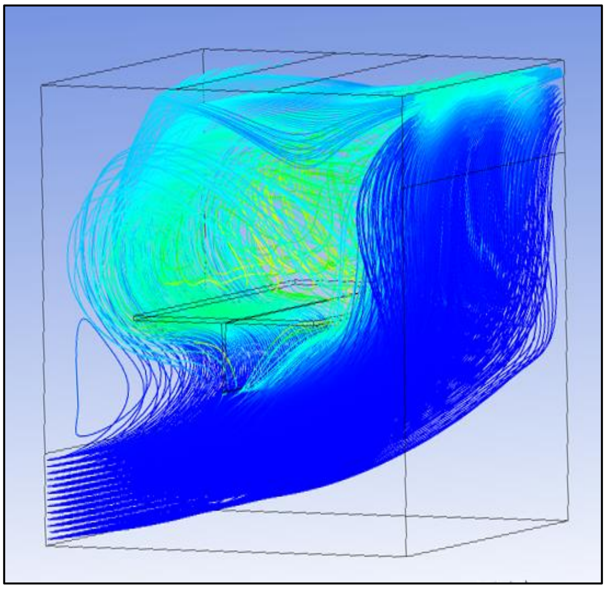

Figure IV.17 *: 3D streamlines for K = 5.05, (Re = 500, Ri = 1, Pr = 0.71).*

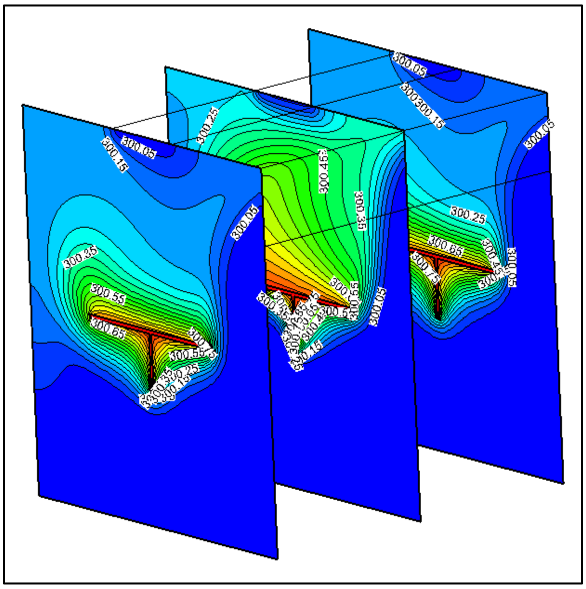

Figure IV.18 *: Slices of isotherms at plans z = 0, 0.5, 1 for (K = 5.05, Re =500, Ri = 1, Pr = 0.71).*

IV.5 Effects of geometrical parameters

In this section, the emphasize is on the effective geometry parameters for the studied problem, therefore all following simulations were conducted for constant Reynolds number (Re = 500), Richardson number (Ri = 1), Prandtl number (Pr = 0.71) and constant thermal conductivity ratio (K = 0.1), for all cases.

IV.5.1 Effects of the inlet and outlet dimensions

To study the effect of inlet and outlet dimensions on the heat transfer rate, thermal and flow fields, several simulations for different cases were conducted, where all other parameters are fixed, namely, the inlet and outlet configuration (BT), the fin location (at the cavity center), fin length (H_f = 0.3) and the aspect ratio (AR = 1). Only the dimensions of the inlet and outlet were varied ($D_1 = D_2$ = H/5, H/4, H/3 and H/2). It is remarkable from Table IV.2 that the inlet and outlet dimensions has a significant effect on the heat transfer rate since we note that for higher D_1 and D_2 we get high average Nusselt number values.

The thermal and flow fields for the different inlet and outlet dimension is shown in Figure IV.19. We can note that isothermal lines gets denser around the fin with the augmentation of the inlet and outlet dimensions (D1 = D2 = H/2 - H/5), which indicates that for low values of D_1 and D_2, the natural convection gets more dominant. It is also can be remarked from the streamlines contours, which shows a vortex on top of the fin surface gets bigger when D_1 and D_2 are at high values.

***Table IV.2** : Average Nu number for different inlet and outlet dimensions.*

$D_1 = D_2$ (m)	Nu_{ave}
H/5	11.85527
H/4	11.79651
H/3	11.86793
H/2	12.68214

(a)

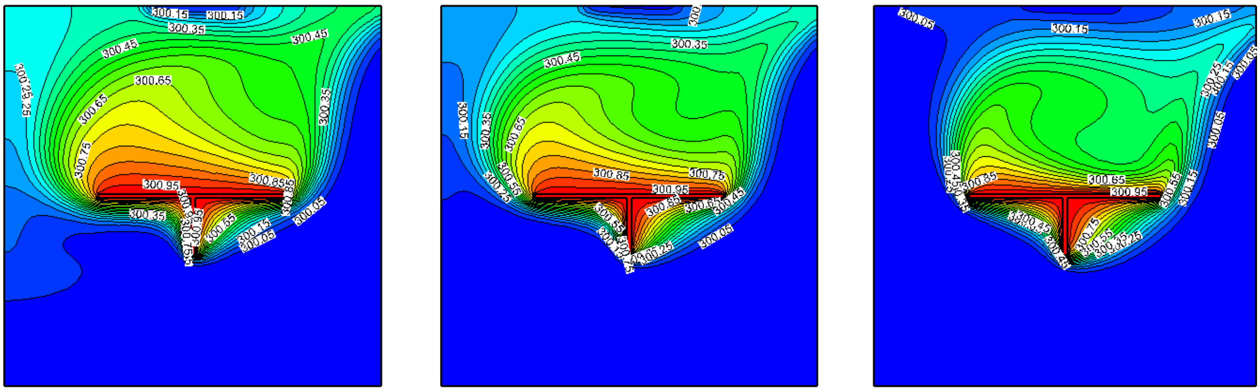

(b)

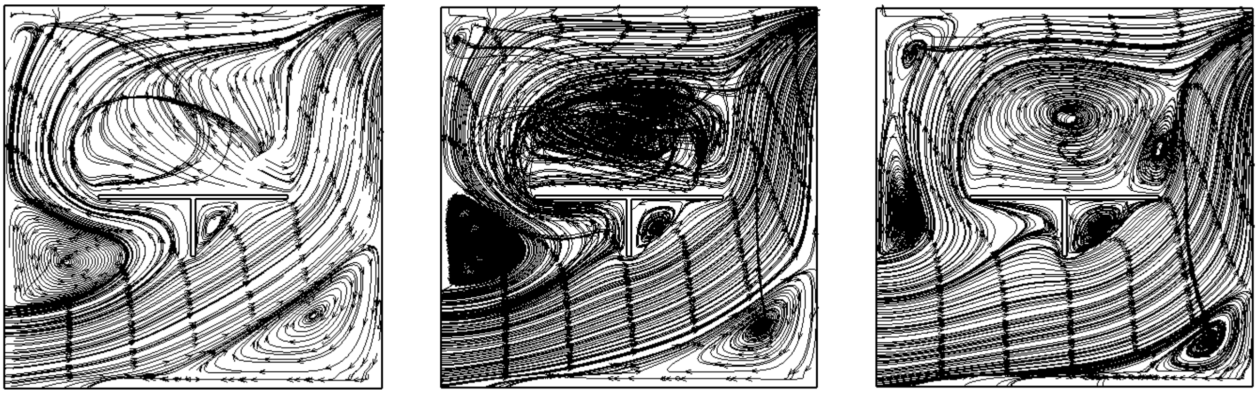

D1 = D2 = H/5 D1 = D2 = H/4 D1 = D2 = H/3

(a) (b)

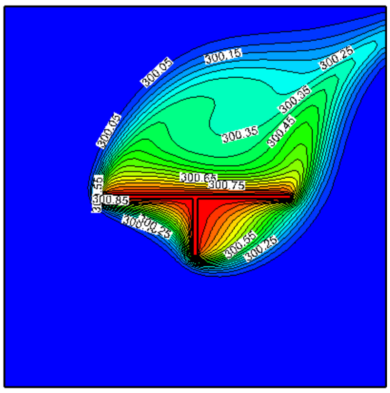

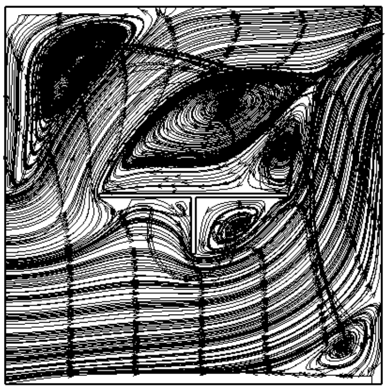

$D_1 = D_2 = H/2$

***Figure IV.19** : Temperature contours (a) and streamlines (b) for different inlet and outlet dimensions (BT configuration, H_f = 0.3, fin at the center, AR = 1).*

IV.5.2 Effects of inlet and outlet locations

Variation of average Nusselt number for different inlet and outlet configuration is presented in Table IV.**3** for $D_1 = D_2 = H/5$, $H_f = 0.3$, fin at the cavity center and AR = 1. It is noticeable that maximum Nu_{ave} values (12.51129 as an average) are measured when the inlet is at the middle of the cavity for all outlet positions. That value is decreased as the inlet is at the bottom of the cavity with an outlet at the top and middle opposite side of the cavity and at its minimum value for a BB configuration. When the inlet is at top side of the cavity, Nu_{ave} reaches its minimum limit for a TM and TT configurations respectively, except for the case when the outlet is at the cavity bottom.

Isotherm and streamlines contours are shown in Figure IV.20 as $D_1 = D_2 = H/5$, $H_f = 0.3$, fin at the cavity center and AR = 1. We can note that for bottom inlet, a wider isotherms distribution as the outlet is moved from the top side of the cavity towards its bottom and the presence of big vortex for the last configuration, which indicates the increased dominance of the buoyancy driven flow convection and confirms the decrease in Nu_{ave} in Table IV.**3**. For a middle cavity inlet and all outlet configurations, isotherms contours shows a dense isotherm lines surrounding the fin, and the air flow covers most of the fin surface, this shows the dominance of the forced convection and reveals the reason behind the optimum values of Nu_{ave}. For an inlet at the top of the cavity, and as the outlet gets shifted down from top to bottom, the isotherms gets denser and closer to the fin surface. We also note a decrease in the vortex size in the cavity, this manifest the transition of the convection regime from natural to mixed, this agrees with the increase in Nu_{ave} in the table below.

***Table IV.3** : Average Nusselt number for different inlet and outlet locations.*

Configuration	Nu_{ave}
BT	11.85527
BM	9.817084
BB	5.488905
MT	12.19863
MM	12.8905
MB	12.44476
TT	4.160865
TM	5.421927
TB	10.98742

(a)

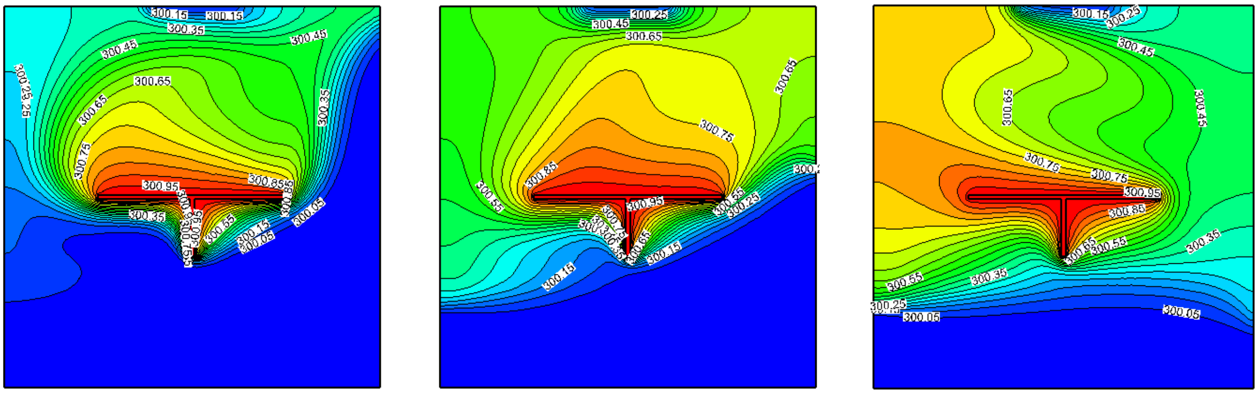

(b)

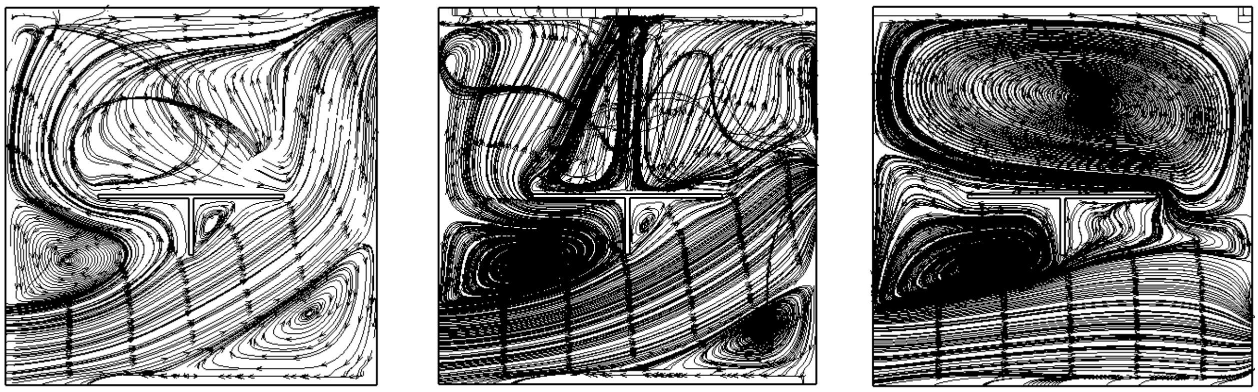

BT configuration BM configuration BB configuration

(a)

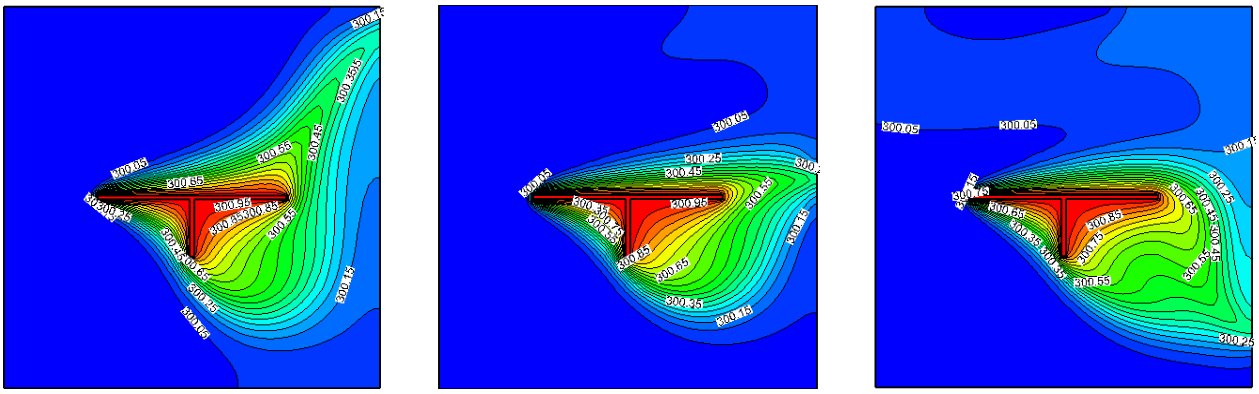

(b)

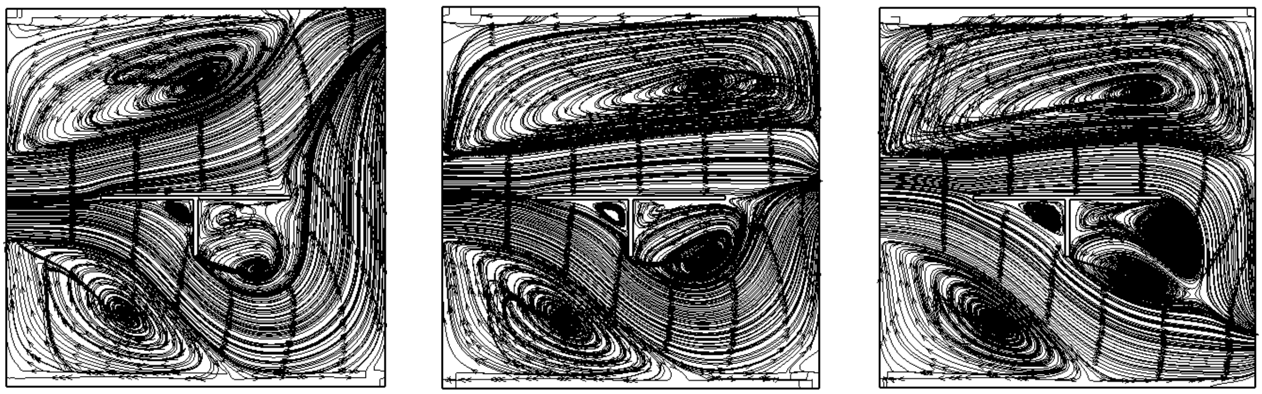

MT configuration MM configuration MB configuration

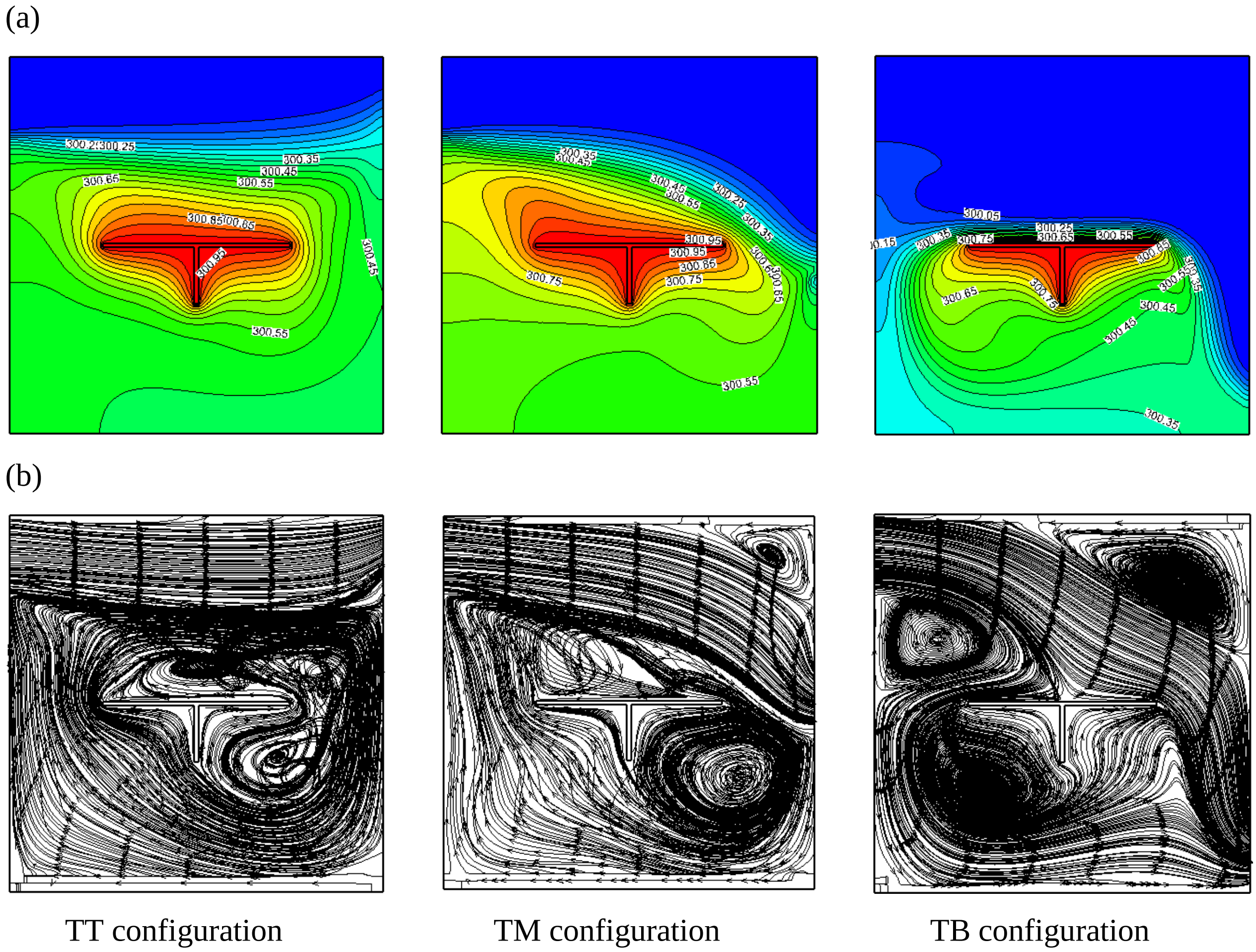

Figure IV.20 *: Temperature contours (a) and streamlines for the different configurations ($D_1 = D_2 = H/5$, $H_f = 0.3$, fin at the center, AR = 1).*

IV.5.3 Effects of fin location

Table IV.**4** shows the variation of average Nu number for different fin locations for $D_1 = D_2 = H/5$, BT configuration, $H_f = 0.3$, and AR = 1. It is evident that the heat transfer rate can be significantly affected by fin location since the average Nusselt number was varied from 5.2155 for the top left side fin location, to 11.8552 for a cavity center fin location. This is due to the change of the thermal and flow fields, and the dominance of the convection regimes one over the other.

The flow and thermal fields for different fin locations are presented in Figure IV.21. It is noted form the isotherm contours that the isotherm lines spreads wider as the fin get closer to the inlet (BL and BR locations), which is also shown in the streamline contours, as the fin gets in the way of the air flow, a bigger vortex is developed on the top side of the fin surface. The average Nusselt number for different fin location also confirms this.

When the fin is at the top of the cavity, the isotherm and streamlines distribution changes significantly, for the TL location the isotherms spreads wider from the fin surface and less fluid is on contact with the fin surface, this indicates the dominance of the natural convection for this configuration. On the other hand, when the fin is in TR location, it is notable that the isotherms are clustered around the fin surface; this is attributed to the higher forced convection currents.

Table IV.4 *: Average Nu number for different fin locations ($D_1 = D_2 = H/5$, $H_f = 0.3$, fin at the canter, AR = 1).*

Location	Nu
BL	10.63233
BR	11.18585
TL	5.215505
TR	11.52942
Center	11.85527

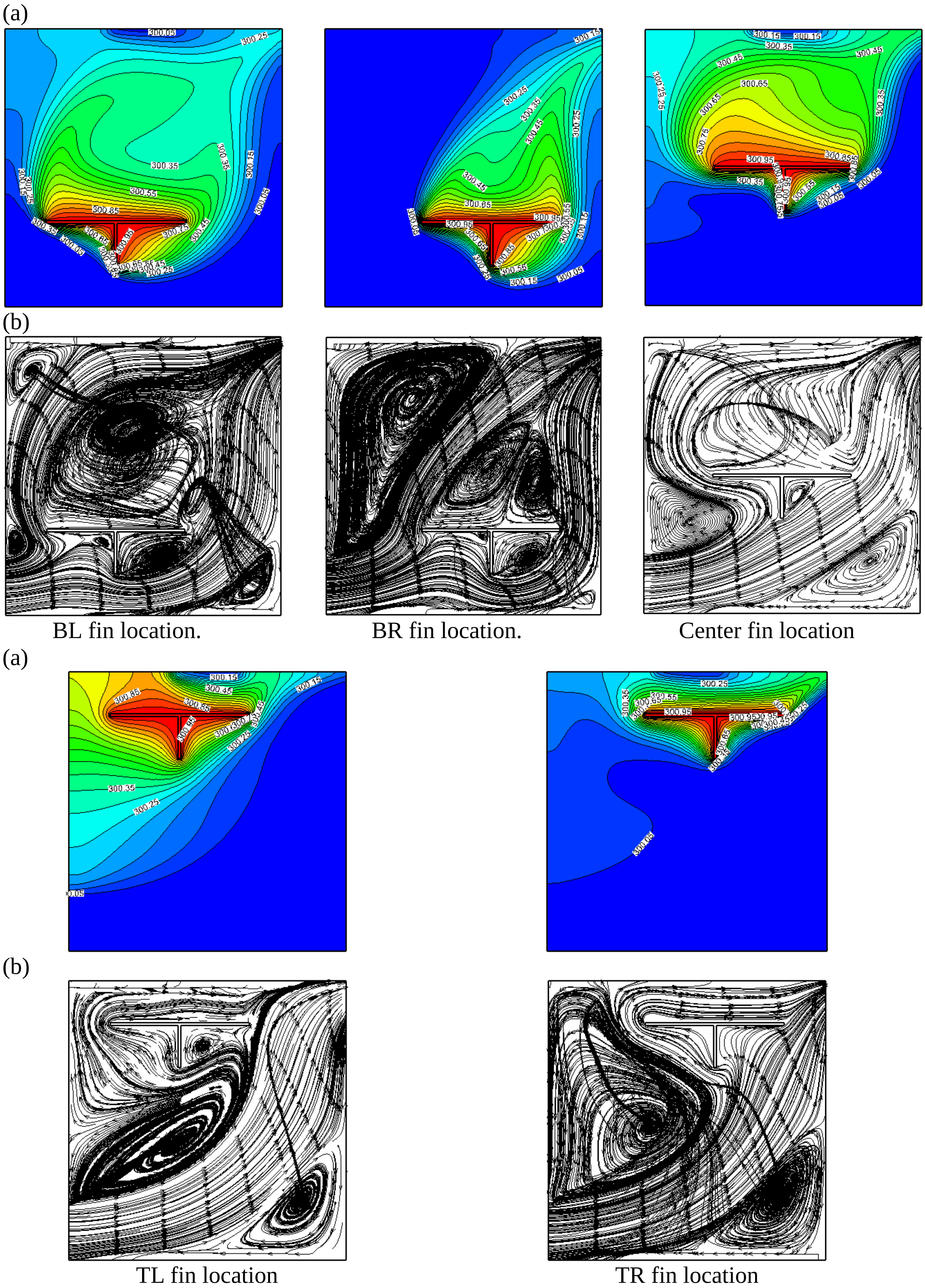

***Figure IV.21** : Temperature contours (a) and streamlines (b) for different fin locations.*

IV.5.4 Effects of fin length

Average Nusselt number for different fin length while $D_1 = D_2 = H/5$, BT configuration, fin location at the cavity center, and AR = 1, is shown in Table IV.**5**, it is clearly evident that there is a decrease in Nu_{ave} from 13.88489 to 11.49496 as the fin length H_f increases from 0.1 to 0.4. This change in the average Nusselt number can attributed to the change in the thermal boundary layers and temperature gradient over the fin surface.

Figure IV.22 illustrates the changes in the thermal and flow fields due to the change of fin length H_f, the variation in the thermal field is clearly noticed. For $H_f = 0.1$ the temperature gradient surrounding the fin clearly dense, and it is propagated wider and far from the fin surface as its length increases ($H_f = 0.4$).

The reason for the thermal field changes is shown in Figure IV.22 through streamlines contours as it exhibits an appearing vortex as H_f increases. It is also evident that as the fin length is increased, the mainstream flow gets away from the fin bottom right side.

Table IV.5 *: Average Nu number for different fin length H_f.*

H_f	Nu_{ave}
0.1	13.88489
0.2	12.92308
0.3	11.85527
0.4	11.49496

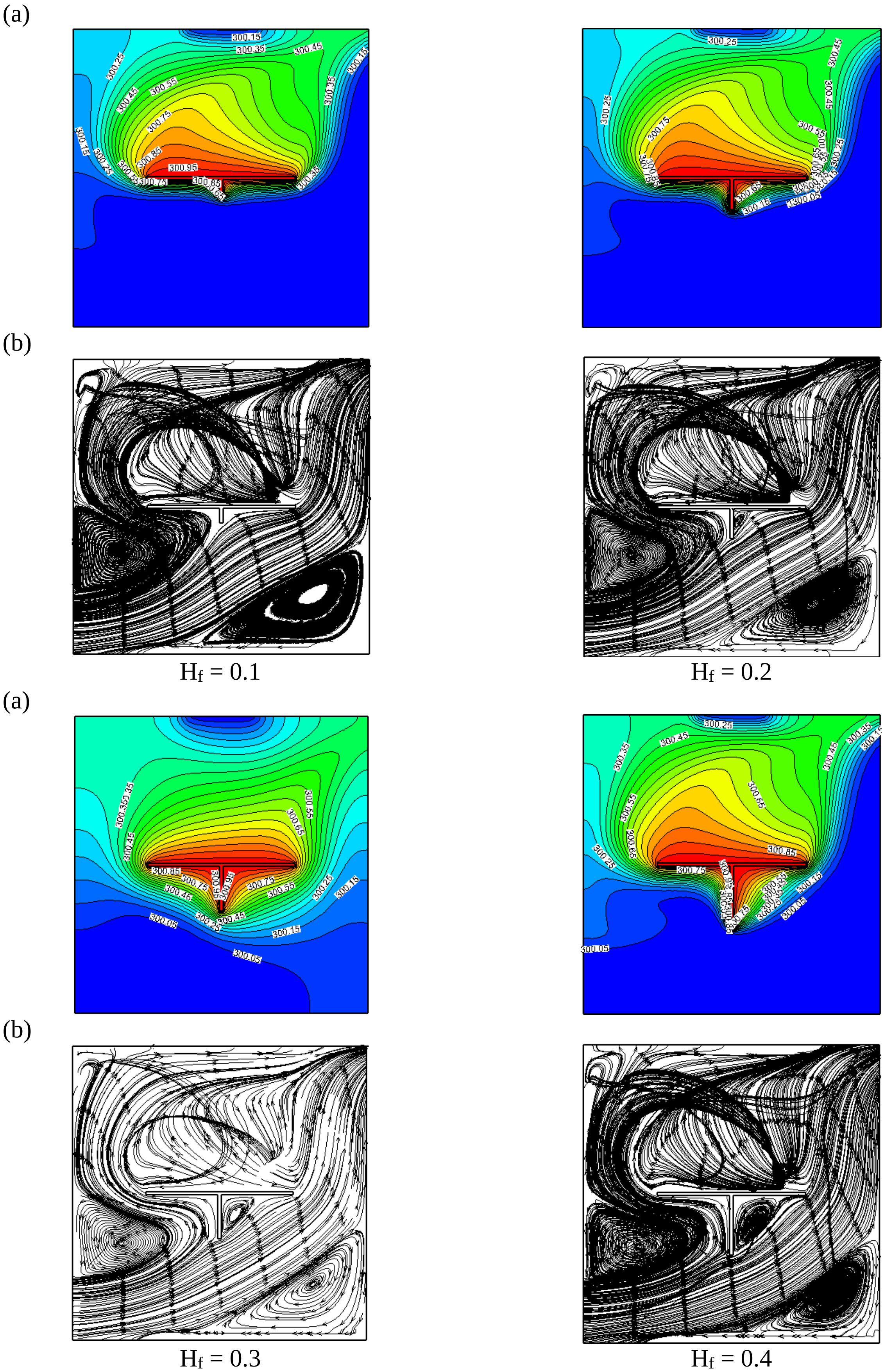

Figure IV.22 *: Temperature contours (a) and streamlines (b) for different fin lengths.*

IV.5.5 Effects of the aspect ratio (AR)

The effects of cavity aspect ratio on average Nusselt number while $D_1 = D_2 = H/5$, BT configuration, $H_f = 0.3$, fin at the cavity center is revealed in Table IV**.6**. From the table below, it is observed that as the aspect ratio is increased from 1 to 2, the average Nusselt number is decreased, while increasing it from 0.5 to 1, Nu_{ave} gets slightly increased. Thus we can say that an aspect ratio of 1 (AR = 1) is the optimum configuration that provides maximum average Nusselt number, and therefore the best thermal performance.

Thermal and flow fields for $D_1 = D_2 = H/5$, BT configuration, $H_f = 0.3$, and the fin at the cavity center are shown in Figure IV.23. The figure outlines the effect of different aspect ratios through isotherms and streamlines. For an aspect ratio of 0.5, it is evident that convection regime is dominant by the forced convection since the isotherm lines are the closest to the fin surface; the flow is surrounding the fin surface, with the presence of small vortices on top and bottom sides of the fin as well as at the cavity corners. When the cavity is a square (AR = 1), the isotherms are more wider in the vertical direction (y direction) which can indicate that the convection regime is now mixed, and that is confirmed as the average Nusselt number is at its maximum values for AR = 1, For aspect ratios of 1.5 and 2, the flow field is almost identical. However, the thermal field is not, we can note that for AR of 1.5, the convection regime is still mixed, but with more natural convection dominance, this dominance of the buoyancy driven flow convection is increased as the aspect ratio is increased to 2, which explains the decrease in Nu_{ave}, as shown in the table below.

Table IV.6 *: Average Nusselt number for different aspect ratios ($D_1 = D_2 = H/5$,BT configuration, $H_f = 0.3$, fin at the cavity center).*

AR	Nu_{ave}
0.5	11.6224
1	11.85527
1.5	11.07772
2	9.089359

(a)

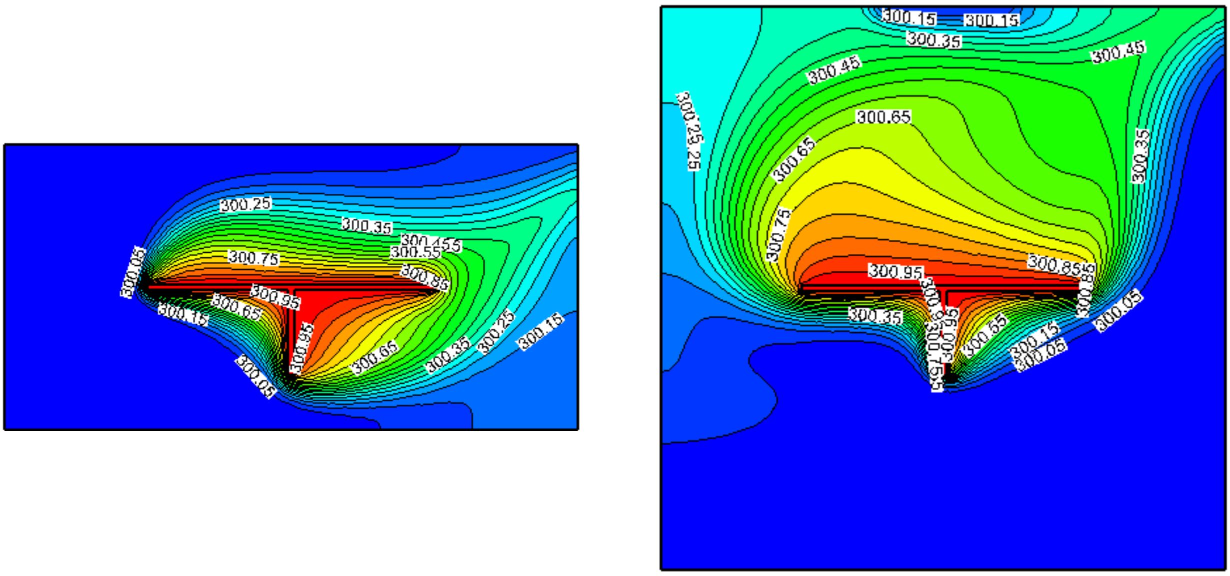

(b)

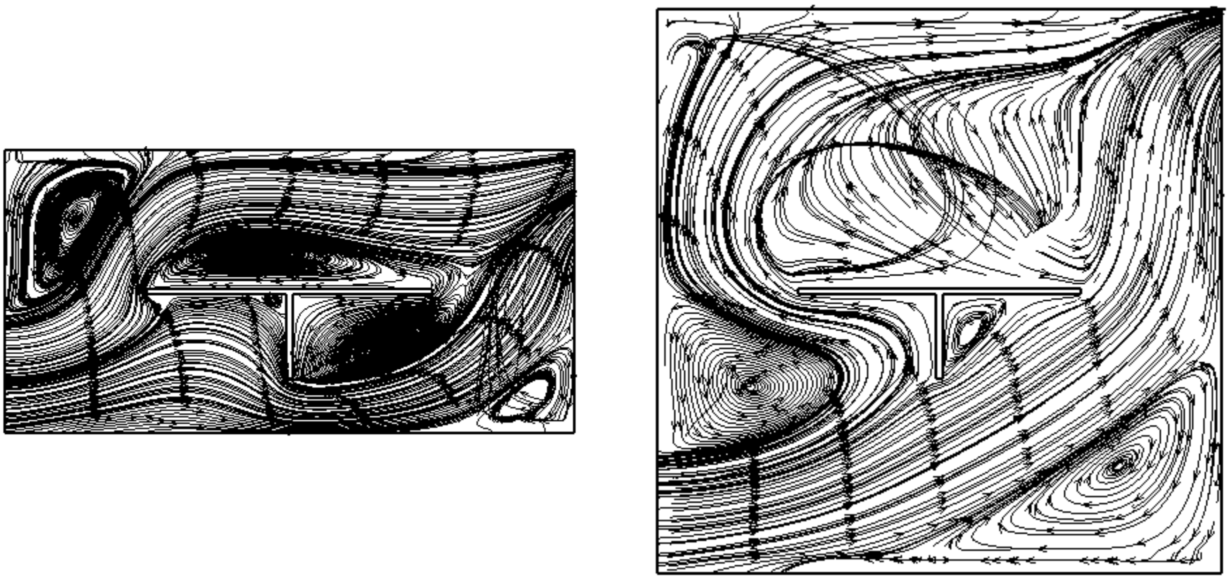

AR = 0.5 AR = 1

(a)

(b)

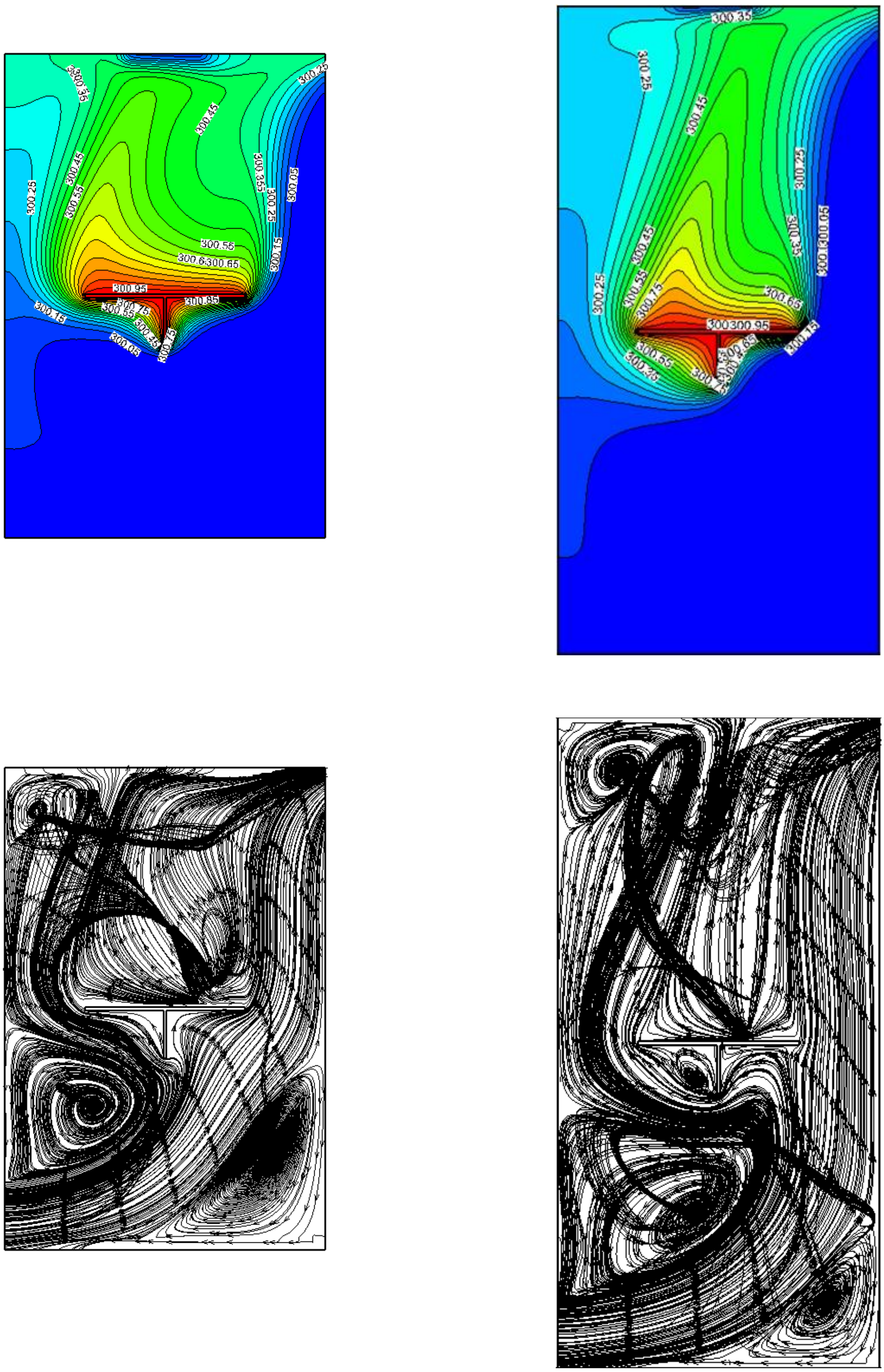

AR = 1.5 AR = 2

***Figure IV.23** : Temperature contours and streamlines for different aspect ratios.*

IV.6 Overall effects of Re and Ri numbers

To further emphasize on the combined influence of the dimensionless parameters. Namely Reynolds and Richardson numbers, and confirm or deny the assumption proposed at the end of CHAPTER II, additional cases were studied were all geometrical parameters were kept constant, ($D_1 = D_2 = H/5$, BT configuration, fin at the cavity center, $H_f = 0.3$ and $AR = 1$), in addition to Prandtl number ($Pr = 0.71$) and the thermal conductivity ratio ($K = 0.1$). So that the variation of the heat transfer rate (measured through the evaluation of average Nusselt number) exclusively depends on Re and Ri values, results are shown in Table IV.7.

The set of data of the table below recapitulates the results of the 81 cases studied in this section, it is noted form the values of average Nusselt number that for a low values of Re number, the rate of change in Nu_{ave} is insignificant. However, the rate increases with the increase in Re number. On the other hand, even for low Ri numbers, the increase in Nu_{ave} due to the increase of Re number is clearly important, and even more significant at higher Ri number values.

Table IV.7 *: Average Nusselt number for a wide range of Re (10 - 1500) and Ri (0.1 - 10) numbers.*

	Ri								
Re	0.1	0.5	1	2	4	6	8	9	10
10	1.7796	1.7802	1.7947	1.7804	1.7947	1.8014	1.8175	1.8383	1.88596
50	3.6947	3.7015	3.7084	3.7242	3.7452	3.7651	3.7961	3.7885	3.81480
100	5.0731	5.1045	5.1167	5.1912	5.2876	5.4191	5.6670	5.7657	5.87514
300	8.3981	8.5174	8.6712	9.4899	10.048	10.487	10.870	11.150	11.2843
500	11.032	11.366	11.855	13.274	13.829	14.513	15.171	15.600	15.8854
700	13.365	13.720	14.501	15.884	17.000	17.581	18.997	19.359	19.8446
900	15.415	15.767	16.891	17.899	19.725	21.110	22.282	22.926	23.9679
1200	18.169	18.5315	19.8024	20.8547	23.9170	25.2221	26.9907	27.9469	28.55202
1500	20.518	20.9061	21.6393	23.2862	27.1845	28.5622	30.4749	32.2730	33.21859

The data of Table IV.7 is represented in three-dimensional plot (Figure IV.24) to point out the variation of average Nusselt number with Re and Ri numbers. The figure below shows that for a fixed Ri number, there is a significant and quick increase in average Nusselt number due to the increase of Re number. However, when Re is fixed, the increase in average Nu number due to variation of Ri number is small or even insignificant for low Re number values.

Thus, the natural convection induced by the increase of Ri number (due to the increase of Grashof number) contributes with less effects on overall heat transfer performance within the cavity in compered with forced convection due to the increase of Re number.

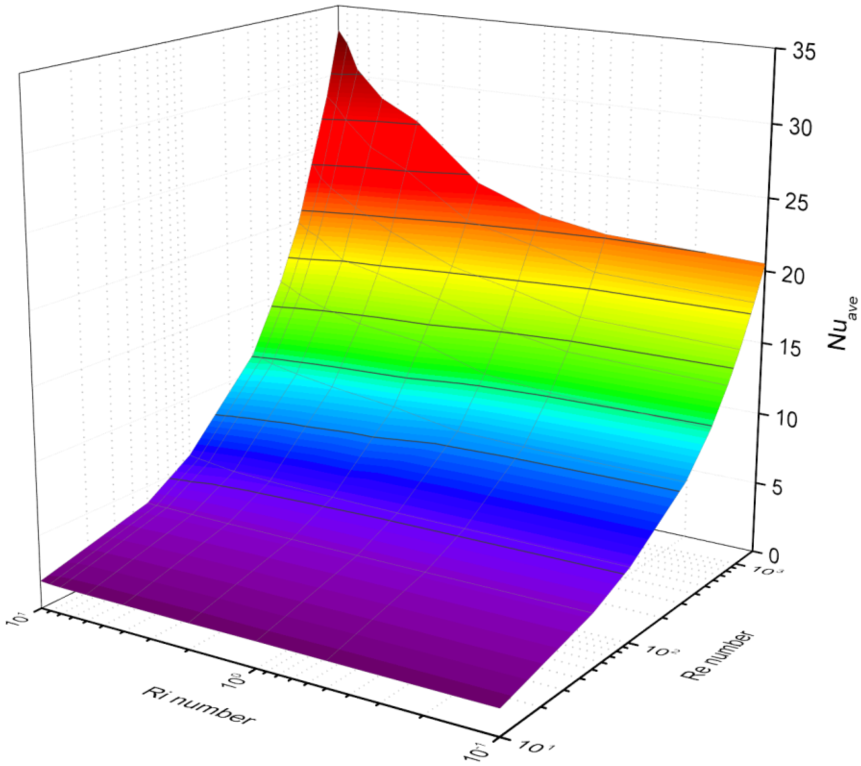

***Figure IV.24** : 3D plot of average Nusselt number as a function of Re and Ri numbers.*

One of the principle objectives of this study was to develop a correlation to predict the average Nusselt number for a given Reynolds and Richardson numbers and relate the non-dimensional parameters. The correlation provided in the present study (equation IV.1) is casted in the terms of the following power low

$$Nu_{ave} = 0.29633Re^{0.6001}Ri^{0.11052} \qquad \text{IV.1}$$

The correlation was obtained for range of Reynolds number of 10 – 1500 and Richardson number 0.1 – 10, while Prandtl is 0.71, the Figure IV.25 represents a party plot of the numerical average Nusselt number and the obtained correlation-based one. Consequently, the goodness of the fit is clearly evident.

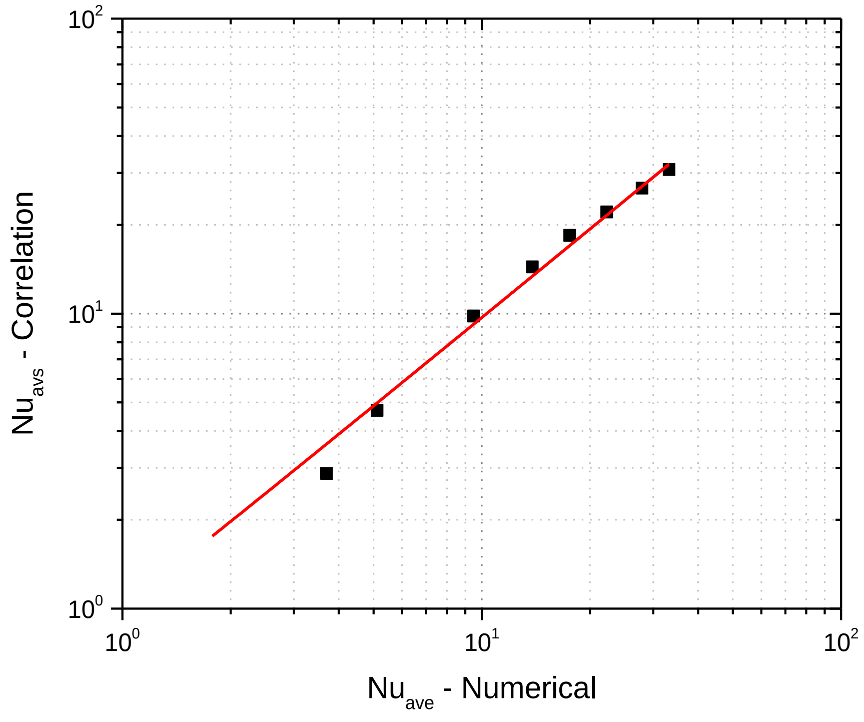

***Figure IV.25** : Party plot showing agreement between numerical and correlation-based average Nusselt number.*

The correlation provided in present work is compared with the correlations of the works of Moallemi and Jang [45], and the correlation provided by the experimental study of Radhakrishnan et al [46], those two studies yielded the following correlations respectively:

$$Nu_{ave} = A.Re^{0.5}.Pr^{m}\left[1 + B\left(\frac{Ri}{Pr^{n}}\right)^{q}\right] \quad \text{IV.2}$$

$$Nu_{ave} = A.Re^{0.69}\left(\frac{Ri}{1 + Ri}\right)^{0.0331} \quad \text{IV.3}$$

Were A and B are constants, the exponents m and n are 0.4 and 0 for Pr < 1 and q is a constant of the order 0.2 to 0.25. For the present comparison, those constant were set in the following manner: for equation IV.2, A = 0.33522, B = 0.5, m = 0.4, n = 0, and q = 0.2, while for equation IV.3, the value of the constant A was set of the range (0.142 to 0.2) depending on the value of Ri number. Results of the comparison are shown in Figure IV.26, which indicate that it is clearly evident that present work results, and correlation tends to have an excellent agreement with correlations and the predicted average Nu number of equations IV.2 and IV.3.

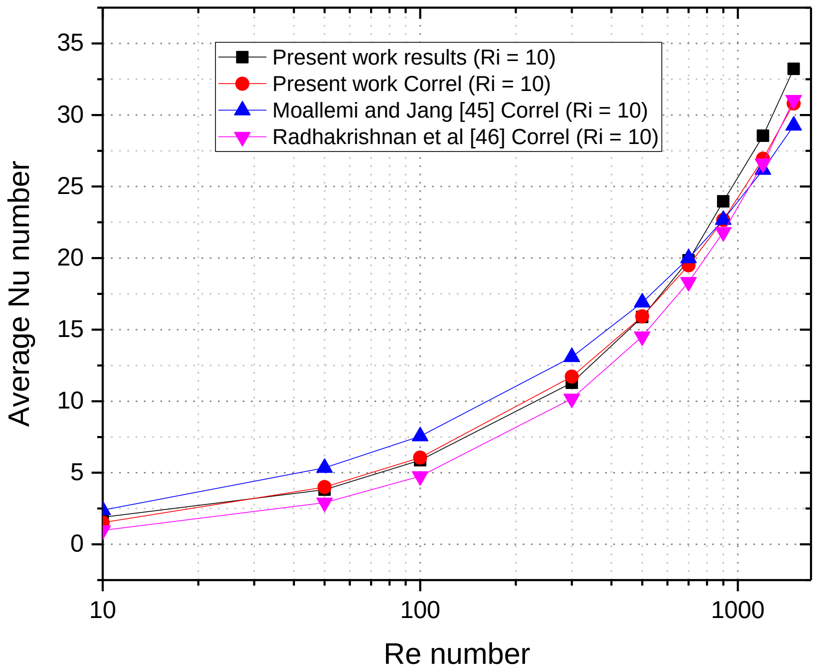

Figure IV.26 *: Comparison of Nu_{ave} results and correlations for present work, and the studies of Moallemi and Jang [45] and Radhakrishnan et al [46] for Ri = 10.*

IV.7 Conclusion

In this Chapter of present work, results of numerical study of mixed convection in rectangular ventilated cavity with T-shaped heat fin has been presented and discussed in details, several dimensionless and geometrical parameters were considered.

After a short introduction about the general scope of this study is conducted, a mesh sensitivity test was performed to select the optimal mesh configurations, afterwards, validation of the present model with the experimental and numerical study of B. Calcagni et al [16] was carried out. Then the effects of the dimensionless parameters was examined, the steeper effect of Re number was clearly evident on the augmentation of average Nu number, while it was found that the augmentation of K causes a decrease in Nu_{ave} values. For the geometrical parameters, it was found that the inlet and outlet configuration has the most significant effect on the average Nu number, the flow and thermal fields, on the opposite to their dimensions.

Those results allows us to say that the selection of the ventilation speed, its type, the cooling fluid properties, and the convection regime, as well as the cavity configuration, and the fin properties and location can enhance significantly the thermal performance.

GENERAL CONCLUSION

Mixed convective heat transfer in ventilated rectangular cavity in presence of a T-shaped heat fin has been studied numerically. Investigating the enhancement of the thermal performance, the study was carried out by solving the Navier-Stokes equations, continuity and energy equation using the FVM based CFD code of ANSYS fluent, and the SIMPLE algorithm. The analysis was accomplished for a wide range of physical parameters, namely Reynolds number (Re = 10 - 1500), Richardson number (0.1 - 10), Prandtl number (0.71 – 7.10) and the thermal conductivity ratio K (0.1 - 10). Furthermore, the influence of several geometrical parameters on the thermal performance such as the inlet and outlet dimensions, locations, fin length and position, and AR was examined. The analysis was performed qualitatively and quantitatively, the latter was in terms of average Nusselt number indicating the thermal performance, while the other in terms of temperature and streamlines contours, from this analysis the following outcomes can be drawn.

The ventilation velocity of the cavity (Re number) has a significant influence on the thermal performance in the cavity and Nu_{ave} reaches maximum values at maximum Re number, the latter has also a significant effect on the flow and thermal fields.

The effect of Richardson number was also important, however, more significant at high Re numbers and the shear driven flow convection is more significant than buoyancy driven one.

The influence of Pr number and K was the opposite for each other, an augmentation in Pr number presented an increase in Nu_{ave} and affected the thermal and flow fields, meanwhile, as K was augmented Nu_{ave} was decreasing, and no significant effect on the flow fields.

The geometric parameters influence was also present and considerable; the change of inlet and outlet dimensions and locations caused important changes in Nu_{ave}, flow and thermal fields. The fin length and location also introduced significant changes in Nu_{ave}, and affected the flow and thermal fields; however this was not the case for the aspect ratio of the cavity. This indicated that the thermal performance could be enhanced through either physical or geometrical parameters.

The present work has the potential to be further extended for more studies, such as considering a turbulent flow since laminar is not practical for many cases, it is also possible to extend the study to unsteady state and investigate the effects of other parameters such as the cold wall dimension, and furthermore it can be examined experimentally.

REFERENCES

[1] A. Bejan, *Convection heat transfer*, FOURTH EDITION ed.: John wiley & sons, 2013.

[2] A. J. G. Yunus A. Çengel, *Heat and mass transfer: fundamentals and applications*, FIFTH EDITION ed. New York: McGraw-Hill Education, 2015.

[3] R. W. Serth, *Process heat transfer*: Elsevier, 2010.

[4] T. L. Bergman, F. P. Incropera, D. P. DeWitt, and A. S. Lavine, *Fundamentals of heat and mass transfer*: John Wiley & Sons, 2011.

[5] D.-Y. Shang and L.-C. Zhong, *Heat transfer of laminar mixed convection of liquid*: Springer, 2016.

[6] E. M. M. Alam, "Numerical study on conjugate effect of conduction and mixed convection flow in a rectangular ventilated cavity with a heat generating circular block," Post graduate Thesis of Mathematics (Math), Department of Mathematics, Bangladesh University of Engineering and Technology, 2012.

[7] S. Izadi, T. Armaghani, R. Ghasemiasl, A. J. Chamkha, and M. Molana, "A comprehensive review on mixed convection of nanofluids in various shapes of enclosures," *Powder technology*, vol. 343, pp. 880-907, 2019.

[8] C. Sun, B. Yu, H. F. Oztop, Y. Wang, and J. Wei, "Control of mixed convection in lid-driven enclosures using conductive triangular fins," *International Journal of Heat and Mass Transfer*, vol. 54, pp. 894-909, 2011.

[9] M. Edalatpour and J. P. Solano, "Thermal-hydraulic characteristics and exergy performance in tube-on-sheet flat plate solar collectors: Effects of nanofluids and mixed convection," *International Journal of Thermal Sciences*, vol. 118, pp. 397-409, 2017.

[10] Y. R. Sekhar, K. Sharma, and S. Kamal, "Nanofluid heat transfer under mixed convection flow in a tube for solar thermal energy applications," *Environmental Science and Pollution Research*, vol. 23, pp. 9411-9417, 2016.

[11] Ç. Y. Yurddaş Ali, "Numerical analysis of natural convection effects in flat-plate solar collector with Al2O3-H2O and Cu-H2O nanofluids," in *International Advanced Researches & Engineering Congress (IAREC'17)*, Osmaniye, Turkey, 2017.

[12] J. T. Mahdi, "Solar Pond is a New Technique of Supplying Thermal Energy," *Journal of kerbala university*, vol. 10, pp. 339-347, 2012.

[13] S. kakaç, *Cooling of Electronic Systems*, 1 ed.: Springer Netherlands, 1994.

[14] S. C. Sugarman, *HVAC Fundamentals*, Second Edition ed.: The Fairmont Press, Inc, 2007.

[15] D.-H. Shin, C. S. Kim, G.-C. Park, and H. K. Cho, "Experimental analysis on mixed convection in reactor cavity cooling system of HTGR for hydrogen production," *International Journal of Hydrogen Energy*, vol. 42, pp. 22046-22053, 2017.

[16] B. Calcagni, F. Marsili, and M. Paroncini, "Natural convective heat transfer in square enclosures heated from below," *Applied thermal engineering,* vol. 25, pp. 2522-2531, 2005.

[17] E. Sourtiji, S. Hosseinizadeh, M. Gorji-Bandpy, and J. Khodadadi, "Computational study of turbulent forced convection flow in a square cavity with ventilation ports," *Numerical Heat Transfer, Part A: Applications,* vol. 59, pp. 954-969, 2011.

[18] M. M. Rahman, S. Parvin, N. Rahim, M. Islam, R. Saidur, and M. Hasanuzzaman, "Effects of Reynolds and Prandtl number on mixed convection in a ventilated cavity with a heat-generating solid circular block," *Applied Mathematical Modelling,* vol. 36, pp. 2056-2066, 2012.

[19] S. K. Gupta, D. Chatterjee, and B. Mondal, "Investigation of mixed convection in a ventilated cavity in the presence of a heat conducting circular cylinder," *Numerical Heat Transfer, Part A: Applications,* vol. 67, pp. 52-74, 2015.

[20] R. Benderradji, H. Gouidmi, D. Taloub, and A. Beghidja, "Numerical study three-dimensional of mixed convection in a cavity: Influence of Reynolds and Grashof numbers," *Journal of Advanced Research in Fluid Mechanics and Thermal Sciences,* vol. 51, pp. 42-52, 2018.

[21] M. Ahammad, M. Rahman, and M. Rahman, "Effect of inlet and outlet position in a ventilated cavity with a heat generating square block," *Engineering e-Transaction,* vol. 7, pp. 107-115, 2012.

[22] H. Doghmi, B. Abourida, H. Belarche, M. Sannad, and M. Ouzaouit, "Effect of the inlet opening on mixed convection inside a three dimensional ventilated cavity," *Thermal Science International Scientific Journal. https://doi. org/10.2298/TSCI170126121D,* 2017.

[23] M. M. Rahman, S. Parvin, M. Hasanuzzaman, R. Saidur, and N. A. Rahim, "Effect of heat-generating solid body on mixed convection flow in a ventilated cavity," *Heat transfer engineering,* vol. 34, pp. 1249-1261, 2013.

[24] F. Karimi, H. Xu, Z. Wang, M. Yang, and Y. Zhang, "Numerical simulation of steady mixed convection around two heated circular cylinders in a square enclosure," *Heat Transfer Engineering,* vol. 37, pp. 64-75, 2016.

[25] M. Mamun, M. Rahman, M. Billah, and R. Saidur, "A numerical study on the effect of a heated hollow cylinder on mixed convection in a ventilated cavity," *International Communications in Heat and Mass Transfer,* vol. 37, pp. 1326-1334, 2010.

[26] A. J. Chamkha, S. H. Hussain, and Q. R. Abd-Amer, "Mixed convection heat transfer of air inside a square vented cavity with a heated horizontal square cylinder," *Numerical Heat Transfer, Part A: Applications,* vol. 59, pp. 58-79, 2011.

[27] M. Shahi, A. H. Mahmoudi, and F. Talebi, "Numerical study of mixed convective cooling in a square cavity ventilated and partially heated from the below utilizing nanofluid," *International Communications in Heat and Mass Transfer,* vol. 37, pp. 201-213, 2010.

[28] J. D. Anderson and J. Wendt, *Computational fluid dynamics* vol. 206: Springer, 1995.

[29] A. C. Yunus, John M Cimbala, *Fluid Mechanics: Fundamentals And Applications (Si Units)*, THIRD EDITION ed. New York: Tata McGraw Hill Education Private Limited, 2014.

[30] L. M. Jiji, *Heat convection*: Springer, 2006.

[31] Y. Song, D. Cheng, and L. Zhao, *Microfluidics: Fundamentals, Devices, and Applications*: John Wiley & Sons, 2018.

[32] B. Zohuri, *Compact Heat Exchangers: Selection, Application, Design and Evaluation*: Springer, 2017.

[33] G. Prager, *Practical Pharmaceutical Engineering*: Wiley, 2018.

[34] B. Lin, *Microfluidics: technologies and applications* vol. 304: Springer, 2011.

[35] H. D. Baehr and K. Stephan, *Heat and Mass Transfer*: Springer Berlin Heidelberg, 2006.

[36] G. Şenay, M. Kaya, E. Gedik, and M. Kayfeci, "Numerical investigation on turbulent convective heat transfer of nanofluid flow in a square cross-sectioned duct," *International Journal of Numerical Methods for Heat & Fluid Flow*, 2019.

[37] F. Moukalled, L. Mangani, and M. Darwish, *The finite volume method in computational fluid dynamics* vol. 113: Springer, 2016.

[38] H. Jasak, "Error analysis and estimation for the finite volume method with applications to fluid flows," 1996.

[39] M. Peric, "A finite volume method for the prediction of three-dimensional fluid flow in complex ducts," Mech. Eng. Dept., University of London, 1985.

[40] H. Hadzic, *Development and application of finite volume method for the computation of flows around moving bodies on unstructured, overlapping grids*: Technische Universität Hamburg, 2006.

[41] ANSYS, *ANSYS Fluent Getting Started Guide*, ANSYS Inc ed., 2018.

[42] ANSYS, *ANSYS Fluent Theory Guide*, ANSYS Inc ed., 2018.

[43] J. M. Cimbala, *PROPERTY TABLES AND CHARTS,TABLE A–9, Properties of air at 1 atm pressure*. The Pennsylvania State University, 2018.

[44] ANSYS, *ANSYS Fluent User's Guide*, ANSYS Inc ed., 2018.

[45] M. Moallemi and K. Jang, "Prandtl number effects on laminar mixed convection heat transfer in a lid-driven cavity," *International Journal of Heat and Mass Transfer*, vol. 35, pp. 1881-1892, 1992.

[46] T. Radhakrishnan, A. Verma, C. Balaji, and S. Venkateshan, "An experimental and numerical investigation of mixed convection from a heat generating element in a ventilated cavity," *Experimental Thermal and Fluid Science*, vol. 32, pp. 502-520, 2007.

APPENDICES

Appendix A

A. Non-dimensionalization of the governing equations

A.1 Continuity equation

$$\frac{\partial u}{\partial x}+\frac{\partial v}{\partial y}+\frac{\partial w}{\partial z}=0$$

$$\frac{\partial u}{\partial x}=\frac{\partial u^{*}.u_{\infty}}{\partial x^{*}.L}=\frac{u_{\infty}}{L}\cdot\frac{\partial u^{*}}{\partial x^{*}}$$

$$\frac{\partial v}{\partial y}=\frac{\partial v^{*}.u_{\infty}}{\partial y^{*}.L}=\frac{u_{\infty}}{L}\cdot\frac{\partial v^{*}}{\partial y^{*}}$$

$$\frac{\partial w}{\partial z}=\frac{\partial w^{*}.u_{\infty}}{\partial z^{*}.L}=\frac{u_{\infty}}{L}\cdot\frac{\partial w^{*}}{\partial z^{*}}$$

$$\frac{u_{\infty}}{L}\cdot\frac{\partial u^{*}}{\partial x^{*}}+\frac{u_{\infty}}{L}\cdot\frac{\partial v^{*}}{\partial y^{*}}+\frac{u_{\infty}}{L}\cdot\frac{\partial w^{*}}{\partial z^{*}}=0$$

$$\frac{\partial u^{*}}{\partial x^{*}}+\frac{\partial v^{*}}{\partial y^{*}}+\frac{\partial w^{*}}{\partial z^{*}}=0$$

A.2 Momentum (Navier-Stokes) equations

- **Momentum equation in x-direction**

$$\rho\frac{\partial u}{\partial t}+\rho u\frac{\partial u}{\partial x}+\rho v\frac{\partial u}{\partial y}+\rho w\frac{\partial u}{\partial z}=-\frac{\partial p}{\partial x}+\mu\left(\frac{\partial^{2}u}{\partial x^{2}}+\frac{\partial^{2}u}{\partial y^{2}}+\frac{\partial^{2}u}{\partial z^{2}}\right)$$

$$\frac{\partial u}{\partial t}=\frac{\partial u^{*}.u_{\infty}}{\partial t^{*}.{}^{L}/_{u_{\infty}}}=\frac{u_{\infty}^{2}}{L}\cdot\frac{\partial u^{*}}{\partial t^{*}}$$

$$u\frac{\partial u}{\partial x}=u^{*}.u_{\infty}\cdot\frac{\partial u^{*}.u_{\infty}}{\partial x^{*}.L}=\frac{u_{\infty}^{2}}{L}\cdot u^{*}\cdot\frac{\partial u^{*}}{\partial x^{*}}$$

$$v\frac{\partial u}{\partial y}=v^{*}.u_{\infty}\cdot\frac{\partial u^{*}.u_{\infty}}{\partial y^{*}.L}=\frac{u_{\infty}^{2}}{L}\cdot v^{*}\cdot\frac{\partial u^{*}}{\partial y^{*}}$$

$$w\frac{\partial u}{\partial z}=w^{*}.u_{\infty}\cdot\frac{\partial u^{*}.u_{\infty}}{\partial z^{*}.L}=\frac{u_{\infty}^{2}}{L}\cdot w^{*}\cdot\frac{\partial u^{*}}{\partial z^{*}}$$

$$\frac{\partial P}{\partial x}=\frac{\partial(P^{*}\rho u_{\infty}^{2}+P_{\infty})}{\partial x^{*}\cdot L}=\frac{\partial(P^{*}\rho u_{\infty}^{2})}{\partial x^{*}\cdot L}+\frac{\partial(P_{\infty})}{\partial x^{*}\cdot L}=\frac{\partial(P^{*}\rho u_{\infty}^{2})}{\partial x^{*}\cdot L}=\frac{\rho u_{\infty}^{2}}{L}\cdot\frac{\partial P^{*}}{\partial x^{*}}$$

$$\frac{\partial^{2}u}{\partial x^{2}}=\frac{\partial^{2}(u^{*}.u_{\infty})}{\partial(x^{*}.L)^{2}}=\frac{u_{\infty}}{L^{2}}\cdot\frac{\partial^{2}(u^{*})}{\partial(x^{*})^{2}}$$

$$\frac{\partial^{2}u}{\partial y^{2}}=\frac{\partial^{2}(u^{*}.u_{\infty})}{\partial(y^{*}.L)^{2}}=\frac{u_{\infty}}{L^{2}}\cdot\frac{\partial^{2}(u^{*})}{\partial(y^{*})^{2}}$$

$$\frac{\partial^2 u}{\partial z^2} = \frac{\partial^2 (u^*.u_\infty)}{\partial (z^*.L)^2} = \frac{u_\infty}{L^2} \cdot \frac{\partial^2 (u^*)}{\partial (z^*)^2}$$

$$\rho \frac{u_\infty^2}{L} \cdot \frac{\partial u^*}{\partial t^*} + \rho \frac{u_\infty^2}{L} \cdot u^* \cdot \frac{\partial u^*}{\partial x^*} + \rho \frac{u_\infty^2}{L} \cdot v^* \cdot \frac{\partial u^*}{\partial y^*} + \rho \frac{u_\infty^2}{L} \cdot w^* \cdot \frac{\partial u^*}{\partial z^*}$$

$$= -\frac{\rho u_\infty^2}{L} \cdot \frac{\partial P^*}{\partial x^*} + \mu \frac{u_\infty}{L^2} \left(\frac{\partial^2 (u^*)}{\partial (x^*)^2} + \frac{\partial^2 (u^*)}{\partial (y^*)^2} + \frac{\partial^2 (u^*)}{\partial (z^*)^2} \right)$$

$$\frac{L}{\rho u_\infty^2} \left(\rho \frac{u_\infty^2}{L} \cdot \frac{\partial u^*}{\partial t^*} + \rho \frac{u_\infty^2}{L} \cdot u^* \cdot \frac{\partial u^*}{\partial x^*} + \rho \frac{u_\infty^2}{L} \cdot v^* \cdot \frac{\partial u^*}{\partial y^*} + \rho \frac{u_\infty^2}{L} \cdot w^* \cdot \frac{\partial u^*}{\partial z^*} \right)$$

$$= \frac{L}{\rho u_\infty^2} \left(-\frac{\rho u_\infty^2}{L} \cdot \frac{\partial P^*}{\partial x^*} + \mu \frac{u_\infty}{L^2} \left(\frac{\partial^2 (u^*)}{\partial (x^*)^2} + \frac{\partial^2 (u^*)}{\partial (y^*)^2} + \frac{\partial^2 (u^*)}{\partial (z^*)^2} \right) \right)$$

$$\frac{\partial u^*}{\partial t^*} + u^* \cdot \frac{\partial u^*}{\partial x^*} + v^* \cdot \frac{\partial u^*}{\partial y^*} + w^* \cdot \frac{\partial u^*}{\partial z^*} = -\frac{\partial P^*}{\partial x^*} + \frac{\mu}{L \rho u_\infty} \left(\frac{\partial^2 (u^*)}{\partial (x^*)^2} + \frac{\partial^2 (u^*)}{\partial (y^*)^2} + \frac{\partial^2 (u^*)}{\partial (z^*)^2} \right)$$

$$\frac{\partial u^*}{\partial t^*} + u^* \cdot \frac{\partial u^*}{\partial x^*} + v^* \cdot \frac{\partial u^*}{\partial y^*} + w^* \cdot \frac{\partial u^*}{\partial z^*} = -\frac{\partial P^*}{\partial x^*} + \frac{1}{Re} \left(\frac{\partial^2 (u^*)}{\partial (x^*)^2} + \frac{\partial^2 (u^*)}{\partial (y^*)^2} + \frac{\partial^2 (u^*)}{\partial (z^*)^2} \right)$$

- **Momentum equation in y-direction**

$$\rho \frac{\partial v}{\partial t} + \rho u \frac{\partial v}{\partial x} + \rho v \frac{\partial v}{\partial y} + \rho w \frac{\partial v}{\partial z} = -\frac{\partial p}{\partial y} + \mu \left(\frac{\partial^2 v}{\partial x^2} + \frac{\partial^2 v}{\partial y^2} + \frac{\partial^2 v}{\partial z^2} \right)$$

$$\frac{\partial v}{\partial t} = \frac{\partial v^*.u_\infty}{\partial t^*.{}^{L}/_{u_\infty}} = \frac{u_\infty^2}{L} \cdot \frac{\partial v^*}{\partial t^*}$$

$$u \frac{\partial v}{\partial x} = u^*.u_\infty \cdot \frac{\partial v^*.u_\infty}{\partial x^*.L} = \frac{u_\infty^2}{L} \cdot u^* \cdot \frac{\partial v^*}{\partial x^*}$$

$$v \frac{\partial v}{\partial y} = v^*.u_\infty \cdot \frac{\partial v^*.u_\infty}{\partial y^*.L} = \frac{u_\infty^2}{L} \cdot v^* \cdot \frac{\partial v^*}{\partial y^*}$$

$$w \frac{\partial v}{\partial z} = w^*.u_\infty \cdot \frac{\partial v^*.u_\infty}{\partial z^*.L} = \frac{u_\infty^2}{L} \cdot w^* \cdot \frac{\partial v^*}{\partial z^*}$$

$$\frac{\partial P}{\partial y} = \frac{\partial (P^* \rho u_\infty^2 + P_\infty)}{\partial y^* \cdot L} = \frac{\partial (P^* \rho u_\infty^2)}{\partial y^* \cdot L} + \frac{\partial (P_\infty)}{\partial y^* \cdot L} = \frac{\partial (P^* \rho u_\infty^2)}{\partial y^* \cdot L} = \frac{\rho u_\infty^2}{L} \cdot \frac{\partial P^*}{\partial y^*}$$

$$\frac{\partial^2 v}{\partial x^2} = \frac{\partial^2 (v^*.u_\infty)}{\partial (x^*.L)^2} = \frac{u_\infty}{L^2} \cdot \frac{\partial^2 (v^*)}{\partial (x^*)^2}$$

$$\frac{\partial^2 v}{\partial y^2} = \frac{\partial^2 (v^*.u_\infty)}{\partial (y^*.L)^2} = \frac{u_\infty}{L^2} \cdot \frac{\partial^2 (v^*)}{\partial (y^*)^2}$$

$$\frac{\partial^2 v}{\partial z^2} = \frac{\partial^2 (v^*.u_\infty)}{\partial (z^*.L)^2} = \frac{u_\infty}{L^2} \cdot \frac{\partial^2 (v^*)}{\partial (z^*)^2}$$

$$\rho \frac{u_\infty^2}{L} \cdot \frac{\partial v^*}{\partial t^*} + \rho \frac{u_\infty^2}{L} \cdot u^* \cdot \frac{\partial v^*}{\partial x^*} + \rho \frac{u_\infty^2}{L} \cdot v^* \cdot \frac{\partial v^*}{\partial y^*} + \rho \frac{u_\infty^2}{L} \cdot w^* \cdot \frac{\partial v^*}{\partial z^*}$$

$$= -\frac{\rho u_\infty^2}{L} \cdot \frac{\partial P^*}{\partial y^*} + \mu \frac{u_\infty}{L^2} \cdot \frac{\partial^2 (v^*)}{\partial (x^*)^2} + \mu \frac{u_\infty}{L^2} \cdot \frac{\partial^2 (v^*)}{\partial (y^*)^2} + \mu \frac{u_\infty}{L^2} \cdot \frac{\partial^2 (v^*)}{\partial (z^*)^2}$$

$$\frac{L}{\rho u_\infty^2}\left(\rho\frac{u_\infty^2}{L}\cdot\frac{\partial v^*}{\partial t^*}+\rho\frac{u_\infty^2}{L}\cdot u^*\cdot\frac{\partial v^*}{\partial x^*}+\rho\frac{u_\infty^2}{L}\cdot v^*\cdot\frac{\partial v^*}{\partial y^*}+\rho\frac{u_\infty^2}{L}\cdot w^*\cdot\frac{\partial v^*}{\partial z^*}\right)$$

$$=\frac{L}{\rho u_\infty^2}\left(-\frac{\rho u_\infty^2}{L}\cdot\frac{\partial P^*}{\partial y^*}+\mu\frac{u_\infty}{L^2}\left(\frac{\partial^2(v^*)}{\partial(x^*)^2}+\frac{\partial^2(v^*)}{\partial(y^*)^2}+\frac{\partial^2(v^*)}{\partial(z^*)^2}\right)\right)$$

$$\frac{\partial v^*}{\partial t^*}+u^*\cdot\frac{\partial v^*}{\partial x^*}+v^*\cdot\frac{\partial v^*}{\partial y^*}+w^*\cdot\frac{\partial v^*}{\partial z^*}=-\frac{\partial P^*}{\partial y^*}+\frac{\mu}{L\rho u_\infty}\left(\frac{\partial^2(v^*)}{\partial(x^*)^2}+\frac{\partial^2(v^*)}{\partial(y^*)^2}+\frac{\partial^2(v^*)}{\partial(z^*)^2}\right)$$

$$\frac{\partial v^*}{\partial t^*}+u^*\cdot\frac{\partial v^*}{\partial x^*}+v^*\cdot\frac{\partial v^*}{\partial y^*}+w^*\cdot\frac{\partial v^*}{\partial z^*}=-\frac{\partial P^*}{\partial y^*}+\frac{1}{Re}\left(\frac{\partial^2(v^*)}{\partial(x^*)^2}+\frac{\partial^2(v^*)}{\partial(y^*)^2}+\frac{\partial^2(v^*)}{\partial(z^*)^2}\right)$$

- **Momentum equation in z-direction**

$$\rho\frac{\partial w}{\partial t}+\rho u\frac{\partial w}{\partial x}+\rho v\frac{\partial w}{\partial y}+\rho w\frac{\partial w}{\partial z}=-\frac{\partial p}{\partial z}+\mu\left(\frac{\partial^2 w}{\partial x^2}+\frac{\partial^2 w}{\partial y^2}+\frac{\partial^2 w}{\partial z^2}\right)-\rho g$$

$$\frac{\partial w}{\partial t}=\frac{\partial w^*.u_\infty}{\partial t^*.{}^{L}/_{u_\infty}}=\frac{u_\infty^2}{L}\cdot\frac{\partial w^*}{\partial t^*}$$

$$u\frac{\partial w}{\partial x}=u^*.u_\infty\cdot\frac{\partial w^*.u_\infty}{\partial x^*.L}=\frac{u_\infty^2}{L}\cdot u^*\cdot\frac{\partial w^*}{\partial x^*}$$

$$v\frac{\partial w}{\partial y}=v^*.u_\infty\cdot\frac{\partial w^*.u_\infty}{\partial y^*.L}=\frac{u_\infty^2}{L}\cdot v^*\cdot\frac{\partial w^*}{\partial y^*}$$

$$w\frac{\partial w}{\partial z}=w^*.u_\infty\cdot\frac{\partial w^*.u_\infty}{\partial z^*.L}=\frac{u_\infty^2}{L}\cdot w^*\cdot\frac{\partial w^*}{\partial z^*}$$

$$\frac{\partial P}{\partial z}=\frac{\partial(P^*\rho u_\infty^2+P_\infty)}{\partial z^*\cdot L}=\frac{\partial(P^*\rho u_\infty^2)}{\partial z^*\cdot L}+\frac{\partial(P_\infty)}{\partial z^*\cdot L}=\frac{\partial(P^*\rho u_\infty^2)}{\partial z^*\cdot L}=\frac{\rho u_\infty^2}{L}\cdot\frac{\partial P^*}{\partial z^*}$$

$$\frac{\partial^2 w}{\partial x^2}=\frac{\partial^2(w^*.u_\infty)}{\partial(x^*.L)^2}=\frac{u_\infty}{L^2}\cdot\frac{\partial^2(w^*)}{\partial(x^*)^2}$$

$$\frac{\partial^2 w}{\partial y^2}=\frac{\partial^2(w^*.u_\infty)}{\partial(y^*.L)^2}=\frac{u_\infty}{L^2}\cdot\frac{\partial^2(w^*)}{\partial(y^*)^2}$$

$$\frac{\partial^2 w}{\partial z^2}=\frac{\partial^2(w^*.u_\infty)}{\partial(z^*.L)^2}=\frac{u_\infty}{L^2}\cdot\frac{\partial^2(w^*)}{\partial(z^*)^2}$$

$$\rho\frac{u_\infty^2}{L}\cdot\frac{\partial w^*}{\partial t^*}+\rho\frac{u_\infty^2}{L}\cdot u^*\cdot\frac{\partial w^*}{\partial x^*}+\rho\frac{u_\infty^2}{L}\cdot v^*\cdot\frac{\partial w^*}{\partial y^*}+\rho\frac{u_\infty^2}{L}\cdot w^*\cdot\frac{\partial w^*}{\partial z^*}$$

$$=-\frac{\rho u_\infty^2}{L}\cdot\frac{\partial P^*}{\partial z^*}+\mu\frac{u_\infty}{L^2}\cdot\frac{\partial^2(w^*)}{\partial(x^*)^2}+\mu\frac{u_\infty}{L^2}\cdot\frac{\partial^2(w^*)}{\partial(y^*)^2}+\mu\frac{u_\infty}{L^2}\cdot\frac{\partial^2(w^*)}{\partial(z^*)^2}-\rho g$$

$$\frac{L}{\rho u_\infty^2}\left(\rho\frac{u_\infty^2}{L}\cdot\frac{\partial w^*}{\partial t^*}+\rho\frac{u_\infty^2}{L}\cdot u^*\cdot\frac{\partial w^*}{\partial x^*}+\rho\frac{u_\infty^2}{L}\cdot v^*\cdot\frac{\partial w^*}{\partial y^*}+\rho\frac{u_\infty^2}{L}\cdot w^*\cdot\frac{\partial w^*}{\partial z^*}\right)$$

$$=\frac{L}{\rho u_\infty^2}\left(-\frac{\rho u_\infty^2}{L}\cdot\frac{\partial P^*}{\partial z^*}+\mu\frac{u_\infty}{L^2}\left(\frac{\partial^2(w^*)}{\partial(x^*)^2}+\frac{\partial^2(w^*)}{\partial(y^*)^2}+\frac{\partial^2(w^*)}{\partial(z^*)^2}\right)-\rho g\right)$$

$$\frac{\partial w^*}{\partial t^*} + u^* \cdot \frac{\partial w^*}{\partial x^*} + v^* \cdot \frac{\partial w^*}{\partial y^*} + w^* \cdot \frac{\partial w^*}{\partial z^*}$$

$$= -\frac{\partial P^*}{\partial z^*} + \frac{\mu}{L\rho u_\infty}\left(\frac{\partial^2(w^*)}{\partial(x^*)^2} + \frac{\partial^2(w^*)}{\partial(y^*)^2} + \frac{\partial^2(w^*)}{\partial(z^*)^2}\right) - g\,\frac{L}{u_\infty^2}$$

$$\frac{\partial w^*}{\partial t^*} + u^* \cdot \frac{\partial w^*}{\partial x^*} + v^* \cdot \frac{\partial w^*}{\partial y^*} + w^* \cdot \frac{\partial w^*}{\partial z^*}$$

$$= -\frac{\partial P^*}{\partial z^*} + \frac{1}{Re}\left(\frac{\partial^2(w^*)}{\partial(x^*)^2} + \frac{\partial^2(w^*)}{\partial(y^*)^2} + \frac{\partial^2(w^*)}{\partial(z^*)^2}\right) - g\,\frac{L}{u_\infty^2}$$

A.3 Energy equation

$$\frac{\partial T}{\partial t} + u\frac{\partial T}{\partial x} + v\frac{\partial T}{\partial y} + w\frac{\partial T}{\partial z} = \frac{K}{\rho C_p}\left(\frac{\partial^2 T}{\partial x^2} + \frac{\partial^2 T}{\partial y^2} + \frac{\partial^2 T}{\partial z^2}\right)$$

$$\frac{\partial T}{\partial t} = \frac{\partial(T^*.\Delta T + T_\infty)}{\partial t^*.\,{}^{L}/_{u_\infty}} = \frac{\Delta T.u_\infty}{L} \cdot \frac{\partial T^*}{\partial t^*}$$

$$u\frac{\partial w}{\partial x} = u^*.u_\infty \cdot \frac{\partial(T^*.\Delta T + T_\infty)}{\partial x^*.L} = \frac{\Delta T.u_\infty}{L} \cdot u^* \cdot \frac{\partial T^*}{\partial x^*}$$

$$v\frac{\partial w}{\partial y} = v^*.u_\infty \cdot \frac{\partial(T^*.\Delta T + T_\infty)}{\partial y^*.L} = \frac{\Delta T.u_\infty}{L} \cdot v^* \cdot \frac{\partial T^*}{\partial y^*}$$

$$w\frac{\partial w}{\partial z} = w^*.u_\infty \cdot \frac{\partial(T^*.\Delta T + T_\infty)}{\partial z^*.L} = \frac{\Delta T.u_\infty}{L} \cdot w^* \cdot \frac{\partial T^*}{\partial z^*}$$

$$\frac{\partial^2 T}{\partial x^2} = \frac{\partial^2\left((T^*.\Delta T + T_\infty)\right)}{\partial(x^*.L)^2} = \frac{\Delta T}{L^2} \cdot \frac{\partial^2(T^*)}{\partial(x^*)^2}$$

$$\frac{\partial^2 T}{\partial y^2} = \frac{\partial^2\left((T^*.\Delta T + T_\infty)\right)}{\partial(y^*.L)^2} = \frac{\Delta T}{L^2} \cdot \frac{\partial^2(T^*)}{\partial(y^*)^2}$$

$$\frac{\partial^2 T}{\partial z^2} = \frac{\partial^2\left((T^*.\Delta T + T_\infty)\right)}{\partial(z^*.L)^2} = \frac{\Delta T}{L^2} \cdot \frac{\partial^2(T^*)}{\partial(z^*)^2}$$

$$\frac{\Delta T.u_\infty}{L} \cdot \frac{\partial T^*}{\partial t^*} + \frac{\Delta T.u_\infty}{L} \cdot u^* \cdot \frac{\partial T^*}{\partial x^*} + \frac{\Delta T.u_\infty}{L} \cdot v^* \cdot \frac{\partial T^*}{\partial y^*} + \frac{\Delta T.u_\infty}{L} \cdot w^* \cdot \frac{\partial T^*}{\partial z^*}$$

$$= \frac{K}{\rho C_p} \cdot \frac{\Delta T}{L^2} \cdot \frac{\partial^2(T^*)}{\partial(x^*)^2} + \frac{K}{\rho C_p} \cdot \frac{\Delta T}{L^2} \cdot \frac{\partial^2(T^*)}{\partial(y^*)^2} + \frac{K}{\rho C_p} \cdot \frac{\Delta T}{L^2} \cdot \frac{\partial^2(T^*)}{\partial(z^*)^2}$$

$$\frac{\Delta T.u_\infty}{L} \cdot \frac{\partial T^*}{\partial t^*} + \frac{\Delta T.u_\infty}{L} \cdot u^* \cdot \frac{\partial T^*}{\partial x^*} + \frac{\Delta T.u_\infty}{L} \cdot v^* \cdot \frac{\partial T^*}{\partial y^*} + \frac{\Delta T.u_\infty}{L} \cdot w^* \cdot \frac{\partial T^*}{\partial z^*}$$

$$= \frac{K}{\rho C_p} \cdot \frac{\Delta T}{L^2}\left(\frac{\partial^2(T^*)}{\partial(x^*)^2} + \frac{\partial^2(T^*)}{\partial(y^*)^2} + \frac{\partial^2(T^*)}{\partial(z^*)^2}\right)$$

$$\frac{L}{\Delta T.u_\infty}\left(\frac{\Delta T.u_\infty}{L} \cdot \frac{\partial T^*}{\partial t^*} + \frac{\Delta T.u_\infty}{L} \cdot u^* \cdot \frac{\partial T^*}{\partial x^*} + \frac{\Delta T.u_\infty}{L} \cdot v^* \cdot \frac{\partial T^*}{\partial y^*} + \frac{\Delta T.u_\infty}{L} \cdot w^* \cdot \frac{\partial T^*}{\partial z^*}\right)$$

$$= \frac{L}{\Delta T.u_\infty}\left(\frac{K}{\rho C_p} \cdot \frac{\Delta T}{L^2}\left(\frac{\partial^2(T^*)}{\partial(x^*)^2} + \frac{\partial^2(T^*)}{\partial(y^*)^2} + \frac{\partial^2(T^*)}{\partial(z^*)^2}\right)\right)$$

$$\frac{\partial T^*}{\partial t^*} + u^* \cdot \frac{\partial T^*}{\partial x^*} + v^* \cdot \frac{\partial T^*}{\partial y^*} + w^* \cdot \frac{\partial T^*}{\partial z^*} = \frac{K.\nu}{\rho C_p L.u_\infty.\nu}\left(\frac{\partial^2(T^*)}{\partial(x^*)^2} + \frac{\partial^2(T^*)}{\partial(y^*)^2} + \frac{\partial^2(T^*)}{\partial(z^*)^2}\right)$$

$$\frac{\partial T^*}{\partial t^*} + u^* \cdot \frac{\partial T^*}{\partial x^*} + v^* \cdot \frac{\partial T^*}{\partial y^*} + w^* \cdot \frac{\partial T^*}{\partial z^*} = \frac{K}{\mu \, . \, C_p} \cdot \frac{\nu}{L.u_\infty}\left(\frac{\partial^2(T^*)}{\partial(x^*)^2} + \frac{\partial^2(T^*)}{\partial(y^*)^2} + \frac{\partial^2(T^*)}{\partial(z^*)^2}\right)$$

$$\frac{\partial T^*}{\partial t^*} + u^* \cdot \frac{\partial T^*}{\partial x^*} + v^* \cdot \frac{\partial T^*}{\partial y^*} + w^* \cdot \frac{\partial T^*}{\partial z^*} = \frac{1}{Re\,.\,Pr}\left(\frac{\partial^2(T^*)}{\partial(x^*)^2} + \frac{\partial^2(T^*)}{\partial(y^*)^2} + \frac{\partial^2(T^*)}{\partial(z^*)^2}\right)$$

Appendix B

B. Miscellaneous combined effects

B.1 Combined effects of Pr, Re and Ri numbers on Nu_{ave}

The effects of Pr number for different Reynolds and Richardson numbers on the average Nu number at K = 0.1, H/5 inlet and outlet dimensions, BT configuration, fin at the cavity center, H_f = 0.3 and AR = 1, is shown the Tables B.1-3 below.

***Tab B.1**: $Nu_{ave} = f(Pr, Re)$*

Re	Pr	Nu
10	0.71	1.759063
50	1.51	5.010827
100	2.31	7.546913
300	3.11	15.71657
500	3.91	22.11354
700	4.70	26.93288
900	5.50	32.05629
1200	6.30	38.34907
1500	7.10	43.44324

***Tab B.2**: $Nu_{ave} = f(Pr, Ri)$*

Ri	Pr	Nu
0.1	0.71	10.17585
0.5	1.51	14.46915
1	2.31	18.11638
2	3.11	21.6595
4	3.91	24.40684
6	4.70	27.93902
8	5.50	30.58322
9	6.30	32.28561
10	7.10	33.74096

***Tab B.3**: $Nu_{ave} = f(Pr,Re,Ri)$*

Re	Ri	Pr	Nu
10	0.1	0.71	1.849437
50	0.5	1.51	5.013458
100	1	2.31	7.727761
300	2	3.11	16.5935
500	4	3.91	24.52482
700	6	4.7	32.74473
900	8	5.5	39.90809
1200	9	6.3	47.53223
1500	10	7.1	54.95511

The combined effect of Prandtl number and Reynolds number on the average Nusselt number (for Ri = 1) is illustrated in Tab B.1. While the combined effect of Richardson number and Prandtl number (for Re = 500) is shown in Tab B.2, form the two tables above we can note that the effect of the external force convection is more important for the thermal performance since its effect is steeper and more significant than the effect of the buoyancy driven flow convection. A further combination of the effect of the inertia force, external force flow convection and the buoyancy driven flow convection is shown in Tab B.3, in this table, an important note is that the effect of the free convection is insignificant at low Ri values (Ri = 0.1 - 4), and the importance of the latter convection regime appears only at high values of Richardson number, which shows the importance of the inertia force and external force flow convection contribution in the thermal performance, in compered with the contribution of natural convection.

B.2 Combined effects of K, Re and Ri on Nu_{ave}

The influence of the thermal conductivity ratio K for different Reynolds and Richardson numbers on average Nu number at K = 0.1, Pr = 0.71, H/5 inlet and outlet dimensions, BT configuration, fin at the cavity center, $H_f = 0.3$ and AR = 1, is shown the Tables B.1-3 below.

Tab B.4 *: $Nu_{ave} = f(K, Re)$*

Re	K	Nu
10	0.1	1.79556
50	1.3375	3.628971
100	2.575	4.720361
300	3.8125	7.128651
500	5.05	8.630269
700	6.2875	9.344196
900	7.525	9.560268
1200	8.7625	9.55594
1500	10	9.422835

Tab B.5 *: $Nu_{ave} = f(K, Ri)$*

Ri	K	Nu
0.1	0.1	11.02067
0.5	1.3375	10.25618
1	2.575	9.997938
2	3.8125	10.0038
4	5.05	9.404042
6	6.2875	9.105578
8	7.525	8.804329
9	8.7625	8.44853
10	10	8.149605

Tab B.6 *: $Nu_{ave} = f(K, Re, Ri)$*

Re	Ri	K	Nu
10	0.1	0.1	1.907965
50	0.5	1.3375	3.605339
100	1	2.575	4.720361
300	2	3.8125	7.513016
500	4	5.05	9.404042
700	6	6.2875	10.49603
900	8	7.525	11.12044
1200	9	8.7625	11.28661
1500	10	10	11.27091

The combined impact of the thermal conductivity ratio K and Re number (while Ri = 1) is outlined in Tab B.4, while Tab B.5 presents the effect of Richardson number and K combination (at Re = 500) on the average Nu number. The first table indicates a significant effect of the increased Re number which produced an important increase in Nu_{ave}. However the rate of the increase gets decreased and then reversed at high Re number and this shows the importance of the thermal conductivity effect on the heat flux and thermal performance, on the other hand, although we increase Ri number, Nu_{ave} is decreasing which makes it possible to say that the effect of K is more significant on the dominant natural convection regime. The combination of the previously mentioned cases (i.e. $Nu_{ave} = f(K, Re, Ri)$) is depicted in Tab B.6, it is clearly evident that the latter combination results are similar to that when Nu_{ave} is affected by a combination of Re and K values which indicates and emphasizes ones again the importance of the forced convection contribution in the thermal performance.

Thème de mémoire: Etude numérique de la convection mixte dans une cavité ventilée contenant une ailette.

Auteurs: Abdelhak KEDDOUDA, Mohammed Ridha BOUDEBIA. Département de génie mécanique, Université d'El-Oued.

Master: Energétique.

Résumé

Le transfert de chaleur par convection mixte à l'intérieur d'une cavité rectangulaire ventilée avec une ailette chauffée en forme de T a été étudié numériquement, de large intervalles des nombres de Re (10 - 1500), Ri (0,1 - 10) et Pr (0,71 - 7,10) ont été considérées dans le présent travail, les effets de la conductivité thermique solide-fluide (K = 0,1 - 10) ont été également étudiés. En outre, les effets de plusieurs paramètres géométriques ont été examinés, à savoir, les dimensions d'entrée et de sortie (D_1 et D_2), leur positions, l'emplacement de l'ailette, sa longueur (H_f) et le rapport d'aspect de la cavité (AR). Le modèle étudié est régi par un ensemble d'équations aux dérivées partielles, et soumis à des conditions aux limites selon les hypothèses considérées; le modèle mathématique a été transformé en une forme adimensionnelle, puis résolu en utilisant le code CFD de ANSYS Fluent basé sur la méthode des volumes finis. Les résultats ont été présentés en termes d'isothermes, des lignes de courant et de nombre de Nusselt moyen pour une multitude de combinaison des paramètres gouvernantes. Les résultats indiquent que le champ thermique et le champ d'écoulement, le taux de transfert de chaleur et le nombre de Nusselt moyen sur la surface de l'ailette, ainsi que la dominance d'un régime de convection sur l'autre, dépendent significativement des paramètres mentionnés ci-dessus.

Mots clés : convection mixte, ailette, ANSYS Fluent, méthode des volumes finis, nombre de Nusselt.

عنوان المذكرة: دراسة عددية للحمل الحراري المختلط في تجويف يحتوي على زعنفة حرارة.

الكاتب: كدودة عبد الحق, بوضبية محمد رضا, قسم الهندسة الميكانيكية, جامعة الوادي.

مـاستر: طـاقوية

ملخص

تم دراسة الحمل الحراري المختلط عدديا في تجويف مستطيل في وجود زعنفة حرارية على شكل T يتم تسخينها بدرجة حرارة ثابتة, تم اعتبار مجال واسع من كل من عدد رينولدز (10 − 1500), عدد ريشاردسون (0.1 − 10) و عدد برانتل (0.71 − 7.10) قصد الدراسة خلال هذا العمل. اضافة الى هذا, تم دراسة تأثير نسبة الموصلية الحرارية مائع−صلب ($K = 10 - 0.1$). علاوة على ذلك تم فحص تأثير عدة عوامل هندسية اخرى و هي أبعاد فتحتي المدخل و المخرج (D_1 و D_2), مواضعهما, موضع الزعنفة, طولها (H_f) و نسبة طول التجويف الى ارتفاعه (AR). يحكم النموذج المدروس مجموعة من المعادلات التفاضلية الجزئية, و يخضع لشروط حدية بحسب الفرضيات المعتبرة, تم تحويل النموذج الرياضي الى شكلٍ بلا أبعاد و من ثم حله باستخدام طريقة الحجوم المنتهية لكود الـ CFD من ANSYS Fluent. تم عرض النتائج في صيغة خطوط درجة حرارة ثابتة, خطوط جريان و متوسط عدد نوسلت من أجل مجموعات مختلفة من العوامل المتحكمة. تشير النتائج الى أن الحقل الحراري و حقل الجريان, معدل نقل الحرارة عند سطح الزعنفة, و كذا هيمنة نمط حمل حراري على الاخر يعتمد بشكل ملحوظ على العوامل المذكورة أعلاه.

كلمات مفتاحية : الحمل الحراري المختلط, زعنفة حرارة, ANSYS Fluent, طريقة الحجوم المنتهية, عدد نوسلت.

Thesis title: Numerical study of mixed convection heat transfer in a ventilated cavity containing a heat fin.

Authors: Abdelhak KEDDOUDA, Mohammed Ridha BOUDEBIA**.** Department of mechanical engineering, University of El-Oued.

Master: Energetics.

Abstract

Mixed convection heat transfer inside rectangular ventilated cavity with an isothermally heated T-shaped heat fin have been investigated numerically, wide range of Re number (10 - 1500), Ri number (0.1 - 10) and Pr number (0.71 – 7.10) were covered in the present work, moreover the effects of the fluid-solid thermal conductivity (K = 0.1 – 10) has been also investigated. Furthermore, the effects of several geometrical parameters have been examined, namely, the inlet and outlet dimensions (D_1 and D_2), locations, fin location, its length (H_f), and the aspect ratio of the cavity (AR). The studied model is governed by a set of partial differential equations, and subjected to a boundary conditions according to the considered assumptions; the mathematical model was transformed to a dimensionless form, and then solved using ANSYS Fluent (finite volume method based CFD code). Results were presented in terms of isotherms, streamlines and average Nusselt number for multiple combinations of the governing parameters. The results indicates that the thermal and flow fields, the heat transfer rate and the average Nusselt number over the fin surface, as well as the dominance of a convection regime over the other, depends significantly on the above mentioned parameters.

Keywords: Mixed convection, Heat fin, ANSYS Fluent, Finite Volumes Method, Nusselt number.